Tekniska Högskolan i Lund
Avdelningen för Bärande Konstruktioner

Lund Institute of Technology
Department of Structural Engineering

Lund 1993

Report TVBK-5067

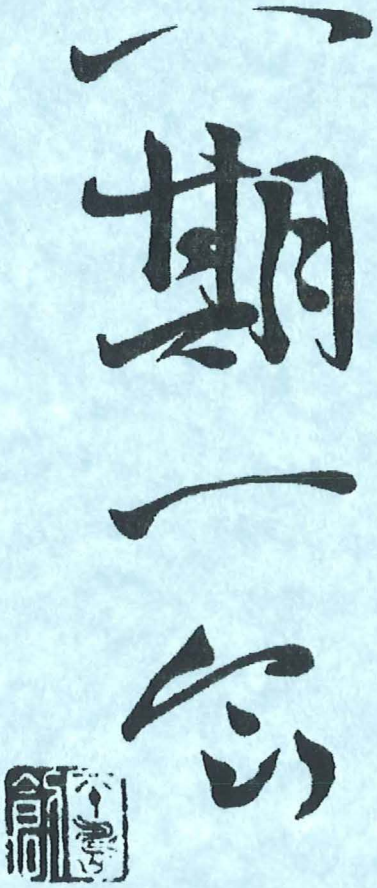

Aramid Fiber Rods as Reinforcement in Concrete

Ola Gunnarsson

Jonas Hjalmarsson

Department of Civil Engineering
Division of Structural Engineering
Lund Institute of Technology
Box 118
S-221 00 Lund
Sweden

ARAMID FIBER RODS AS REINFORCEMENT IN CONCRETE

Part I: ARAMID FIBER REINFORCED PLASTICS AND MISCELLANEOUS APPLICATIONS

Ola Gunnarsson, Jonas Hjalmarsson

Part II: STATIC AND IMPACT FLEXURAL BEHAVIOR OF PRESTRESSED CONCRETE BEAMS REINFORCED WITH BRAIDED ARAMID FIBER RODS AS PC-TENDONS

Ola Gunnarsson, Jonas Hjalmarsson
Dr. Hiroshi Mikami, Nakajima Norimichi

Supervisor: Assoc. professor Lars Sentler

1993

Abstract:

The use of fiber composites in concrete structures is an alternative to conventional steel reinforcement and several structures employing fiber composites have already been built in Japan, Europe and USA. Fiber composites offer high strength, high durability and low weight. Another property is high elastic elongation which is an advantage in structures acting under impact load. Part I of this report deals with the possible use of aramid fiber reinforced plastics as a reinforcing material and part II deals specially with aramid-rods as dampers for impact loads in prestressed concrete beams.

Report TVBK-5067
ISSN 0349-4969
ISRN: LUTVDG/TVBK--5067-SE

EXAMENSARBETE TVBK-5067

Handledare: Lars Sentler

Ola Gunnarsson
Jonas Hjalmarsson

LUND April 1993

Part I: ARAMID FIBER REINFORCED PLASTICS AND MISCELLANEOUS APPLICATIONS

Part I:

ARAMID FIBER REINFORCED PLASTICS AND MISCELLANEOUS APPLICATIONS

Ola GUNNARSSON, Jonas HJALMARSSON
Lund Institute of Technology, Lund, Sweden

1 Introduction

New high-tech materials has been developed to meet growing demands as longer life cycles and lower production costs in the construction sector.

Fiber materials such as glass fiber, carbon fiber, aramid fiber and other plastics were introduced in the concrete industry in late 1970s. Their excellent properties in terms of strength, weight and durability in aggressive environments attracted interest of engineers. At an early stage of development, short discrete fibers were successfully used by mixing uniformly with concrete in the manufacturing of precast concrete elements. In addition to short discrete fibers used in fiber reinforced concrete (FRC) long fibers has also been developed, pultruded or braided, to replace conventional reinforcing steel. Out of these long fibers Fiber Reinforced Plastic (FRP) rods have been manufactured. These rods have been used a lot in fabrication of precast concrete elements for facade or wall panels of buildings. Another promising field is prestressed concrete. Research has been carried out on many different applications. Several bridges and other utilizations employing FRP have already been built.

2 History

During this last decade great efforts has been made in research and development of Fiber Reinforced Plastics, FRP, as reinforcing materials in concrete. In the front-line of this R&D today we find Japan which, because of positive economic growth, has been able to invest a great deal of money in developing new and better building materials. Most of the big construction companies have taken part in this race and many different materials have been investigated.

The original reason for developing fiber composites was the rising demand of high-performance materials mainly within aircraft and space technology. The most important property of the material was a high strength in addition to a low weight and a high durability under extreme environmental conditions. The most common material at the time was aluminum, but its fatigue and corrosion performance was not satisfactory. Therefore the development of new materials was the only way to deal with the problem. The real break-through for composite materials came in the early fifties and there has been an enormous progress in development of new materials ever since.

3 A brief description of fiber composite materials

A fiber composite material is a symbiosis between two or several materials to improve certain qualities of the material performance, usually the tensile strength by adding fibers into the material. By choosing the right combination of materials the properties can be improved in several ways.

Fiber composites is not a new invention as one can see simply by looking at a piece of wood. Wood is a natural fiber composite used by mankind through thousands of years. The new fiber composites cannot show such a long period of documented performance which affects the practical use of fiber composites. This is changing rapidly because a number of structures employing FRP have already been built and others are about to come.

Within the field of building construction materials many materials requires improvements to respond to an extended use in different aggressive environments. One of the weak points of reinforced concrete is the steel reinforcement and its high potential to corrode. Therefore the research has focused on the possible use of other kinds of high-strength material also including non-corrosive and alkali-resistant properties.

Fiber composite materials have been considered interesting with respect to lower energy consumption costs and reduced health hazards during manufacturing, low weight providing reduced costs of transportation to site and easier installation, lower depletion of resources and reduced maintenance costs of buildings and bridges./4/

4 Material properties

4.1 Fiber

The possibility to produce fiber materials with good properties has accelerated rapidly through the last decades. The progress has been directed towards new and better fibers with high strength to minimize the use of material, especially for use in the aircraft industry. The price of fibers has decreased the last years mainly depending on the reduced demand of fibers for the defence industry. As a consequence there is an urgent need for the manufacturers of fibers to find new markets. In the building industry there is a demand for material in large scale that could lead to lower prices on fibers in a close future. The market price on steel has kept a stable level through this last decade due to governmental subsidues. Therefore it can be expected that the price on FRP decreases and the steel price increases. This will make the use of FRP in the building industry even more interesting as the price reaches the level of steel.

At the moment there are only some fibers that are of interest to the building industry. The main reason is the high price but, material properties as Young's modulus and durability are of importance. The fibers should also be continuos. The fibers of interest at the moment are aramid, carbon and glass fiber and a new material named vinylon.

Table 4.1 General properties of fiber materials

Material	Specific gravity [g/cm^3]	Tensile strength [MPa]	Elastic elongation [%]	Young's modulus [GPa]
E-glass	2.75	2 500	2.5	70
Aramid	1.43	3 200	2.5	130
Carbon HT	1.94	3 400	1.5	230
Carbon HM	1.83	2 300	0.6	360
High per-formance steel	7.95	1 750	0.2*	200

* Plastic elongation >3.5 %

Table 4.1 shows the material properties of the most suitable fiber materials material properties and as comparisons also high-strength steel. The data in table 4.1 shows the elastic material properties derived from short time testing. To find a relevant description of the material properties it is also important, especially for high strength fiber materials, to consider the size and time dependence.

The fiber material considered in this paper is aramid which is an organic fiber material based on aromatic polyamide. Aramid fibers were originally invented by DuPont under the trade name of Kevlar. Today there are three manufacturers of aramid fibers in the world: DuPont of U.S.A. producing Kevlar, Akzo of the Netherlands producing Twaron and Tejin of Japan producing Technora. Another manufacturer is about to start a production in Germany (Hoechst).

Table 4.2 Material properties of aramid

Fiber	Young's modulus [GPa]	Tensile strength [MPa]	Elongation [%]
Kevlar 49	131	2 800	2.8
Twaron HM	125	3 000	2.4
Technora	73	3 400	4.6

During the manufacturing process a suitable thermoplastic is warmed up or dissolved in a solvent. Then it is pressed through a nozzle to an appropriate diameter. Finally the material is heated and stretched 5-10 times. This results in a strong orientation of molecules and crystals providing good strength properties. By aromatic rings attached with nitrogen bonds the molecule chain connects and becomes rigid. It is possible to produce aramid fibers with varying stiffness depending on different levels of orientation of the molecule chains as shown in figure 4.1.

The structural pattern of aramid fiber provides it with high resistance to different corrosive environments except for very acid or basic surroundings. Aramid fibers are possible to use in temperatures up to 200°C without any larger deterioration of the strength properties. The most negative properties are a certain sensitivity to humid air and ultra violet radiation that reduces the tensile strength.

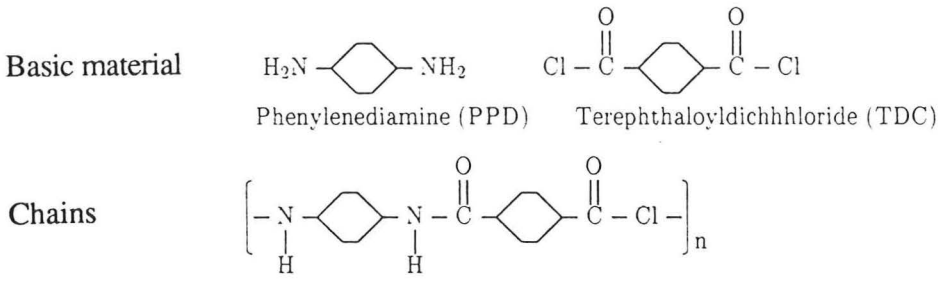

Figure 4.1 Stuctural configuration of aramid fibers

4.2 Matrix

The main purpose of the matrix is to redistribute forces between the fibers and to protect the fiber against aggressive environments. The most common materials available at the moment are the thermo settings polyester, epoxy and vinylester and the thermo plastic modified acrylic. The general properties of these materials are described below (see table 4.3).

Table 4.3 Material properties of matrix materials

Matrix	Young's modulus [GPa]	Tensile strength [MPa]	Elongation [%]
Isopolyester	3.3	62	2.1
Epoxy	3.3	60	—
Epoxy vinylester	3.3	81	5.0
Modified acrylic	3.2	62	2.6

Early information on this matter provided by the manufacturers has been proven wrong. The Young's modulus for polyester and epoxy was at first 6.9 GPa, but is now changed to 3.3 GPa, which makes a considerable difference in calculations. The material properties of the matrixes offer a possibility to compare different matrixes, but the main interest is whether it offers high performance together with the fiber or not.

Epoxy plastics were originally developed in Europe and the United States during the second world war and the name concludes a large group of materials with similar material properties. The most commonly used epoxy resin derives from epichlorhydrin and bisphenol A. The possibilities of varying the manufacturing process and the composition of the contents are several. This offer epoxy resins with a wide spectrum of material properties. The general configuration of epoxy is shown in figure 4.2.

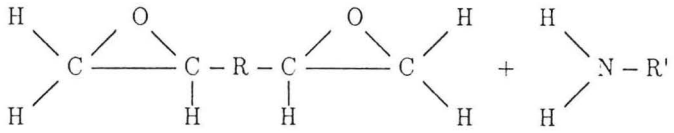

Figure 4.2 The general configuration of epoxy. R and R' are multi functional molecules based on styrene.

5 Aramid Fiber Reinforced Plastics (AFRP)

The different combinations of fibers and matrixes make a very strong, light and corrosion resistant material well suited for use in various concrete structures.

The maximum allowed initial prestresses in aramid fiber and prestressing steel are very close, even if the short-term strength of aramid fiber is about 50% larger compared to prestressing steel (see table 4.1). This phenomena derives from a larger strength reduction of an aramid composite under prolonged prestressing.

The prestress loss due to relaxation of tendon is larger in AFRP compared to steel but due to shrinkage of concrete (creep and dry shrinkage) the relaxation is smaller in AFRP compared to steel. This results that in prestressed concrete, even at high initial stress level, the fiber composite shows a total prestress loss that is almost the same as the prestress loss of prestressed steel.

6 Properties of the FiBRA-rod

6.1 The product

The FiBRA-rod is a braided aramid fiber rod made out of Kevlar 49 fibers using an epoxy resin as matrix material. There are two types of rods, flexible and non-flexible. The braided surface of the rod provides it with good bond properties. In addition to this sand could be adhered to further increase the bond characteristics between rod and concrete.

Table 6.1 FiBRA-rod product series

Type	Diameter [mm]	Sectional area [mm^2]	Weight [g/m]	Tensile strength [kN]
New trade name				
RA7	7.3	42	54	62.7
RA9	9.0	63	82	94.1
RA11	10.4	85	108	125.4
RA13	12.7	127	162	188.2
RA15	14.7	170	216	250.9
FA11	10.4	85	108	117.6
FA13	12.7	127	162	176.4
FA15	14.7	170	216	235.2
Old trade name *				
K8	3.0	6.5	7.5	7.8
K16	4.0	13	15	15.7
K32	6.0	25	30	31.4
K64	8.0	50	60	62.7
K96	10.0	75	90	94.1
K128	12.0	100	120	125.4
K192	14.0	150	180	188.2
K256	16.0	200	240	250.1

* The code could also be KS, where S inicates that silica sand is adhered to the surface

The cross section of a rod consists of about 60 % aramid fibers and 40 % epoxy resin (by volume). Young's modulus is 68.6 GPa, the elongation 2.0 % and Poisson's ratio 0.6. The maximum tensile strength is about 1.48 GPa for the non-flexible type (RA) and 1.38 GPa for the flexible type (FA).

According to the results of the following tension tests and heat and alkali resistance tests FiBRA possesses the properties required for long-term use as a concrete reinforcing material. The relaxation loss and tensile fatigue properties are acceptable for use as prestressing tendons.

The types and dimensions shown in table 6.1 are available on the open market. In addition to these common types other dimensions are manufactured on request, from diameter 3 mm up to 20 mm. Carbon, glass, nylon and vinylon fibers could also be used to produce FiBRA. The table below introduces the new names of the rods and as comparison the old names and their properties are shown as well. Most of the available data on the rods is based on tests with these older names and dimensions, why those are published.

6.2 Manufacturing process

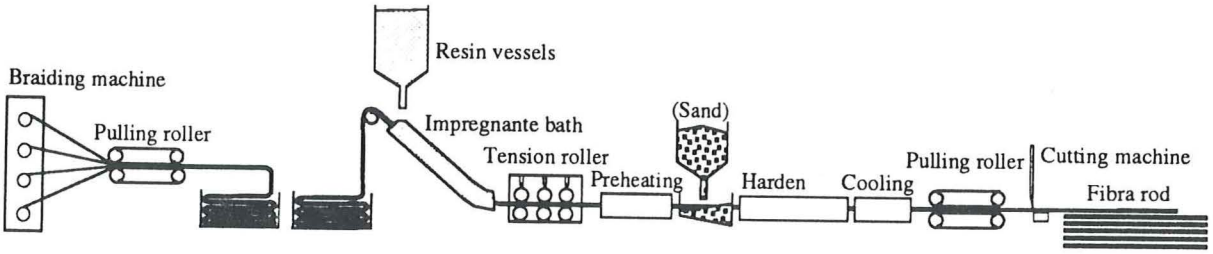

Figure 6.1 The manufacturing process of the FiBRA-rod

The manufacturing process in figure 6.1 only deals with the rod type. The FiBRA rod is made out of continuous aramid fibers woven in braided form and impregnated with epoxy resin and finally hardened. A rod is made out of eight strands and each strand is composed of 1 to 32 yarns. The number of yarns decides the diameter of the rod and each yarn consists of 4 000 Kevlar 49 filaments (6 000 denier* industrial grade). Due to the braided form of the rod there are certain advantages to gain:

— The tensile force applied to the rod is more uniformly distributed to the entire cross section. This makes it possible to manufacture large diameter rods for practical use. If large diameter rods were made by the pultrusion method irregularities among the paralell fibers and stress concentrations at the surface during load would limit the strength characteristics significantly.

— A regular pattern of protrusions and depressions on the braided surface increases the bond force to the concrete. If a pultrusion method is used improvements of the low bond would be required by adding a silica sand finishing to the surface. The treatment of the surface would have to be made in two steps.

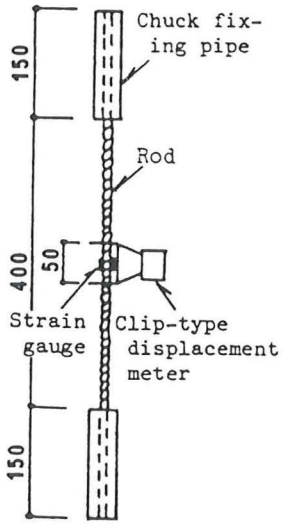

Figure 6.2 Tension test method

* 6 000-denier means that a fiber has a weight of 6 000 gram per 9 000 meter (10 000 yards)

6.3 Tensile characteristics

6.3.1 Tensile strength

The tensile strength properties in the tables above were determined using the tension test method shown in figure 6.2. The Young's modulus of FiBRA is given by the manufacturer as 68.6 GPa (7 000 kgf/cm^2) and the stress-strain behavior of FiBRA is practically linear-elastic up to failure, as could be seen in figure 6.3.

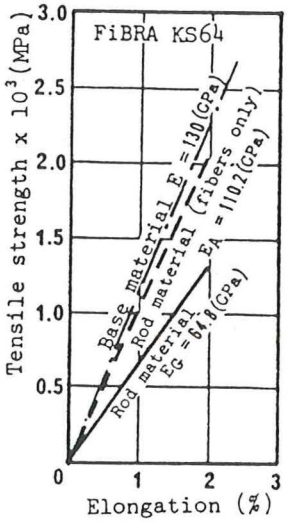

Figure 6.3 Tensile strength and elongation

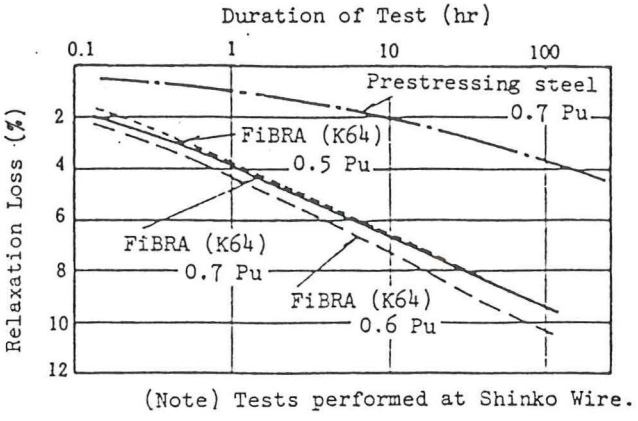

Figure 6.4 Relaxation curve

6.3.2 Tensile fatigue

Partial pulsating tensile fatigue tests were performed on KS64 FiBRA (ø8 mm).The tests were carried out at room temperature varying the stress range with the lower limit load constant at 50 % of actual rupture and the fatigue limit where rupture would not occur even at 2 million cycles was determined. With stress ranges under 374.6 MPa, rupture did not occur even at 2 million cycles, but in case of 443.3 MPa, rupture occurred at approximately 305 000 cycles.

6.3.3 Relaxation

Relaxation tests were performed on KS64 FiBRA under room temperature conditions. The initial loads were 0.5, 0.6 and 0.7 times the tensile strength P_u of KS64. The results of the tests are shown in figure 6.4. The relaxation values of the specimens were 3 to 4 times that of the prestressing steel at 10 hours and 2 to 2.5 at 100 hours. With prestressing steel the relaxation value becomes higher using increasing initial load, but in case of FiBRA, although there was some amount of scatter, there were no differences observed depending on initial load.

6.4 Durability

6.4.1 Heat resistance

Two different tests were performed, dry heat and moist heat, using small-diameter KS16 FiBRA. The purpose was to evaluate the heat resistance in terms of ratio of strength obtained during treatment with strength obtained without treatment (100 %). The results of the test are shown in figure 6.5. Both tests resulted in high resistance to heat up to 220°C. The ratio of strength was at this point about 95 %, which is very high for an organic fiber.

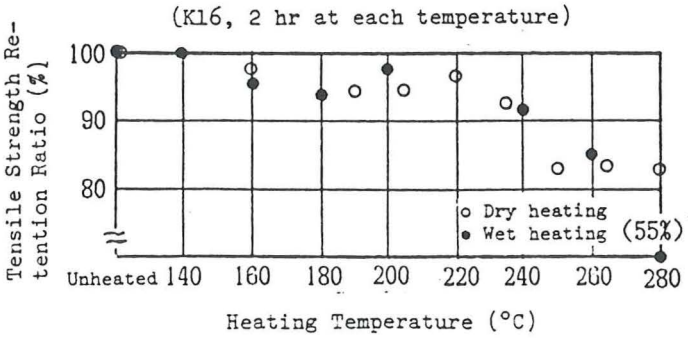

Figure 6.5 Heat resistance test results

6.4.2 Chemical resistance

The test consisted of immersing KS16 FiBRA in a solution of pH=13. The immersion of the bars occurred at four different temperature levels that were room temperature, 40°C, 60°C and 80°C. The alkali resistance was evaluated and expressed by ratio of tensile strength maintained with the strength for no treatment (100 %). Up to 2 000 hours of treatment there was no significant difference between no treatment and treatment up to 40°C. For immersion in 60°C and 80°C the strengths tended to decline slightly when more than 1400 hours had elapsed, but the ratios of strengths maintained were still exceeding 95 %.

7 Properties of the Arapree strip

7.1 The product

Arapree (ARAmid PREstressing Element) is a reinforcement which has been developed jointly by Akzo and HBG (Hollandsche Beton Groep). The tendon is based on the aramid fiber Twaron. An epoxy resin was selected as bonding matrix to recieve good adherence, stability and resistance to chemicals. The elongation of the rod is 2.4 % and Poisson's ratio is 0.38. The volumetric composition of the cross-section of a strip consists of 35-45% Twaron HM and 65-55% resin.

At the moment there are two types of Arapree elements, one with a rectangular cross-section and one with a circular cross-section (see table 7.1). The strip-like or rectangular tendon improves the transfer of forces through effective bond/direct contact with the cement matrix, avoiding the need to insert permanent ducts of metallic terminations in prestressed concrete. The available length of the prestressing elements is almost unlimited due to delivery on coils.

Table 7.1 Arapree product series

Type*	Shape of the cross-section	Size [mm]	Fiber cross-sectional area [mm^2]	Tensile strength [kN]
f 20 000	rectangular	20 x 0.3	2.2	6.6
f 100 000		20 x 1.5	11.1	33.3
f 200 000		20 x 3.0	22.2	66.6
f 400 000		20 x 6.0	44.4	133.2
f 20 000	circular	Ø 2.5	2.2	6.6
f 100 000		Ø 5.0	11.1	33.3
f 200 000		Ø 7.5	22.2	66.6

* equal to number of filaments

7.2 Manufacturing

Non twisted Twaron yarn bundels are formed into a strip by passing eyelets and combs and finally the bundles are impregnated by a resin. The surface is treated before curing to achieve the desired bond properties between prestressing element and concrete which are very effective. This is due to the pattern on the surface of the rectangular strips and the possibility to adhere sand to the surface of the circular shaped rods.

7.3 Tensile characteristics

7.3.1 Stress rupture

An important matter for polymer based high tensile strength fibers is the susceptibility to sustained loading. Mean stress rupture level in tension after 100 years is approximately 65% of short-term strength. A sustained stress in air at a level below 65% of the short-term strength does not lead to stress rupture.

7.3.2 Creep

The creep coefficient can be assumed to be 0.2 after 10^6 h. Due to relaxation, the stress at constant strain will drop to about 85% of the initial value after 10^6 h in air and to about 80% in alkaline solution. In a polymeric material, as this, there is an approximate linear relation between the applied stress and the creep strain.

7.3.3 Relaxation

Relaxation of polymeric materials appears to be nearly the same at different applied stress levels. After 100 years in air there is an estimated relaxation of about 15% and in an alkaline solution this value would be about 20%.

7.3.4 Fatigue

Fatigue tests on bare strands and strands embedded in concrete show that embedded strands perform in the same way as bare strands, which is opposite to steel. Steel usually shows a pronounced decrease of fatigue strength due to embedment. The Arapreee strips with a static fracture load of 35 kN showed a fatigue strength at 3 million cycles of 17.5 to 20 kN at a lower load of 5 kN. Comparison between required fatigue strength for prestressing steel and Arapree showed that the behavior of Arapree was satisfactory.

7.4 Durability

7.4.1 Heat resistance

Since Arapree is an organic material, service temperatures higher than 100°C should be avoided. The strength decrease at 150°C is about10% after 10^3 h. Heat treatment of concrete during hydration has no detrimental effect on the properties of Arapree.

7.4.2 Chemical resistance

In some accelerated tests the influence from the environment on mechanical properties is given. The chemical resistance is outstanding in respect of practically all hazards that could be assumed to exist in or around concrete structures which indicates how useful this material is for exposed structures. The bare fibers must though be prevented from exposure to ultra violet radiation.

8 Properties of the Technora rod

8.1 The product

Technora AFRP consists of Technora fibers strengthened with a resin and formed into rods. The Technora fiber is made out of PPODTA (co-poly-paraphenylen/3,4-oxydiphenylen terephtalamide) and the matrix material is vinylester. The volumetric composition of the cross-section is 65 % fiber and 35% resin. Young's modulus of the rod is 54 GPa, the elongation 3.7 % and Poisson's ratio 0.35. The maximum tensile strength with a bond anchorage is about 1.9 GPa. The types and sizes of Technora rods are presented in table 8.1.

Table 8.1 Technora product series

Type	Diameter [mm]	Sectional area [mm²]	Weight [g/m]	Tensile strength [kN]
Round rod				
ARPR1	3.0	7.07	9	13.0
	4.0	12.56	16	22.7
	6.0	28.26	37	49.9
	8.0	50.24	66	86.1
Spiral wound rod				
ARPD1	3.0	7.07	10	13.0
	4.0	12.56	18	22.7
	6.0	28.26	41	49.9
	8.0	50.24	73	86.1

8.2 Manufacturing process

The Technora rods are manufactured by a pultrusion process as shown in figure 8.1. The straight bundle of Technora fibers is impregnated with a vinylester resin and passed through a die to squeeze the resin. Another fiber is wounded spirally around the bundle and then the resin is cured in an oven. The volume ratio of the fiber and the resin is 2:1. The rods are possible to be wound on a 1.5 m diameter drum. The most practical rod diameters for construction have been found to be 6 and 8 mm.

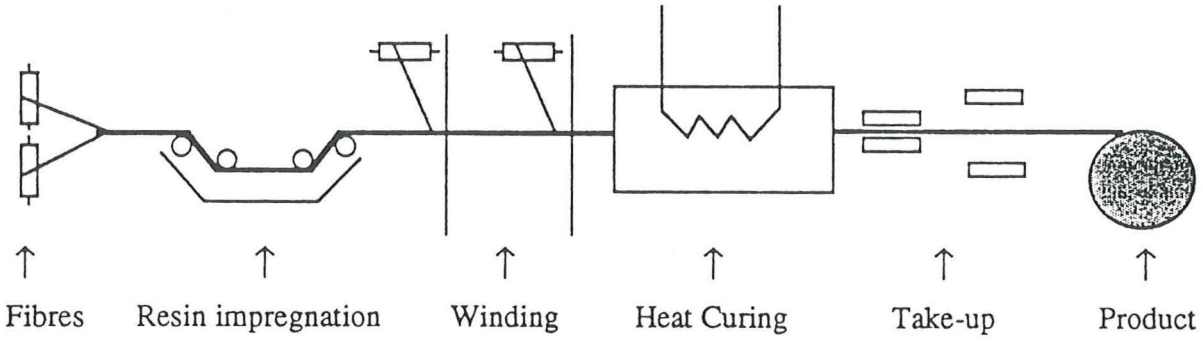

Figure 8.1 Manufacturing process of the Technora rod

8.3 Tensile characteristics

8.3.1 Tensile strength

The tensile strength was tested using a test sample with a length of 600 mm and a tensioning speed of 20 mm/min. The testing showed that the average tensile strength of the rods was 2.14 GPa , or 96 % of the tensile strength of the Technora fiber. Tests were also made to investigate how the tensile strength depends on the tensioning speed.

A slight tendency was observed for the tensile strength to increase as the tensioning increased. Another test was made to investigate how the sample length affected the tensile strength. The test showed that the length of the sample had no effect on the tensile strength.

8.3.2 Fatigue

Fatigue testing was performed varying the lower limit of the stress intensity (σ_L) and the amplitude. The tensile strength after 100 years was estimated through logaritmic scale to be 1.23 GPa, that is about 57 % of the average tensile strength of the rods.

8.3.3 Relaxation

The results presented in figure 8.2 show that the 30 years relaxation rate with a load range of 0.5-0.6 P_u was found to be about 14 %.

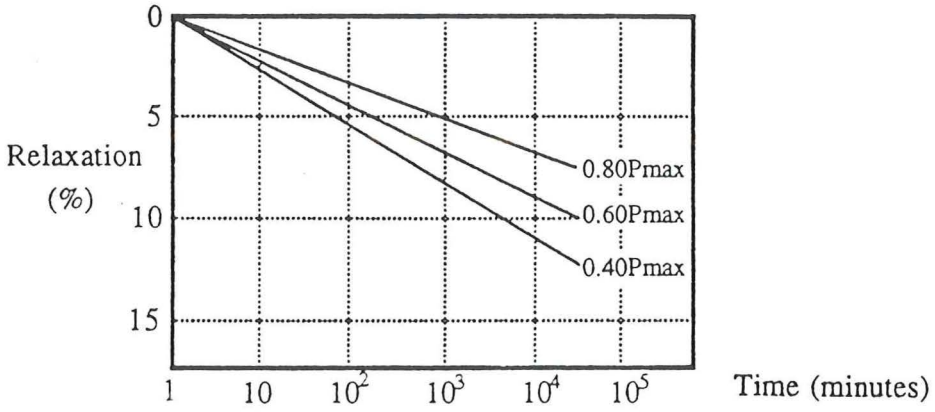

Figure 8.2 Relaxation

8.4 Durability

8.4.1 Chemical resistance

Rods immersed untensioned in water at 60°C, sea water and a pH 13 alkaline solution for 400 days and tensioned rods immersed in an alkaline solution for 200 days were tested for changes in the tensile strength. None of the conditions described caused a decrease in the tensile strength of the rods. These results show that Technora rods are resistant to alkaline hydrolysis.

8.4.2 Weathering properties

The weathering properties were investigated by exposing rods in a well-lit, south-facing position at an angle of 45° for 360 days. The tensile strength, surface hardness and flexural strength were measured. The tensile strength tends to level out at about 90 % of the average strength at a value of 1.93 GPa.

Aramid fibers have a tendency to deteriorate in ultra violet light, but since the effects of this deterioration are limited to the surface of the rods, no further decrease of the tensile strength would be expected as a result of longer exposure. There was no deterioration in the surface hardness and the triaxial bending strength as a result of exposure.

9 Anchorage

The transfer of forces between the prestressing tendon and the anchor is very important. Metallic wedge-type anchors have been developed by FiBRA, Arapree and Technora mainly for short-term pre-, and post-tensioning. For long-term testing mortar grout or resin injection anchors have been developed.

9.1 FiBRA

A steel wedge-type anchor with 1, 3 or 6 tendons applicable in one anchor has been developed. A cone made out of either steel or FRP (aramid or carbon) is used together with a resin as a resin injection anchor for material testing. See figure 9.1 to 9.3.

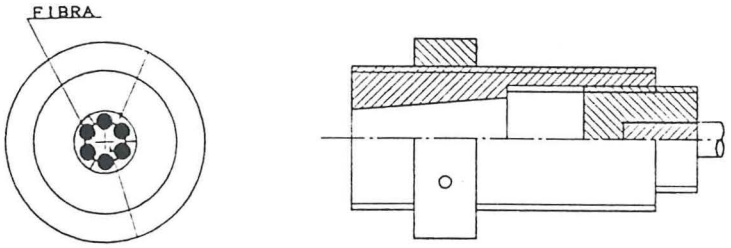

Figure 9.1 FiBRA wedge type anchor (six tendons)

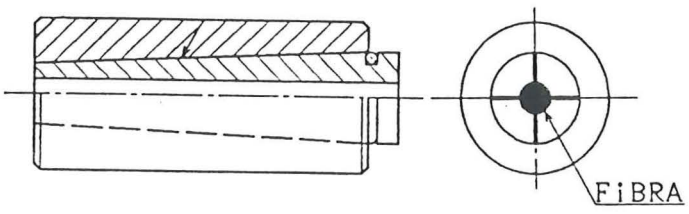

Figure 9.2 FiBRA wedge type anchor (one rod)

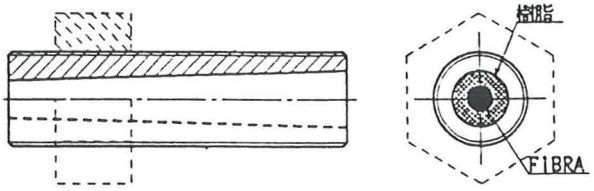

Figure 9.3 FiBRA resin type anchor

9.2 Arapree

The strip-like shape enabled simple anchor devices to be developed. The short-term anchorage has a terminal body of steel and wedges made of polyamid. For long-term testing an anchor consisting of a steel tube which is filled with a cement mortar bond material has been developed. See figure 9.4.

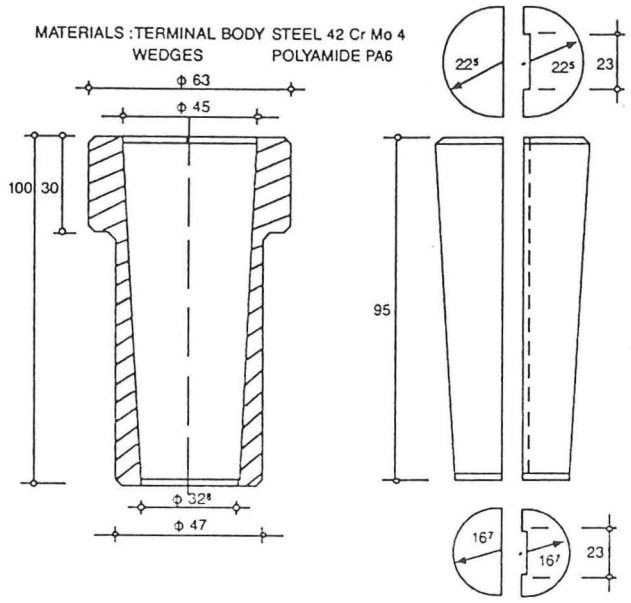

Figure 9.4 Arapree short-term anchor

9.3 Technora

For prestressing applications metallic wedge-type and mortar grout-type anchors have been developed. Anchors for single rods and multiple bundles of rods (3, 4, 7, 12 or 19 rods) are available. A special 7 strand FRP grouted anchorage has been developed for use with external tendons. See figure 9.5 to 9.6.

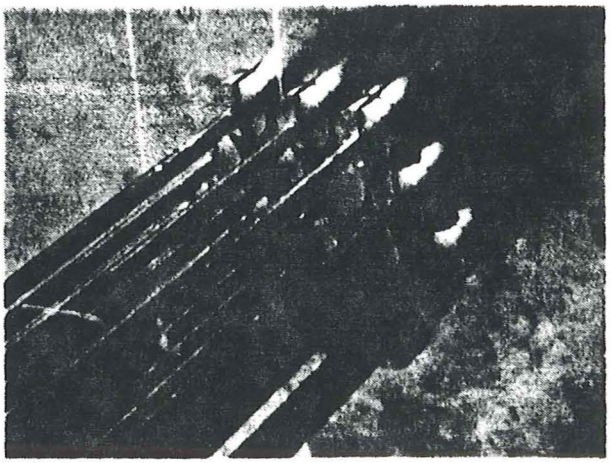

Figure 9.5 Technora multi-wedge type anchor

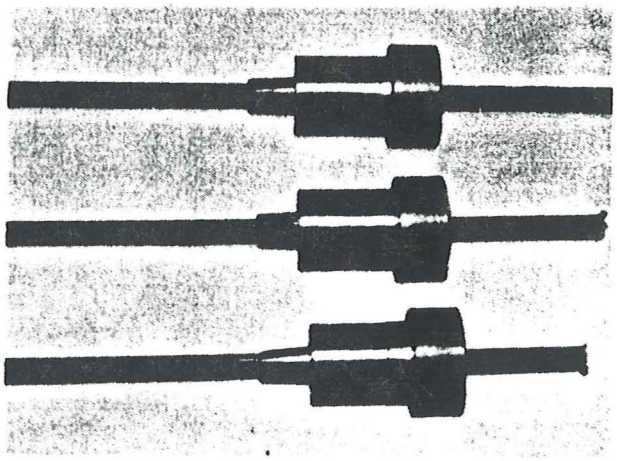

Figure 9.6 Technora single wedge type anchor

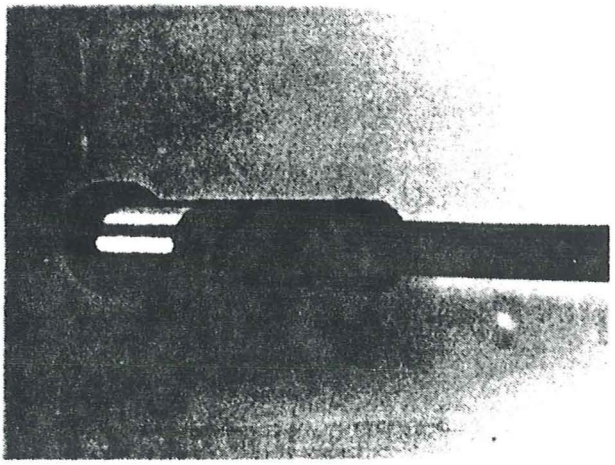

Figure 9.7 Technora 19ϕ6 mm Bonding anchor

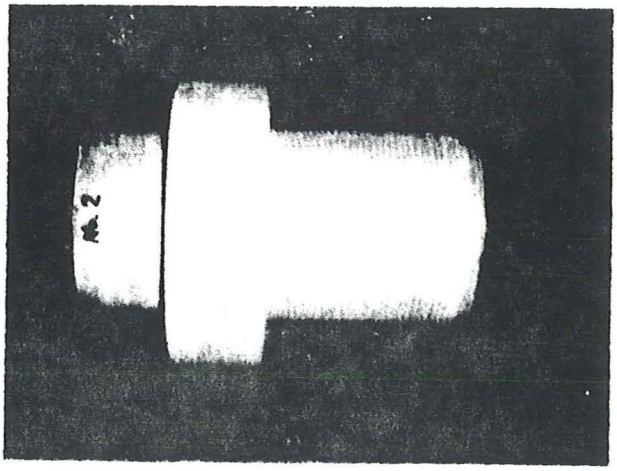

Figure 9.8 Technora 7ϕ6 mm Bonding anchor

10 Applications of fiber reinforced plastics

There is a large number of applications were FRP (fiber reinforced plastics) have been used. This is a brief description of some applications where AFRP have been used and some ideas for the future.

10.1 Bridges reinforced with fiber reinforced plastics

One German construction company together with Bauer have been researching mainly about glass fiber reinforced plastics (GFRP) and they were first used in a prestressed concrete bridge called the Lünen'sche Gasse Bridge (Düsseldorf, 1980). There are some more bridges built using this material, for instance the Ulenberg-Strasse Bridge (Düsseldorf, 1986), the Marienfelde Bridge (Berlin, 1986), the Schiessberg-Strasse Bridge (Leverkusen, June 1990) and the Bridge Nötsch (Kärnten, Austria, October 1990) /7/.

In Japan GFRP have been used in large quantities as a reinforcing material together with shot-crete in tunnels. The Japanese were first to use CFRP strands in a prestressed bridge. Japanese construction companies have built eleven bridges (Summer 1992) using different sorts of FRP as advanced composite materials. These are the Shinmiya Bridge (Ishikawa, Japan, October 1988), the Nakatsugawa Personnel Bridge (Chiba, Japan, March 1989), the Hukui Bicycle Bridge 15th (Ishikawa, Japan, March 1989), the Birdie Bridge (Ibaragi Prefecture, Japan, September 1990), the Nasu Country Pretensioned PC-bridge (Tochigi Prefecture, Japan, 1990), two Sumitomo Demonstration Bridges (Oyama, Japan, 1990), the BASF Railroad Overbridge (Ludwigshafen, Germany, June 1991), the NEFCOM Pedestrian Bridge (Sagamihara, Japan, 1991), the Hakui Bicycle Bridge 16th (Ishikawa, Japan, February 1992) and the Hakui Bicycle Bridge 17th (Ishikawa, Japan, April 1992). These bridges were constructed using either CFRP or AFRP for the prestressing tendons, rods or grids /4/.

In Scotland a pedestrian suspension bridge with a span of 62 meters and a width of two meters was recently build. The weight of this bridge is only 15 ton and the only material used is prefabricated FRP. The pylons were made of GFRP, bridge deck was made of GFRP and polyester and the suspension cable was made of Parafil /16/.

10.2 Documented utilizations of FiBRA applications

10.2.1 Nasu Country Pretensioned PC bridge (Tochigi Prefecture, Japan, 1990)

The bridge is a three-span 36.02 m long, 2.4 m wide pretensioned girder slab bridge spanning a pond. For each span seven I-shaped girders were used. Of the total of 21 girders 3 were made with braided AFRP rods as tendons. The relaxation ratio of the braided AFRP rods is approximately twice that of the prestressing steel strands. The allowable cable tensile force was set to 50% of the manufacturer's guaranteed strength. The effects of concrete creep and drying shrinkage are small because the Young's modulus is one third of steel. This results in an almost equivalent effective coefficient for AFRP and steel.

The three AFRP girders were fabricated simultaneously using the same production line and fabrication procedure as the ordinary girders. In contrast to the curing methods for ordinary girders no accelerated curing was used. The reason for this was that the effects of the braided AFRP rod's coefficient of linear expansion not yet had been clarified. By fabricating a girder equivalent to the actual girder it was possible to verify the bending characteristics and safety of the finished bridge, see table 10.1. Close agreement between the measured and calculated values of fracture load were obtained for every test girder, as shown in table 10.2. The stress-strain curve of the braided AFRP rods was assumed to be linear up to failure. The difference in stirrups results in a slightly lower failure point for TF2 than for TF1 /8/.

Table 10.1 Types of flexural specimens

Denomination	PC-tendon	Stirrup
TF 1	Braided AFRP Rod 8-Ø14 mm	Deformed steel bar D6, c. 200 mm
TF 2	Braided AFRP Rod 8-Ø14 mm	Braided AFRP Rod Ø6 mm, c. 200 mm
TP 1	PC-strand 8-T10.8 mm	Deformed steel bar D6, c. 200 mm

Table 10.2 Testing results

Denomination	Compressive strength of concrete [MPa]	Calculation [kN]			Experiment [kN]	
		Design load	Cracking load	Ultimate load	Cracking load	Ultimate load*
TF 1	57.7	27.4	41.2	122.5	57.8	131.3
TF 2	58.1		41.2	122.5	57.8	123.5
TP 1	54.6		37.2	89.2	57.8	102.9

* Flexural failure (Compression)

10.2.2 Floating bridge Takahiko Three Country Golf Course (Ibaraki Prefecture, Japan)

A precast prestressed concrete floating bridge fulfilling the request for a design which would allow people to cross as close to the water's surface as possible. The construction schedule at the site was tight and therefore it was decided to prefabricate the PC pontoons to the floating bridge. The 56.37 m long and 4 m wide bridge crosses a pond and consists of six PC pontoons. Each pontoon is about 7.6 m long, 3m wide, 1 m high and weighs 14 tons. In figure 10.1 the construction of the bridge is shown. The bridge is reinforced in each side wall with four braided AFRP tendons and continuously spiral formed braided vinylon fibers as stirrups. To connect the six pontoons four AFRP tendons are passed through ducts and tensioned at the outer ends of the pontoon structure.

The prestressing force applied was chosen to not cause tension in the concrete element during lifting, transportation and connecting with the bearers. The use of AFRP as reinforcing materials made it possible to minimize the concrete cover which reduces the overall weight of the structure. A structure as this has an increasing utilization in various marine facilities as offshore artificial islands and offshore airports /9/.

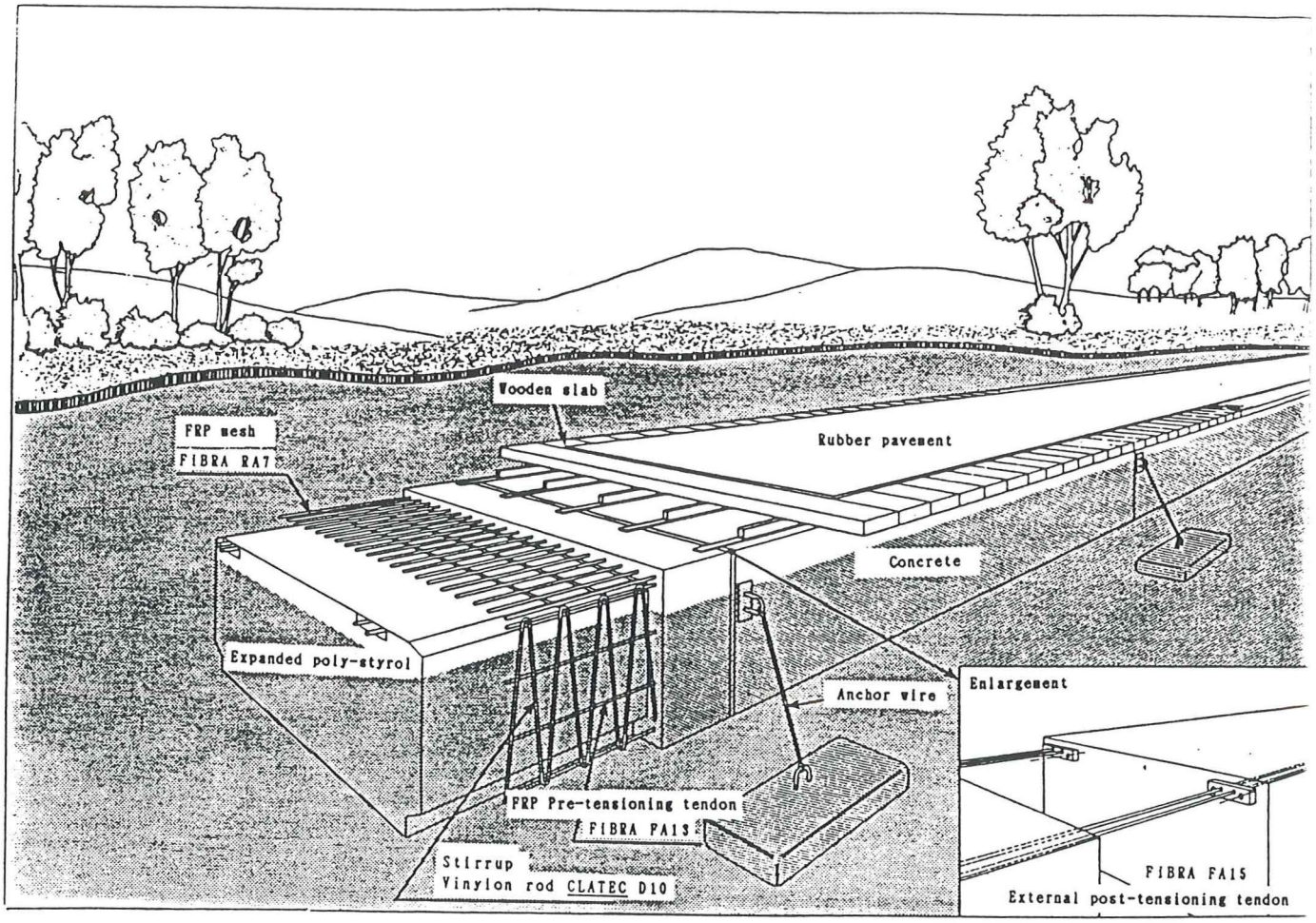

Figure 10.1 View of floating bridge

10.2.3 Miscellaneous applications of FiBRA

Other applications where Fibra has been used are a post-tensioned building floor, a 60x60 mm floor panel for free access floor, a post-tensioned slab for a chemical factory and as permanent and temporary rock bolts which are easy to cut.

10.3 Documented utilizations of Arapree applications

10.3.1 Birdie Bridge (Ibaragi Prefecture, Japan, September 1990)

This unique pedestrian bridge where a combination of several different FRP-materials have been used has an overall bridge length of 54.5 m, with a clear span of 46.5 m. The cross section of the bridge is shown in figure 10.2.

The construction started by casting of the abutments and anchoring them into the sloping river bed faces with ground anchors made from CFRP, initially stressed to 0.5 F_u. A form work was built up from the river bed to support the installation of the precast concrete panels.

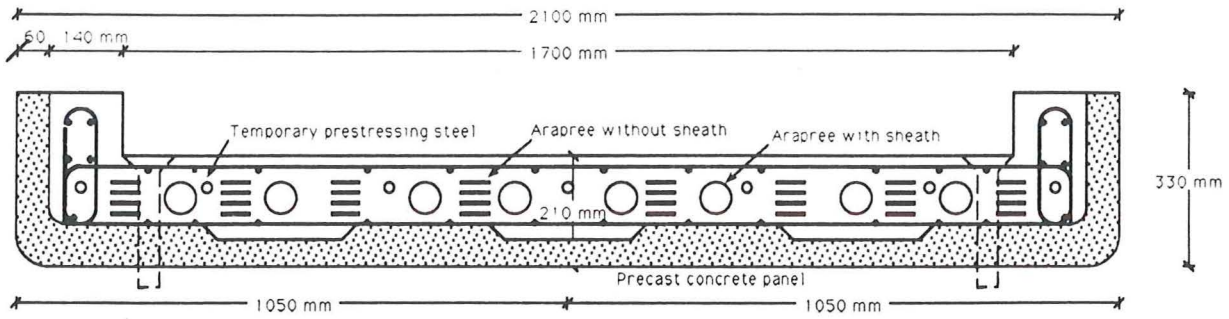

Figure 10.2 Cross section of Birdie bridge

These concrete panels served as permanent outer form work for the bridge. The use of these panels simplified the work at site and gave the bridge an aesthetic surface. The panels were constructed using vinylon short-fiber reinforced concrete, further reinforced with a mechanically connected grid of carbon fiber composite cables. The vinylon fibers were preferred to carbon fibers, because they are less expensive and may easily be mixed in a conventional concrete mixer.

Photo 10.1 Birdie bridge

The prestressing of the bridge consists of AFRP (Arapree) flat bars. During the hoisting there were temporarily prestressed with steel to protect the AFRP-rods from the high shear loads. A total number of sixteen bundles with eight AFRP flat bars in each were used. Half of the bundles were used as pretensioning tendons and the other half as post-tensioning tendons. The prestress level of the tendons was 33% of their tensile strength, but the level is planned to be further increased to 50% or 60% of ultimate tendon strength in future beams. The anchorage was secured by bond with an inorganic mortar in cylinders of metal or FRP /10,11/.

10.3.2 Structural elements reinforced with Arapree

The first practical application of Arapree was in a noise barrier post along a motor way near Rotterdam, Holland. Each post, with an effective cantilever of 3.5 meter, is centrically prestressed with 8 AFRP tendons. A concrete cover of 30 mm was sufficient. Under maximum wind load the concrete of the tensile zone was supposed to crack. The cracks are not any problems as Arapree is resistant to chloride corrosion.

Another use for Arapree was in a hollow core floor slab with a span of 6 m, a width of 1.2 m and depth of 0.26 m.

In a 40 m long and 5 m high prestressed cavity masonry wall Arapree was used to increase the bending stiffness. Due to the effective bond properties of the strip the anchor length was only 75 mm.

Arapree has also been used in fish ladders. These fish ladders are usually made from tropical hardwood. To avoid the use of this wood thin pretensioned concrete planks (35 mm) were used.

Prestressed railway sleepers employing AFRP-tendons combines good durability with excellent fatigue behavior. The shape is optimized to make the sleepers cheap and easy to produce. The sleeper in figure 10.3 has been tested under cyclic loading. The static and fatigue behavior along with the durability, non-conductivity and non-magnetic properties of this sleeper are excellent compared to sleepers using steel as reinforcement /12/.

AFRP-tendons was used in a pedestrian bridge consisting of two prestressed parabolic shells placed closely to each other. No extra protection of the tendon was needed /13/.

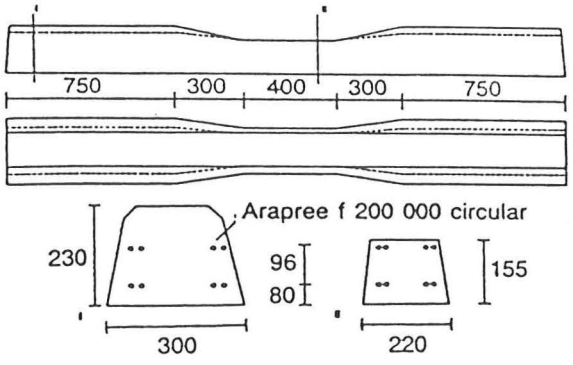

Figure 10.3 Prestressed railway sleeper

10.3.3 Cantilever roadway (Barcelona, Spain, 1990)

This construction is a part of the traffic communications involved in the Summer Olympic Games in 1992. Due to space problems the roadway had to be constructed in two levels where the upper level is a cantilever structure with a span length of 4 m. The length of the structure is 80 m. The 4 m cantilever structure is designed fully prestressed. Therefore no tensile stresses are expected in the structure. Figure 10.4 shows the vertical layout of a precast element. Five empty ducts of 10 cm diameter was placed to fill with steel tendons if the fiber prestressing does not work correctly. The effective prestressing after total losses is approximately 40% of the tensile failure strength of the composite material.

The fiber bar is anchored by bond in the concrete. The connection of the precast elements to the vertical walls is made by means of conventional prestressing bars to avoid tensile stresses in the joint /14/.

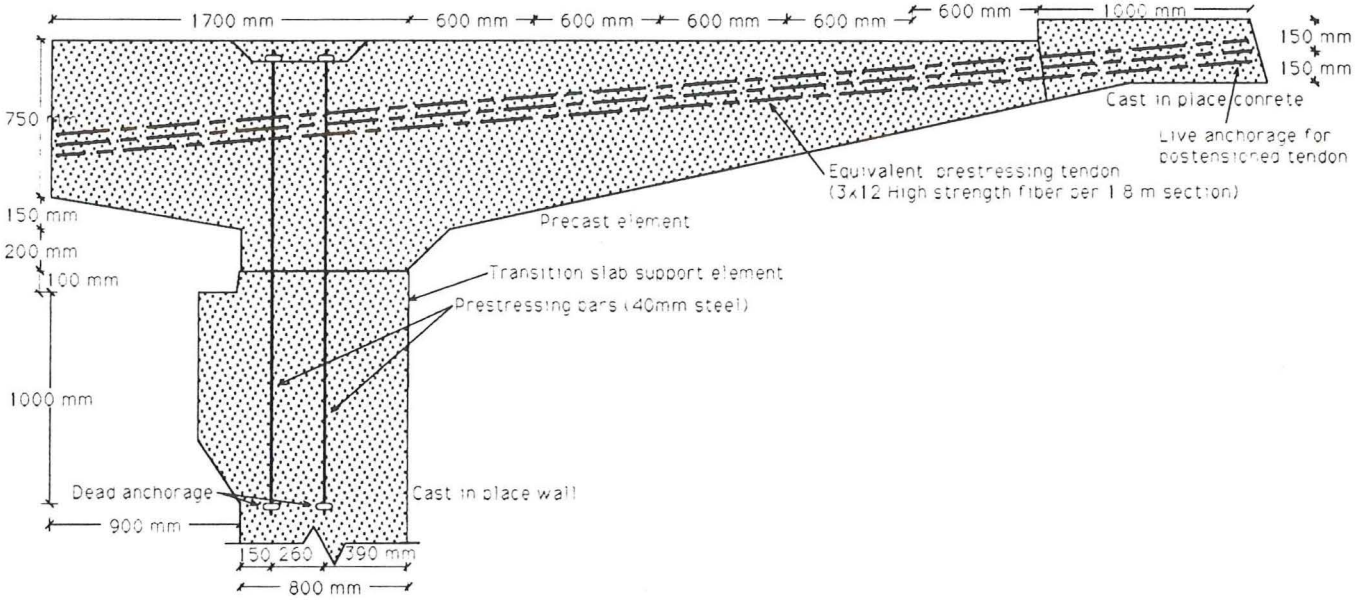

Figure 10.4 Cantilever definition and prestressing arrangement

10.4 Documented utilizations of Technora applications

10.4.1 Sumitomo Demonstration Bridges (Oyama, Japan, 1990)

The first use of Technora aramid fiber reinforced plastic rods were as prestressing tendons in two roadway bridges. In figure 10.5 a plan and a cross section of the two bridges are shown.

The pretensioned bridge has a length of 12.5 m and consists of a slab on top of three pretensioned concrete box girders. Sixteen straight tendon bundles, each bundle consisting of three 6 mm diameter AFRP rods, was used for each girder. In each girder four bundles were placed in the top flange and twelve in the bottom flange. Grouted end anchorages were manufactured for all tendons. Stirrups were constructed of 8 mm diameter AFRP rods and

attached to the prestressing tendons by plastic ties. Bending of the aramid fiber rods to form manufactured stirrups leads to about 60% losses in tensile strength. There was no steel used in any of the three girders. The prestressing tendons were first pretensioned to 0.75 F_u* and then subsequently dropped to 0.70 F_u. It is noted that both these stresses are in the same range as the level customarily used for high strength steel tendons. However the bridge is located in a research establishment where it can be continuously inspected. The deck was reinforced with epoxy coated steel reinforcement and transversely post-tensioned bundles using three 6 mm diameter AFRP rods, spaced at 300 mm centers. After tensioning grout was injected into the sheaths to secure the bond.

The post-tensioned bridge is 25 m long and consists of a single post-tensioned concrete box girder, using ten internal AFRP tendons, five in each web, and six external AFRP tendons, placed above the bottom flange of the box girder. The internal tendons consist of nineteen 6 mm diameter rods, and the straight external tendons consist of seven 6 mm diameter rods. The tensioning used was approximately 60% in the internal tendons and 68% in the external tendons of the specified tensile strength for the bundles. Grouted anchorages with steel casings were used for the internal tendons and special fiber reinforced plastic casings were used to the grouted anchorages for the external tendons. /4/.

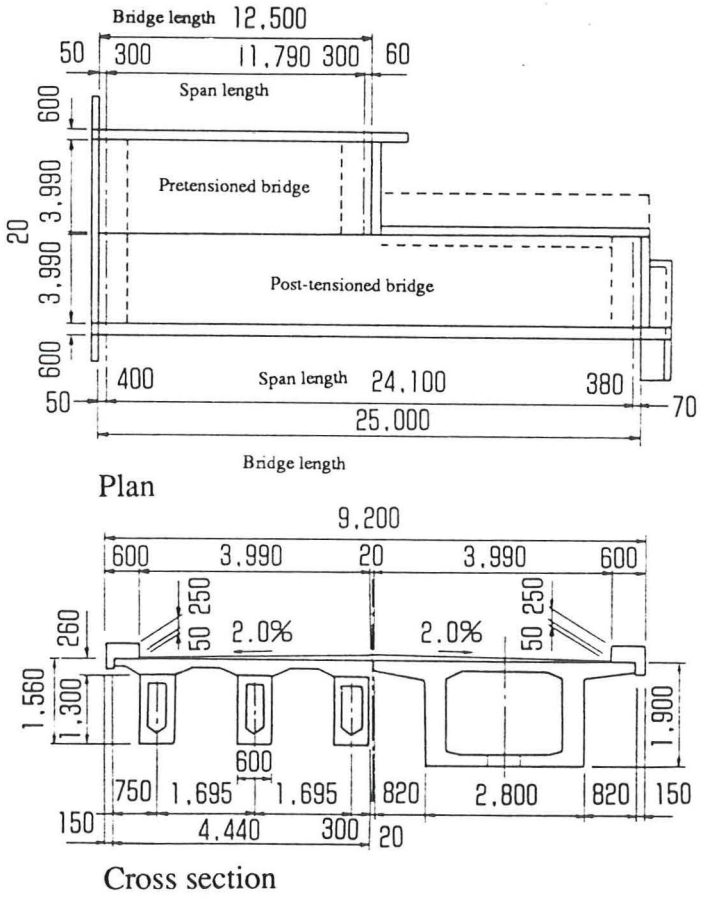

Figure 10.5 Plan and cross section

* Specified tensile strength for bundles with rods and grouted anchorages

10.4.2 Cargo handling prestressed concrete barge (Niihama City, Japan)

The barge was planned as a prestressed concrete slab-construction with simple hollow girders. The total length of the five span barges was 61 m in one of the span (9 m) there were used AFRP tendons as pretensioned reinforcement. The part of the barge using AFRP-tendons for reinforcement consisted of 17 pretensioned hollow girders. Each hollow girder has span length of 8.32 m and a cross-section as shown in figure 10.6 and 10.7 /15/.

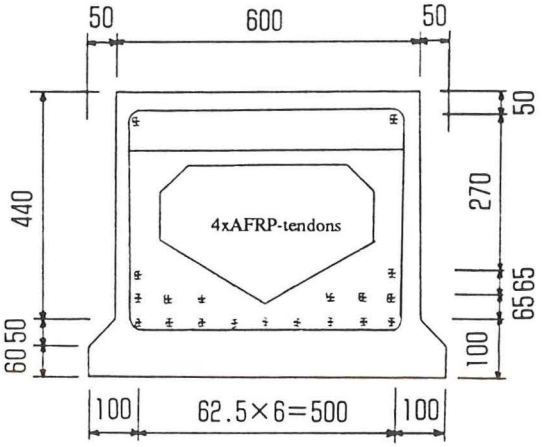

Figure 10.6 Cross section of girder

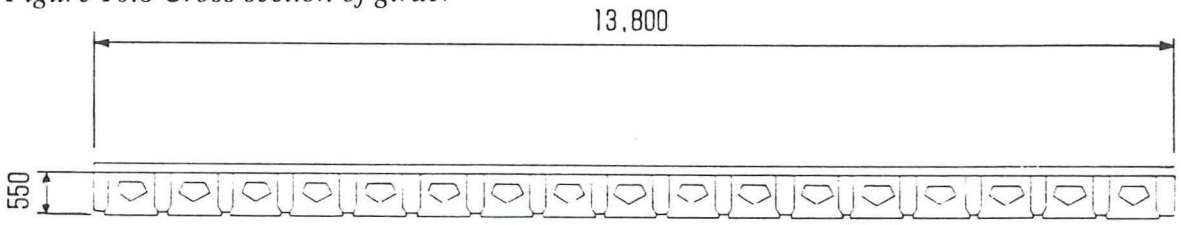

Figure 10.7 Cross section of barge

10.4.3 Ground anchorage for retaining wall

Technora rods have also been used as ground anchors. Since AFRP tendons have a smaller elastic modulus than steel the stress losses due to deformation and creep of the natural ground is also smaller. The low weight also makes it easier to work with on steep slopes. The AFRP ground anchor in this experimental construction was installed as an earth retaining anchor beneath a railway line in Kagawa Prefecture, Japan. The excavation during this work was 10 m deep and the length of the anchor was approximately 12 m. The experimental construction consisted of an AFRP ground anchor and a ground anchor using steel strands installed together so the two types could be compared /15/.

10.5 Miscellaneous and future applications

AFRP and GFRP materials are used as rock bolts in mountain tunneling projects. Rock bolts are driven into the ground before tunneling and used as a temporary support for rock boulders to prevent cave-ins. FRP is more expensive than conventional steel bolts but has lower weight and is easier to cut.

FRP is an outstanding alternative in special applications where non-magnetic and non-electrical conductivity is necessary. One application is the elevated guide way of reinforced concrete girders for the magnetic levitation light-rail system being proposed in Japan.

In reinforced concrete structures as atomic power plants where the reinforced concrete is exposed to radiation there are a strength reduction of the steel. The non-magnetic and non-electrical conductivity properties in FRP are important improvements of the vulnerability.

The present high price of FRP compared to steel must be seen in long term perspective. The price of the reinforcement product mainly depends on the cost of the fiber, which depends on the market volume. At the moment there is a change in the market sector where aramid is used. In sectors where the weight and strength relation are very important the selling today decrease with a lower price as result.

In the future energy and environmental questions will be more important then today. FRP products have a low weight which means cheaper transportation and handling. FRP does not need as much energy as steel to be produced and there is no need for mining to find the raw materials and large plants which is the case for steel production. The life expectancy is longer for FRP than for steel so recycling will not be so often and easier to do.

11 Conclusions

There has been commercial reinforcing products made out of Aramid fiber reinforced plastics (AFRP) for several years on the market

AFRP has already been used as reinforcement for concrete in several applications. In most of these applications the experiences are good and no unexpected behavior has been noticed. AFRP will never replace steel totally, only bee a better alternative in some situations where steel nowadays meets up the requirements.

There still have to be more joint efforts between manufacture and construction industry to develop FRP reinforcing systems that could be a skillful and economically alternative to conventional reinforcement. Design and performance guidelines are needed to ensure safety and simplify the practical utilizations.

There are some examples in which the reliability to FRP was very high with following problems. It is therefore important to act in an inpatient and professional way so the trustworthiness of FRP not will be wasted on default projects.

References

/1/ Mitsui Construction Co.,Ltd.: Technical reports on FiBRA

/2/ Sumitomo Construction Co.,Ltd.: Technical reports on Technora

/3/ Akzo and HBG: Technical reports on Arapree

/4/ Mufti, A.A.; Erki, M-A; Jaeger, L.G.:"Advanced composite materials in bridges and structures in Japan", Canadian Society for Civil engineering, 1992

/5/ Den Uijl, J.A.:"Vorspannen met aramidvezels"; Materialen No. 9, 1988, pp 2-5

/6/ Sentler, Lars:"Fiberkompositer som armering", The Swedish Council for Building Research, Report R10:1992

/7/ "Applications of Heavy Duty Composite Prestressing Tendons"

/8/ Yonekura and Tamura.:"Application of braided AFRP rods to bridges"

/9/ Oriental Construction Co.,Ltd:"Precast prestressed concrete floating bridge using FRP tendons"

/10/ Kubota et al (1990)

/11/ Nojiri (1992)

/12/ Reinhardt et al:"Arapree: a new prestressing material going into practice"

/13/ Gerritse et al:First application of Arapree. In " Fiber reinforced cements and concretes.: Recent developments."

/14/ Casas and Aparicio: "A full scale experiment on a prestressed concrete structure with high strength fibers"

/15/ Noritake et al: Prospectus over "Aramid (Technora) FRP Rod"

/16/ Maunsell House, 160 Croydon Road, Beckenham, Kent BR3 4DE

Part II:

STATIC AND IMPACT FLEXURAL BEHAVIOR OF PRESTRESSED CONCRETE BEAMS REINFORCED WITH BRAIDED ARAMID FIBER RODS AS PC-TENDONS

Ola GUNNARSSON & Jonas HJALMARSSON
Lund Institute of Technology, Lund, Sweden

Dr. Hiroshi MIKAMI & Nakajima NORIMICHI
Mitsui Construction Co., Ltd., Tokyo, Japan

1 Introduction

This report presents information from static and impact tests of concrete beams prestressed with aramid fiber reinforced plastics (AFRP). The objective was to confirm the practical use of AFRP as PC-tendons in concrete beams and to find out their behavior in impact loading. The material AFRP has a high elastic elongation (2%) compared to steel tendons (0.2%). Reinforcement of AFRP in concrete structures is supposed to subdue the impact loads better than steel as a high strain capacity is an advantage. Tests have been carried out on this behavior in RC-beams /1/ and RC-slabs /2-4/ but yet not in PC-beams. These tests are an attempt to achieve a better understanding of the phenomena. If it can be confirmed that concrete structures reinforced with AFRP PC-tendons is a good damper for dynamic and especially impact loads one of the purposes of this test is reached. The static load behavior has been carefully studied in order to learn more about the static behavior and to try to understand the impact behavior.

2 Test specimen

2.1 PC-tendons

The PC-tendons used in the test were of braided AFRP-type. Two different dimensions were used shown in table 2.1.

Table 2.1 Material properties of AFRP-rods

Name	Diameter [mm]	Sectional area [mm^2]	Tensile strength [kN]	Weight [g/m]	Young´s modulus [GPa]	Elongation [%]
FA 11	10.4	85	117.6	108	68.6	2.0
FA 13	12.7	127	176.4	162		

2.2 Concrete

The cement used for the concrete in the test was high-early-strength Portland cement. A maximum aggregate size of 20 mm was used. The curing condition for the beams and the specimens for testing of concrete strength was not the same, which may effect the test data. The properties of the concrete are shown in table 2.2.

Table 2.2 Material properties of concrete

Days after casting	Compressive strength [MPa]	Tensile strength [MPa]	Bending tensile strength [MPa]	Young´s modulus [GPa]
3	31.26	2.70	-	24.97
7	37.55	2.44	5.60	27.12
22	40.50	3.07	5.40	28.04
28	40.75	2.78	6.29	28.92

* Lund Institute of Technology, Lund, Sweden
** Technical Research Institute of Mitsui Construction CO,LTD., Tokyo, Japan

2.3 Beams

A total of six specimens was produced for use in static and dynamic loading test. The test specimens were designed for concrete compression failure. Three different types, shown in figure 2.1 and 2.2, were made employing AFRP as PC-tendons and steel stirrups as shear reinforcement. The reinforcement ratio of the PC-tendons was in type A 1.27 %, in type B 1.69 % and in type C 2.27 %. The amount of longitudinal steel bars was small and they were therefor neglected in the design of the beam. Their function was to make strain measurements possible. In all specimen wire strain gauges were attached to the PC-tendons, the longitudinal steel bars and the stirrups. Two specimens were made of each type. In order to achieve the same pretension in the static and dynamic test the PC-tendons were prestressed in a steel frame continuously through the two specimens of the same type.

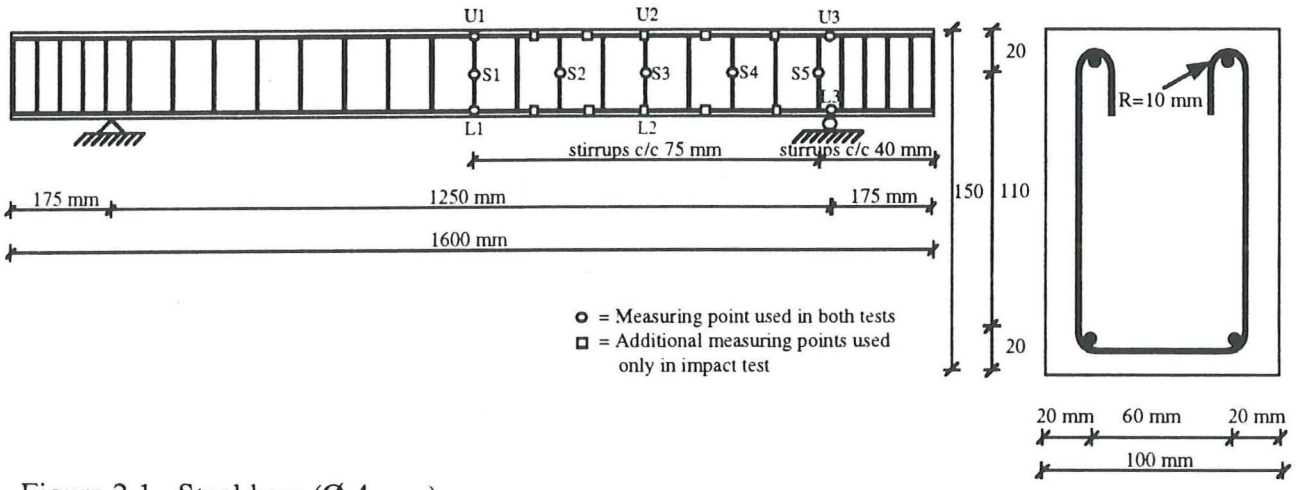

Figure 2.1 Steel bars (Ø 4 mm)

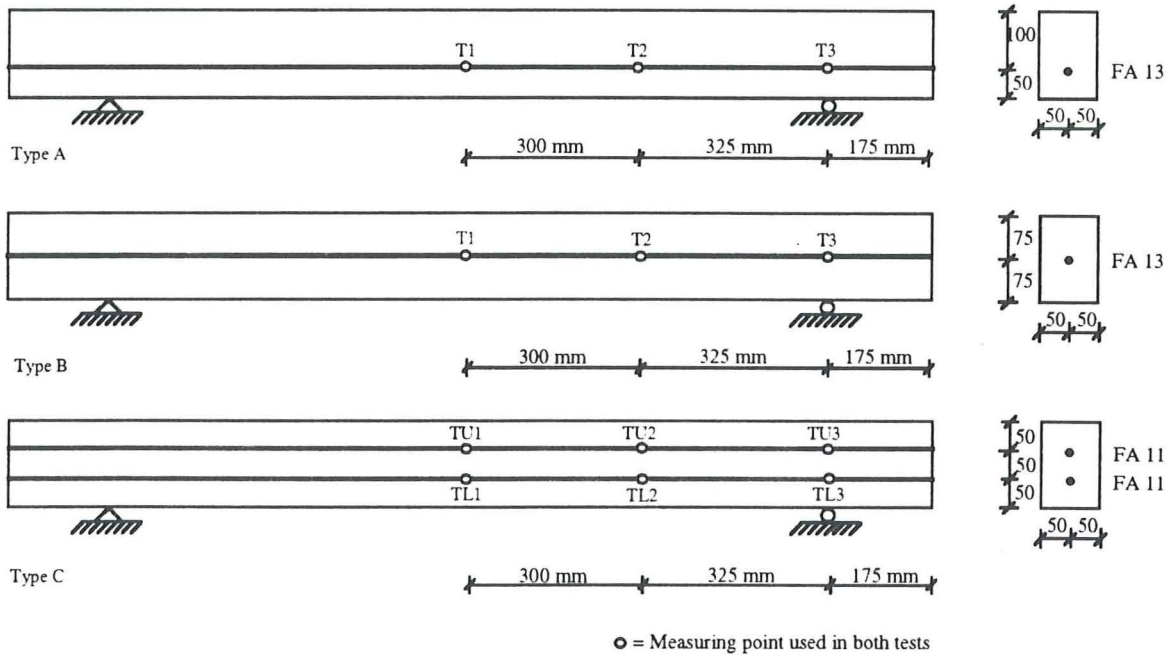

Figure 2.2 PC-tendons

3 Pretensioning

In the ends of the tendon a resin-type of anchor was used and the pretension was applied using a SLP-jack (Hydraulic Jack Center Hole Type). In type A and B the pretension force was calculated to be 73.50 kN (0.42 P_u*) and in type-C 36.75 kN/tendon (0.31 P_u*). Type A,B and C were designed to achieve the same prestress in the center of the beam (4.9 MPa). A reduction of the stress in the tendons occurs depending on pretension losses, relaxation and deformation of the steel frame that was used for the pretensioning. This reduction was estimated to be 15 %. Wire strain gauges were attached on the PC-tendons and the pretension was applied in several steps.

Stress-strain graphs of the pretension process (figure 3.1 to 3.4) were made to clarify which strain gauges that showed an unexpected behavior. Out of these graphs Young's modulus was calculated and a mean value of 70.1 GPa corresponds very well with the value of 68.6 GPa given by the manufacturer. This test result could furthermore be improved to 68.3 GPa by removal of the strain gauge values that showed a strange behavior (table 3.1). Figure 3.1 to 3.4 made it possible to exclude data from table 3.1 when calculating the improved Young's modulus.

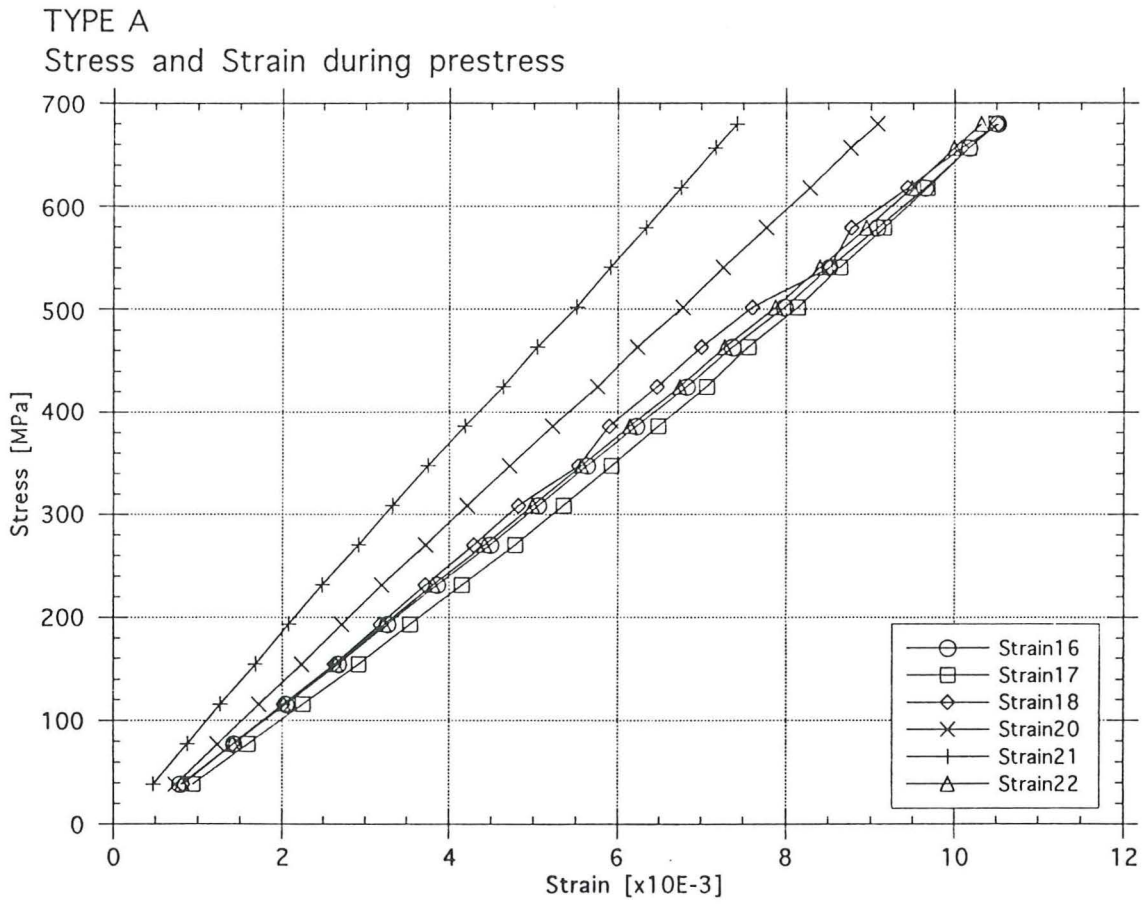

Figure 3.1 Pretensioning

* P_u= Ultimate tensile strength

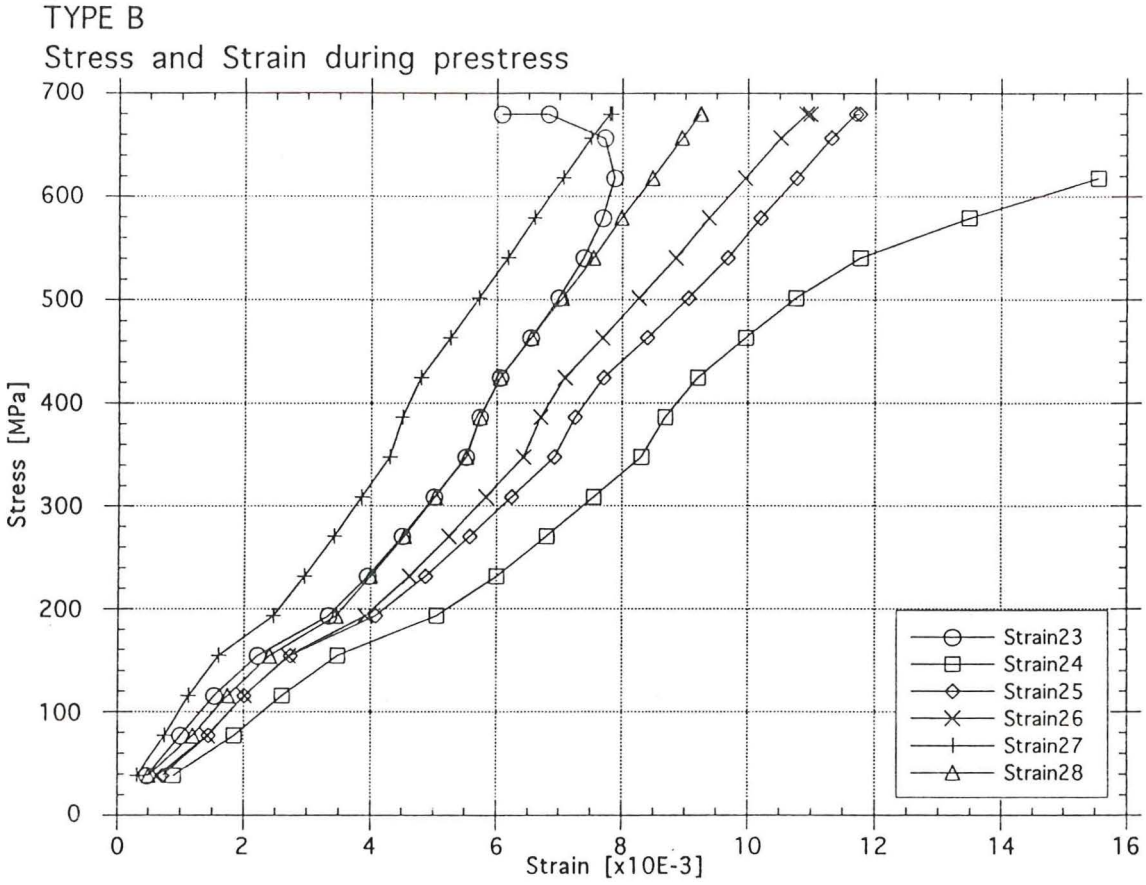

Figure 3.2 Pretensioning

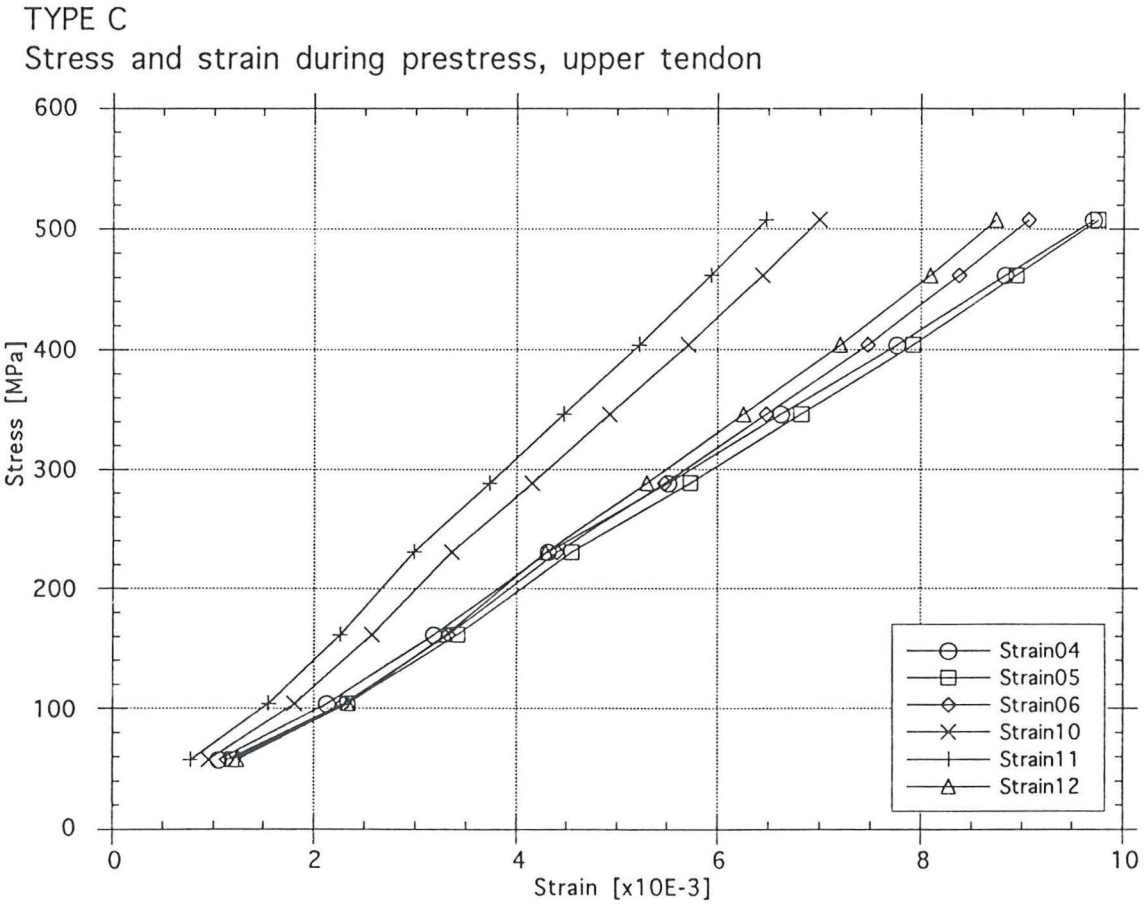

Figure 3.3 Pretensioning

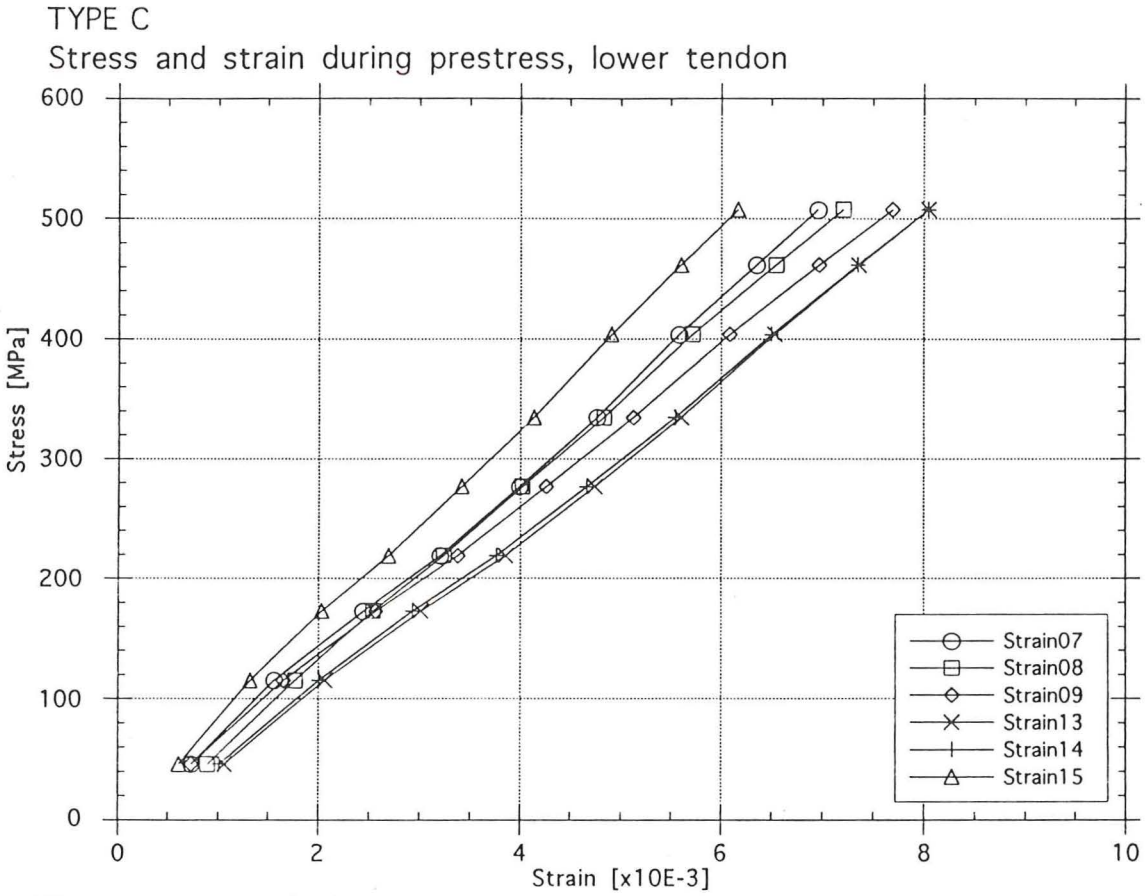

Figure 3.4 Pretensioning

Table 3.1 Young's modulus values derived from pretensioning

Type A	Strain gauge	Gauge Position	Young's modulus [GPa]
Static-test	16	T-1	66.3
	17	T-2	67.4
	18	T-3	67.2
Impact-test	20	T-1	77.2
	21	T-2	91.7
	22	T-3	67.8

Type B	Strain gauge	Gauge Position	Young's modulus [GPa]
Static-test	23	T-1	81.9
	24	T-2	59.5
	25	T-3	59.8
Impact-test	26	T-1	64.9
	27	T-2	87.8
	28	T-3	81.9

Type C Upper	Strain gauge	Gauge Position	Young's modulus [GPa]
Static-test	04	TU-1	52.8
	05	TU-2	53.3
	06	TU-3	57.6
Impact-test	10	TU-1	75.8
	11	TU-2	79.8
	12	TU-3	60.9

Type C Lower	Strain gauge	Gauge Position	Young's modulus [GPa]
Static-test	07	TL-1	73.5
	08	TL-2	72.8
	09	TL-3	66.2
Impact-test	13	TL-1	65.8
	14	TL-2	65.1
	15	TL-3	85.7

4 Static test

4.1 Test method

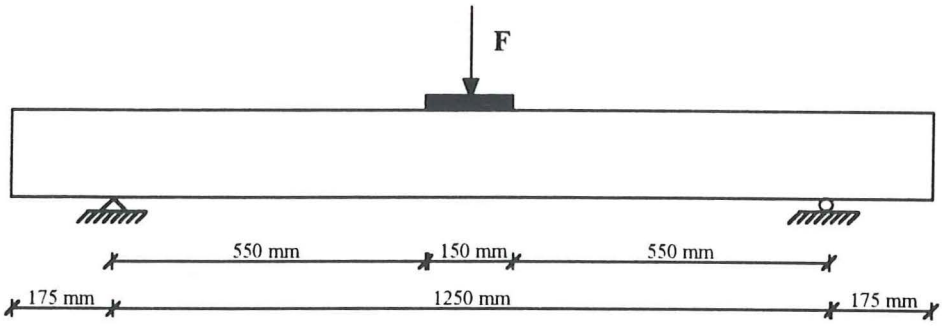

Figure 4.1 Test equipment

The static test was carried out as a one-point load test. The load was applied on a 150x100 mm rigid steel plate. The plate was used to make the loading condition correspond to the one used in the dynamic test, where a Ø 150 mm one-point impact load was used. Strain gauges had been attached on the AFRP PC-tendons, on the lower and upper longitudinal steel bars and on the stirrups (see figure 2.1 and 2.2). Strain gauges were also applied at three positions on the surface of the concrete. Beam displacement was measured on the central longitudinal axis of the beam at five positions.

A continuously increasing static load was applied until the occurrence of the first crack. After the first crack the beam was unloaded and π-gauges, for measuring of the crack width, were attached over the two major cracks. Then the loading started again in steps by 0.2 kN until the load value from the load cell no longer increased. Then the load was slowly decreased down to zero. During the loading process crack sketches were made after each load-step (see figure 4.39).

4.2 Test results

The relationship up to first crack opening and unloading from this point down to zero is excluded in the graphs shown below. This is done to make the graphs more easy to read.

Measured and calculated values of beam displacements, loads and moments are shown in table 4.1. The one-point load application and the shape of the steel plate give the Load-Moment relationship: Load = Moment / 0.294.

Table 4.1 Measured and calculated test results

Type	Measured values				Calculated values			
	Crack moment [kNm]	Max moment [kNm]	Deflection crack moment [mm]	Max center deflection [mm]	Crack moment [kNm]	Max moment [kNm]	Deflection crack moment [mm]	Max center deflection [mm]
A	5.3	11.5	1.8	14.2	6.1	10.8	1.5	19.9
B	4.3	7.4	1.8	8.5	4.0	7.0	1.0	21.9
C	4.4	9.6	1.6	14.9	4.0	8.0	1.0	19.1

4.2.1 Deflection of beam

The graphs in figure 4.2 to 4.4 show the deflection in five positions of the beam. Initially the deflection increases linearly but after crack opening the growth increases drastically. Almost no differences in deflection were measured between the three specimens before reaching the crack load. At a load of 20 kN the following deflections were measured: type A 2.2 mm, type B 4.2 mm and type C 3.2 mm.

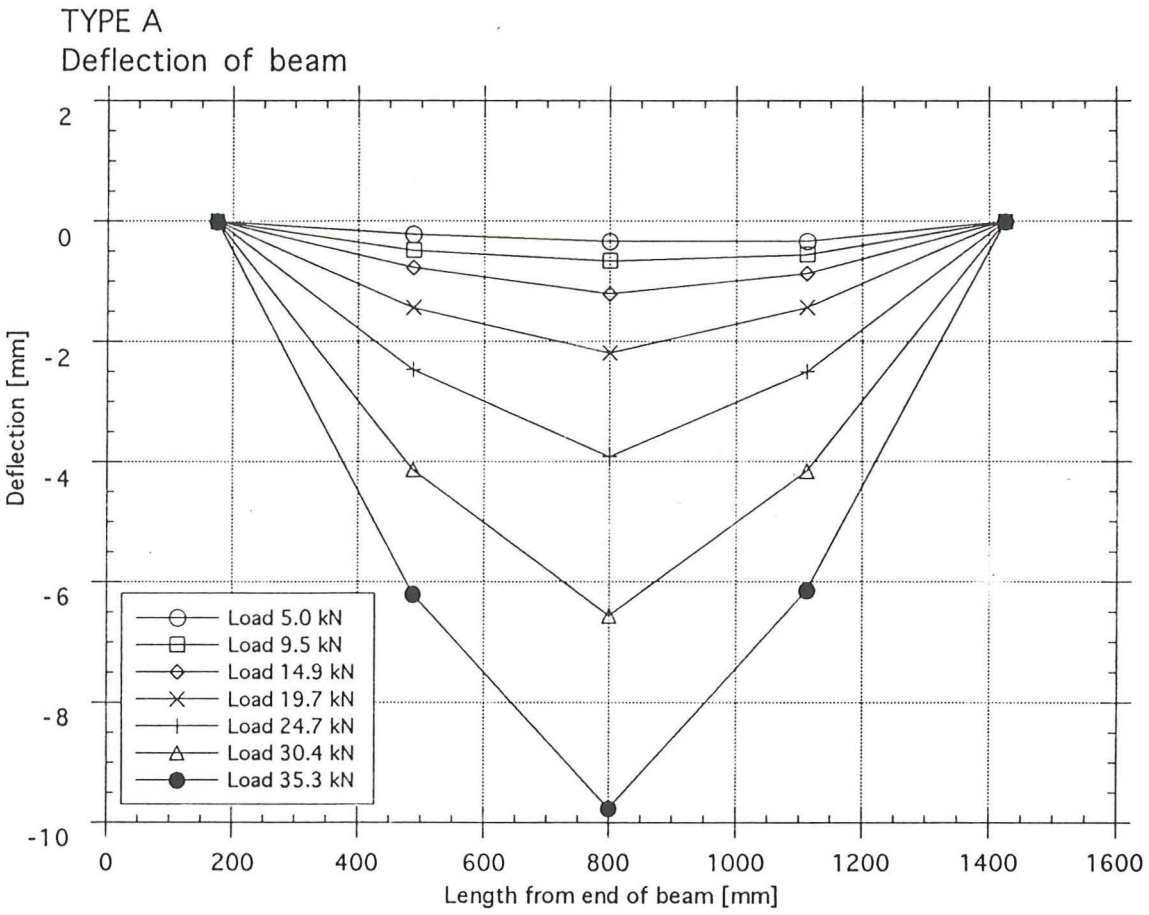

Figure 4.2 Deflection of beam type A

The shape of the cross section of type A with one FA 13 PC-tendon placed low in the tensile zone makes that beam the stiffest, due to higher effective depth and rigidity of the PC-tendon. Type B and C are due to the shape of the cross section less stiff, but there is a notable difference in stiffness between those two beams. The occurrence of major cracks in the center area of the beams results in a V-shaped deformation at high load (see figure 4.2 to 4.4). Observe that the graphs are nearly symmetrical due to the load application and the occurrence of a major crack close to the beam center.

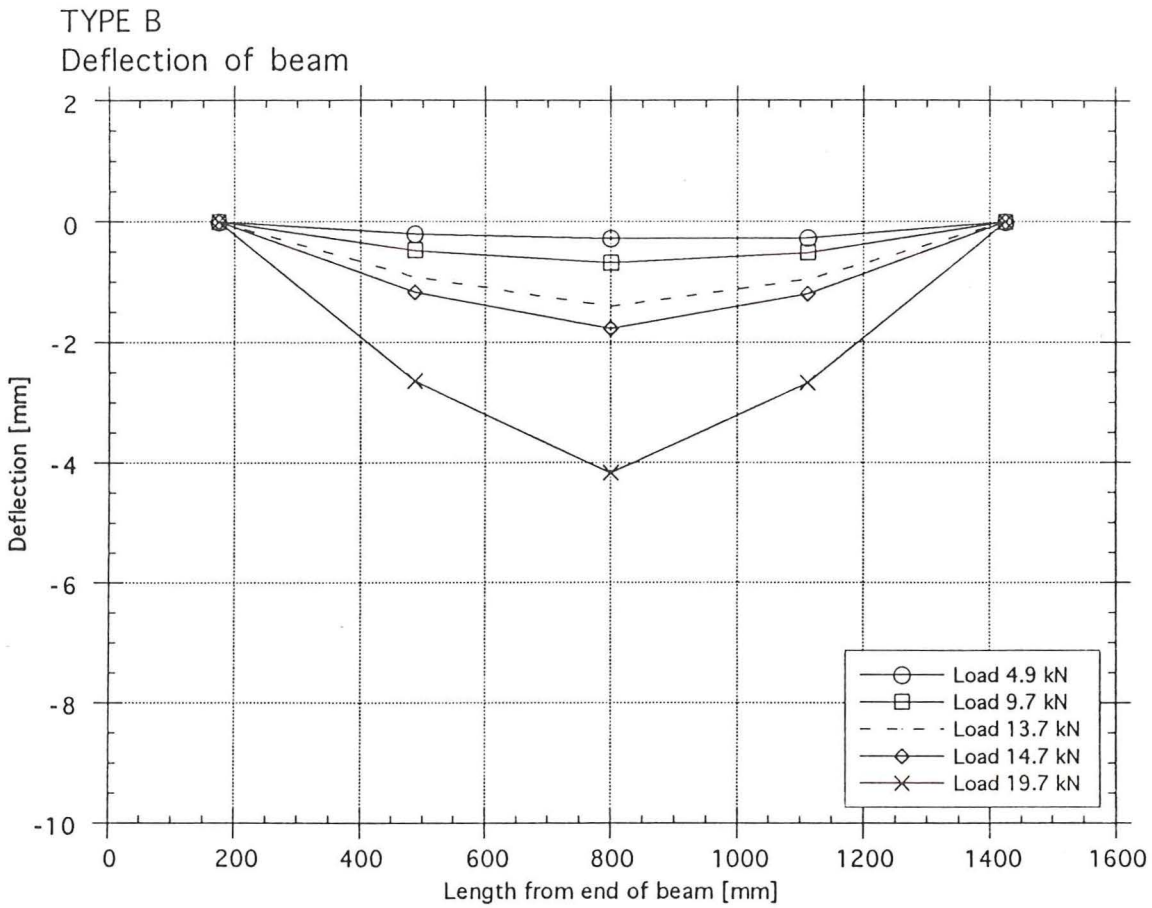

Figure 4.3 Deflection of beam type B

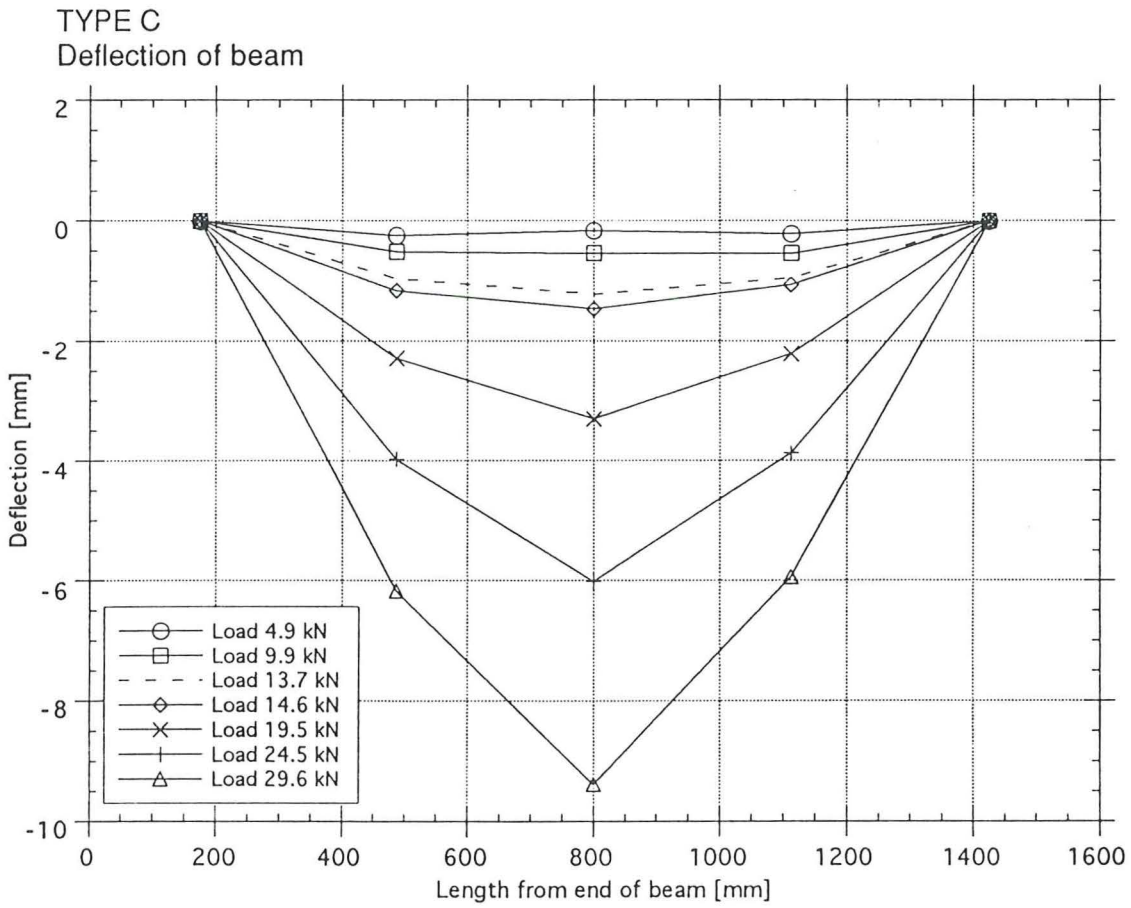

Figure 4.4 Deflection of beam type C

4.2.2 Strain distribution in beam

The graphs in figure 4.5 to 4.14 show the load-strain behavior at three positions of the beam. These positions are beam center, 300 mm from beam center and at support.

In all beams the load-strain relationship is linear in the compression zone up to occurrence of the first crack. In figure 4.11 to 4.14 a drastic change of strain in the type C beam occurs, especially in the upper tendon, when the neutral axis passes above this tendon at a load of about 15 kN which is the crack load. In figure 4.5 to 4.7 (type A) and 4.11 to 4.14 (type C) there is no change in strain of the lower steel bar in the high load area at support and 300 mm from beam center. This may be caused by split cracks or slip of the steel bars.

In all of these graphs the strain in the PC-tendons at support is not equal to zero before failure, probably due to slip of the tendons. Under high load conditions the lower and upper steel bars of the beams yield at beam center and the upper steel bars buckle.

O This turning point shows the area where the cross section changes from non-cracked to totally cracked.

X Compression area due to the position of the neutral axis that is below the level of the PC-tendon.

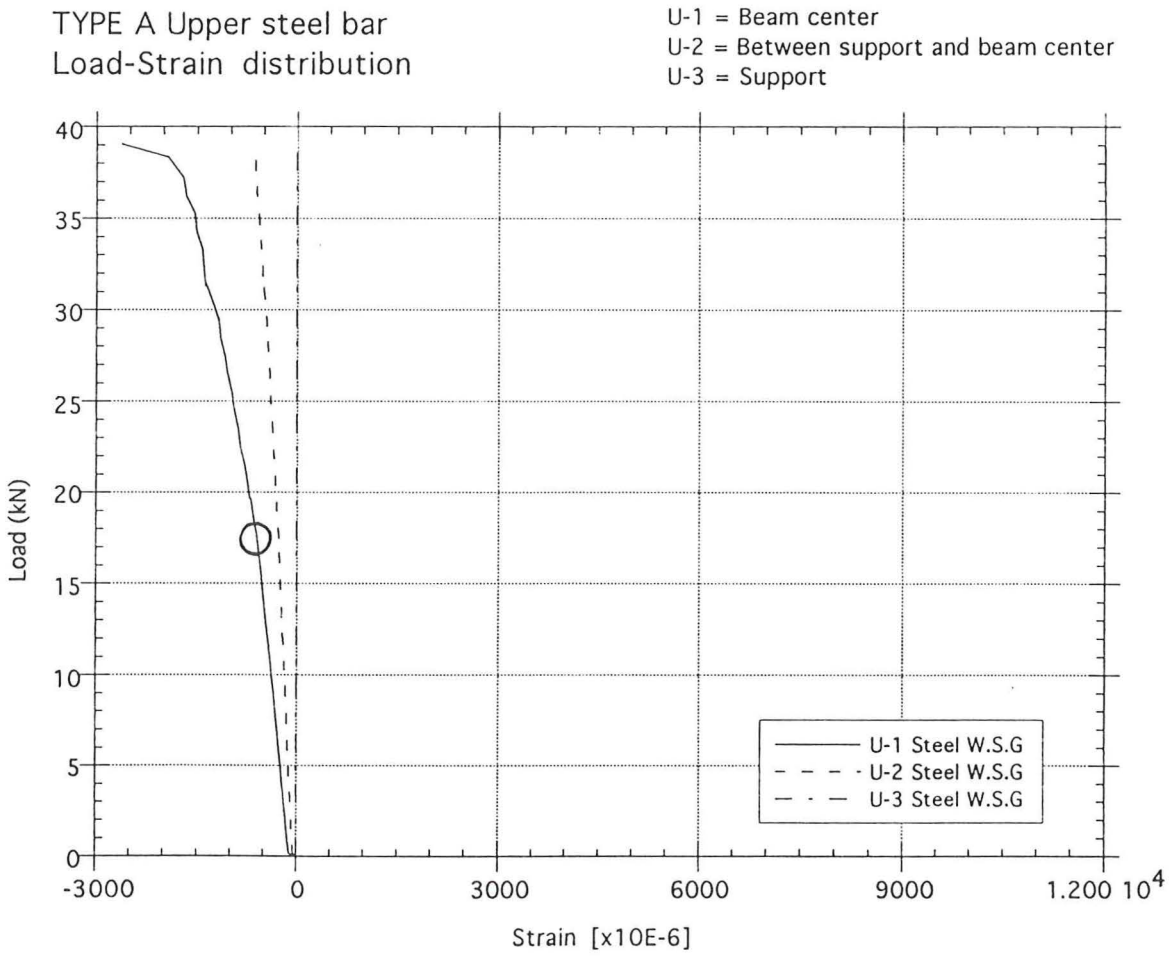

Figure 4.5 Strain distribution

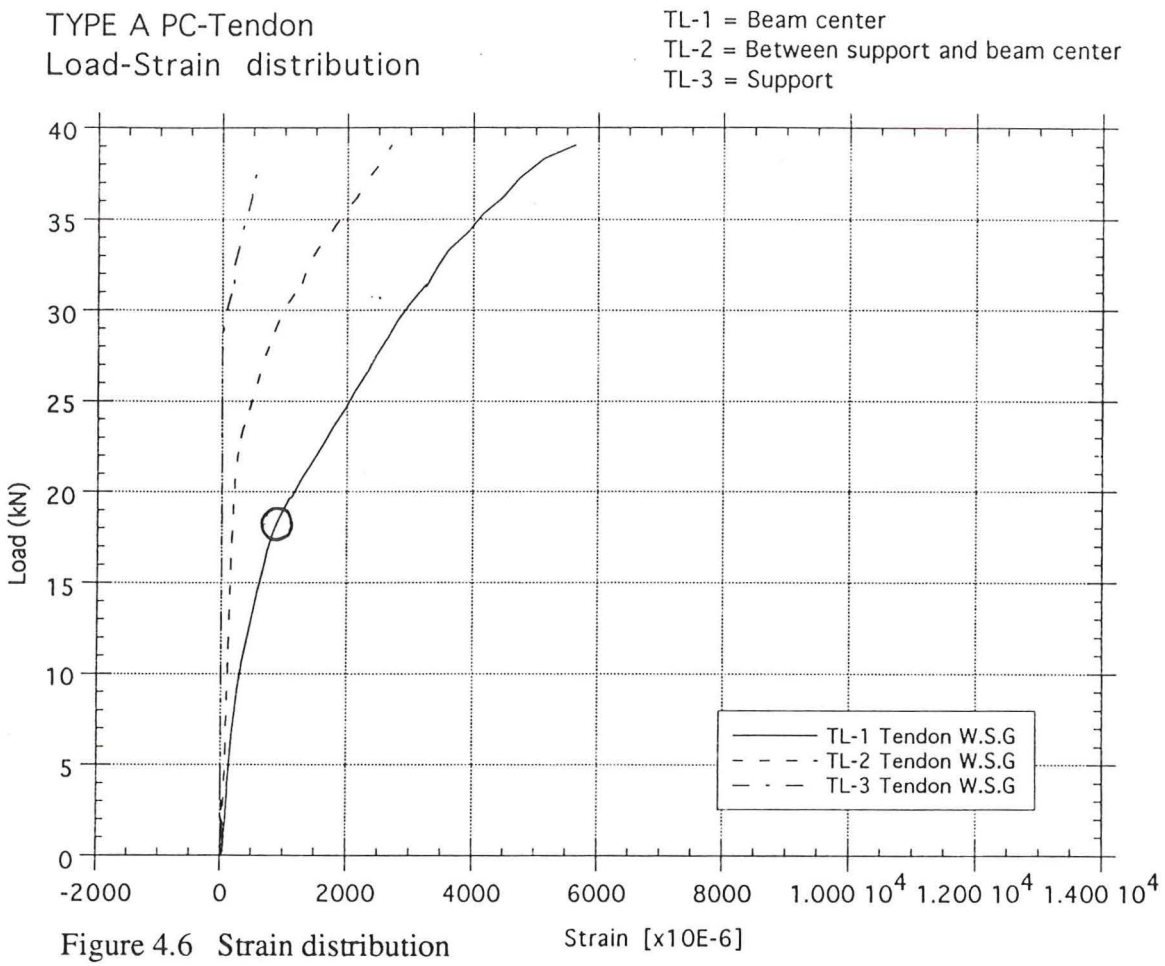

Figure 4.6 Strain distribution

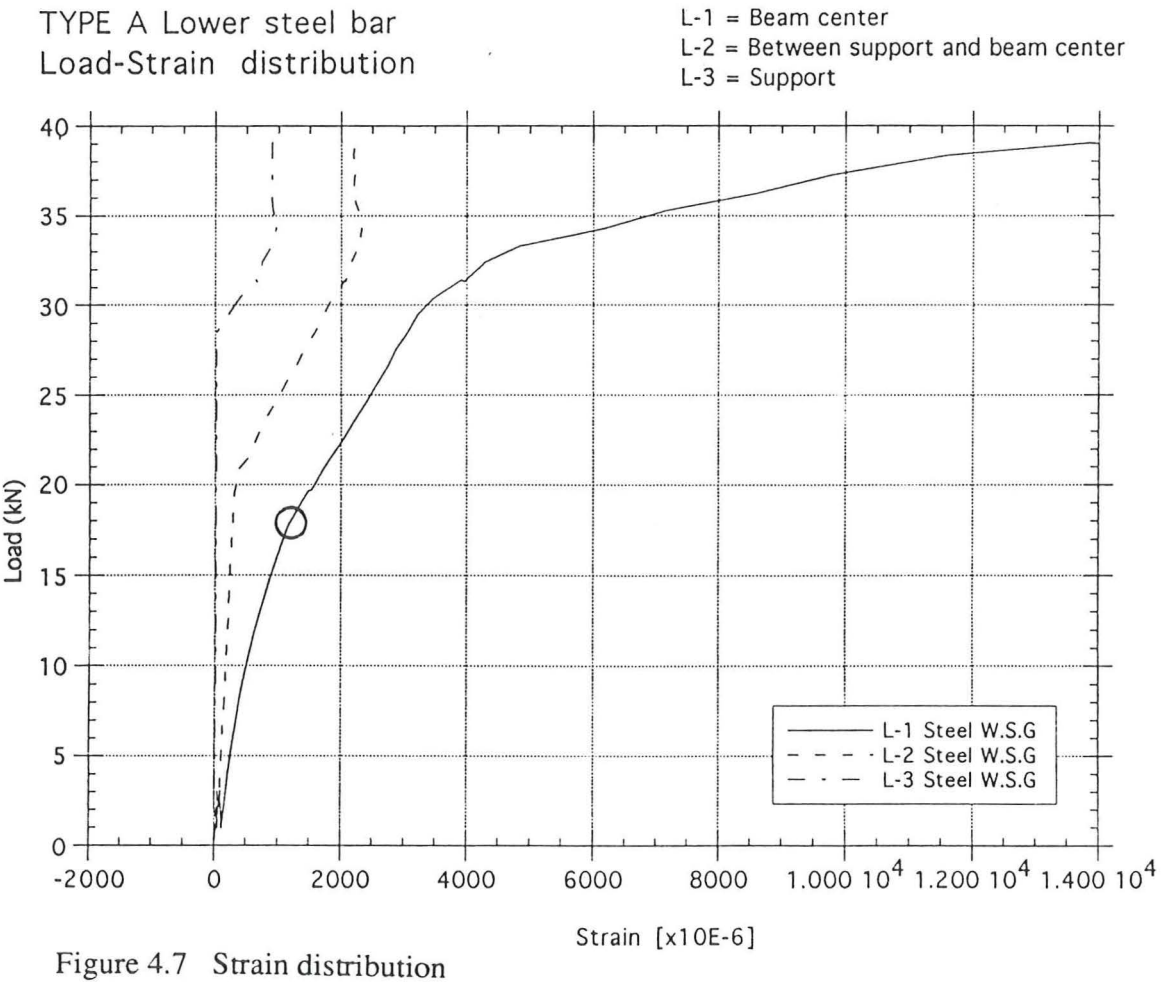

Figure 4.7 Strain distribution

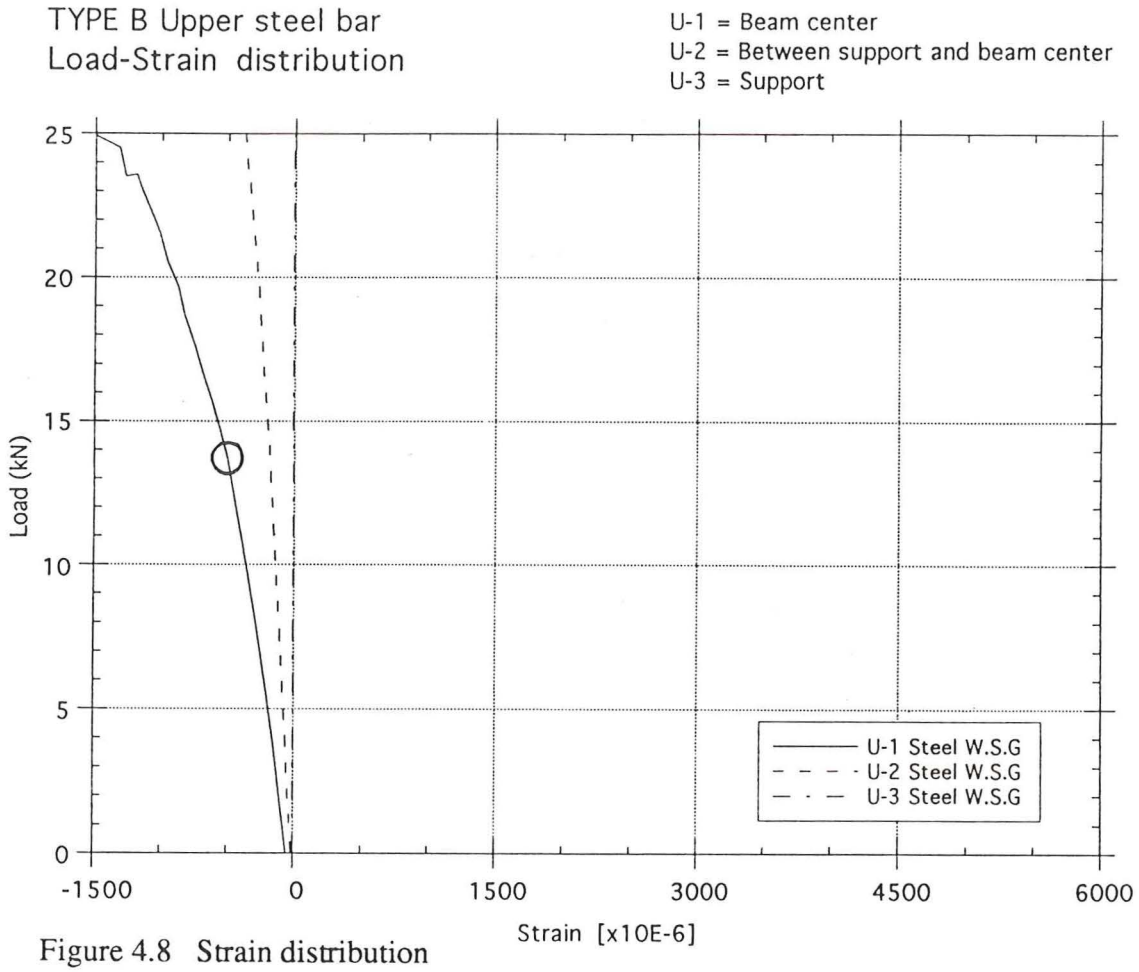

Figure 4.8 Strain distribution

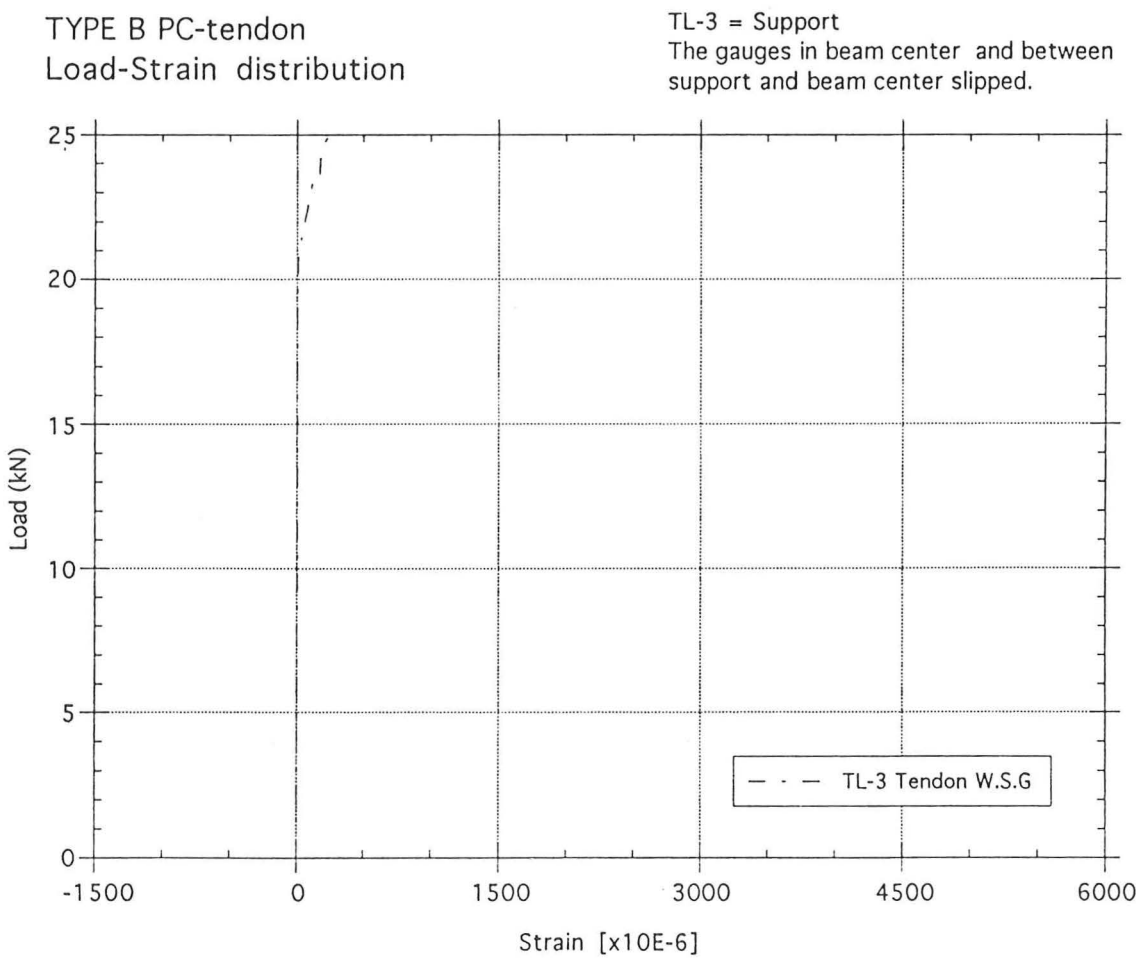

Figure 4.9 Strain distribution

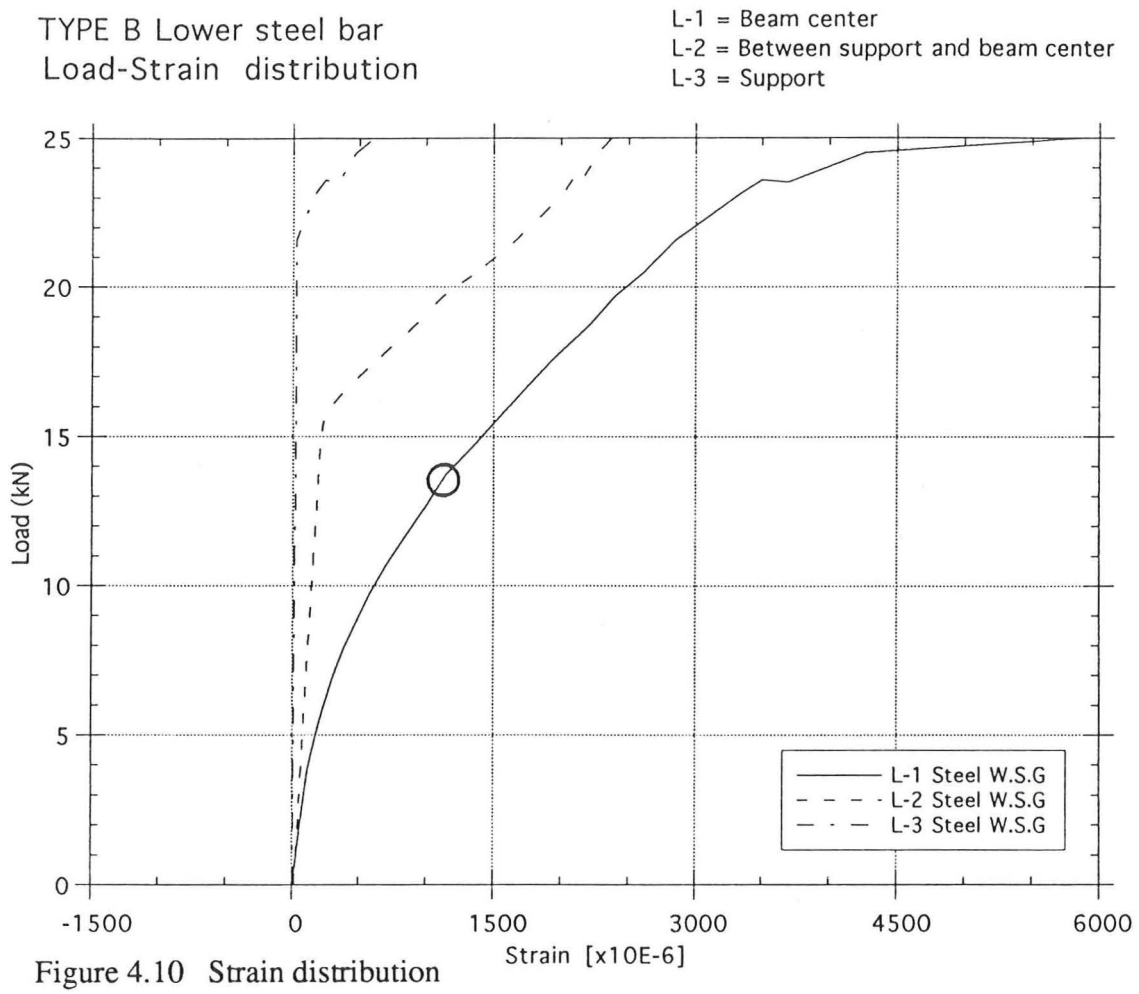

Figure 4.10 Strain distribution

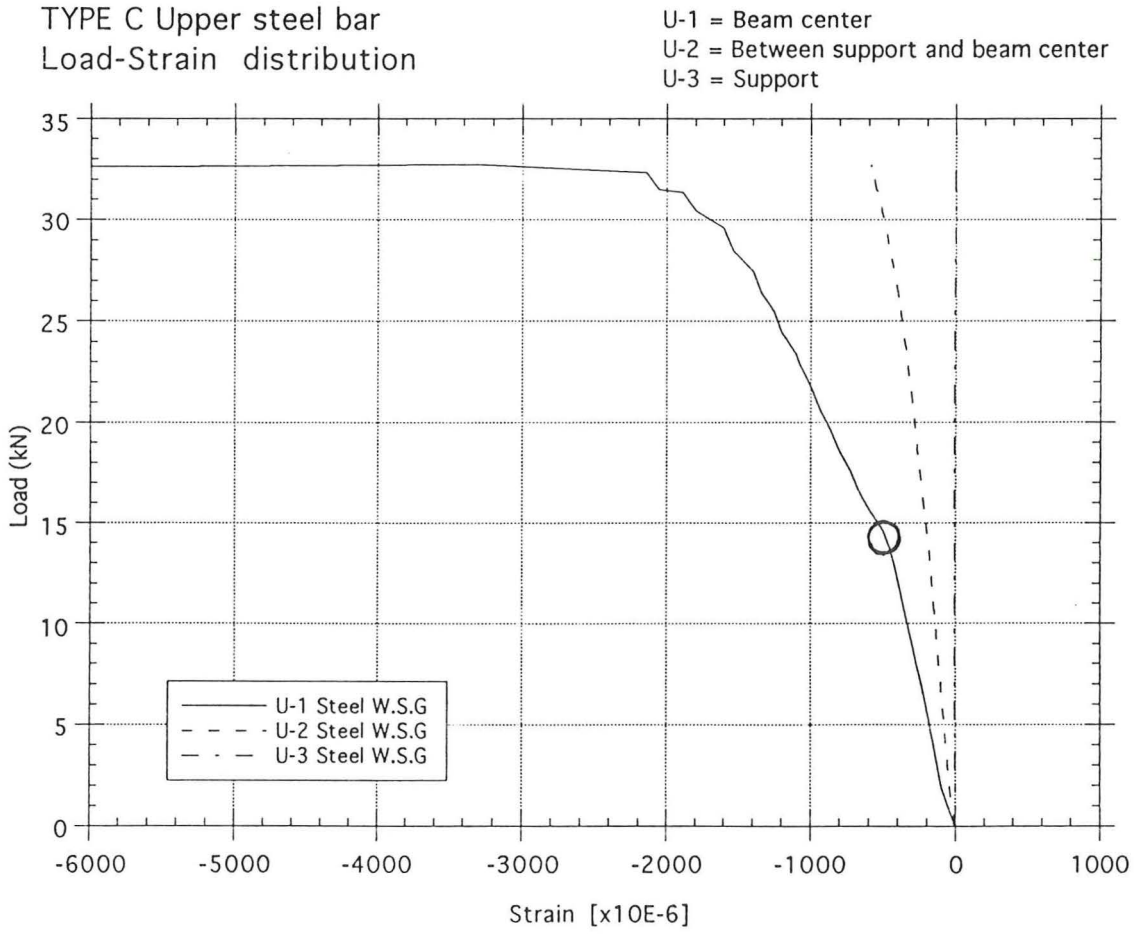

Figure 4.11 Strain distribution

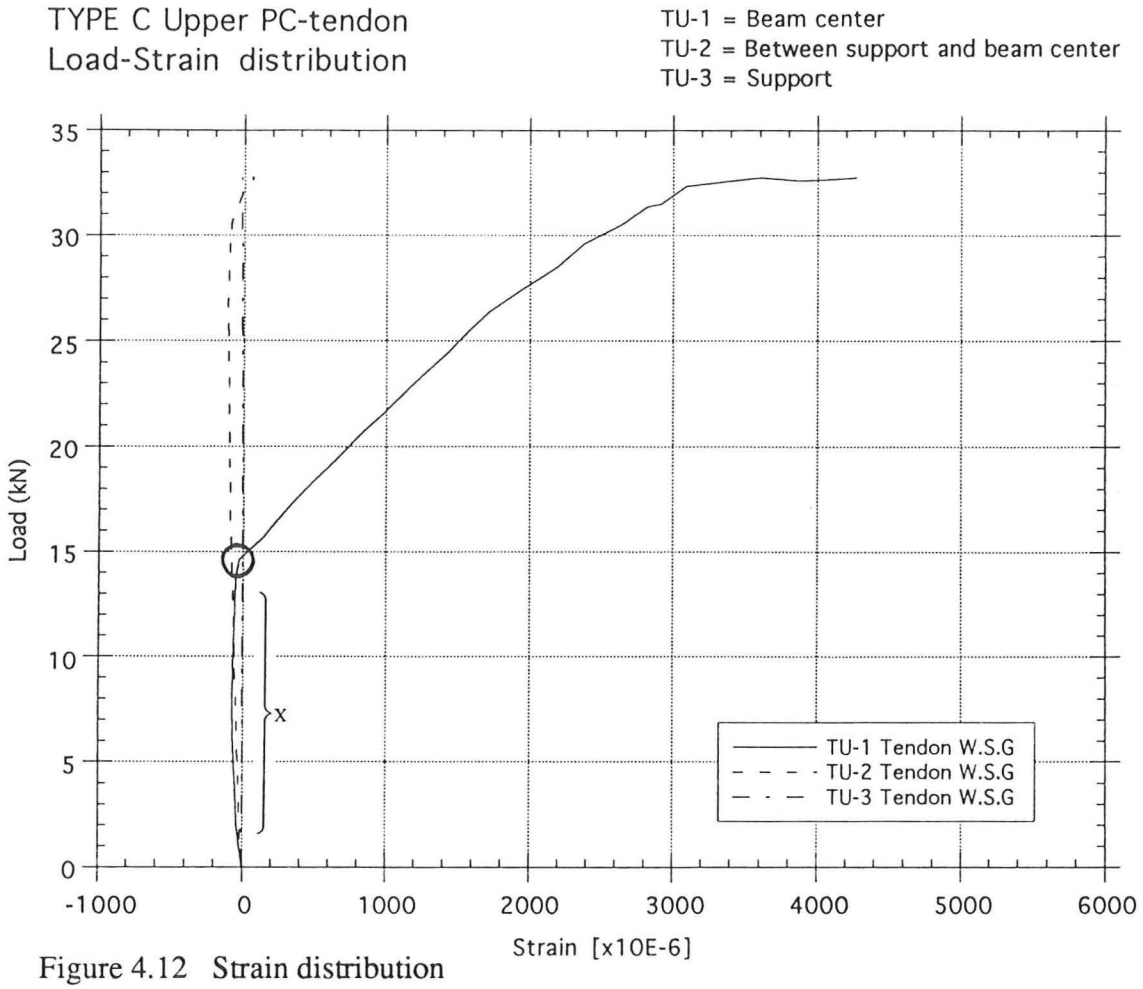

Figure 4.12 Strain distribution

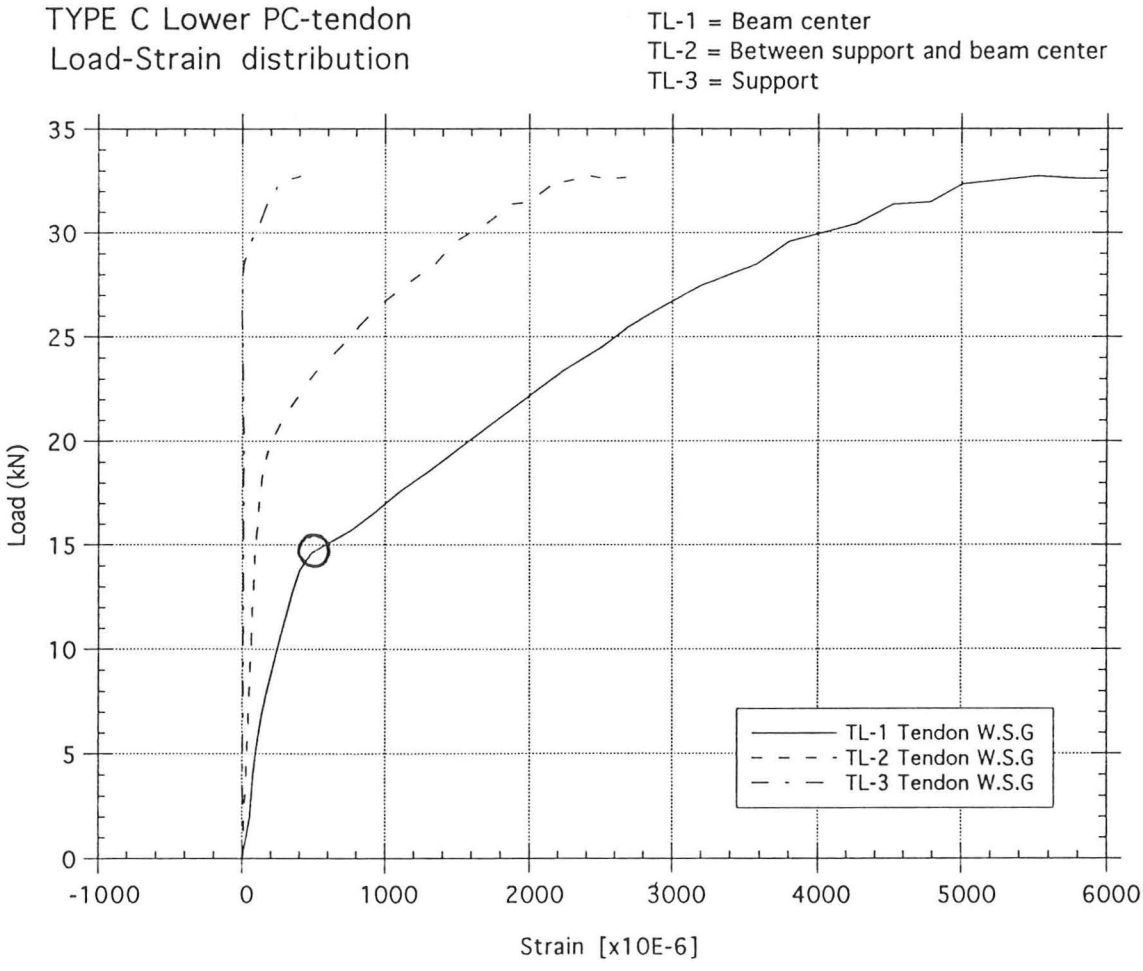

Figure 4.13 Strain distribution

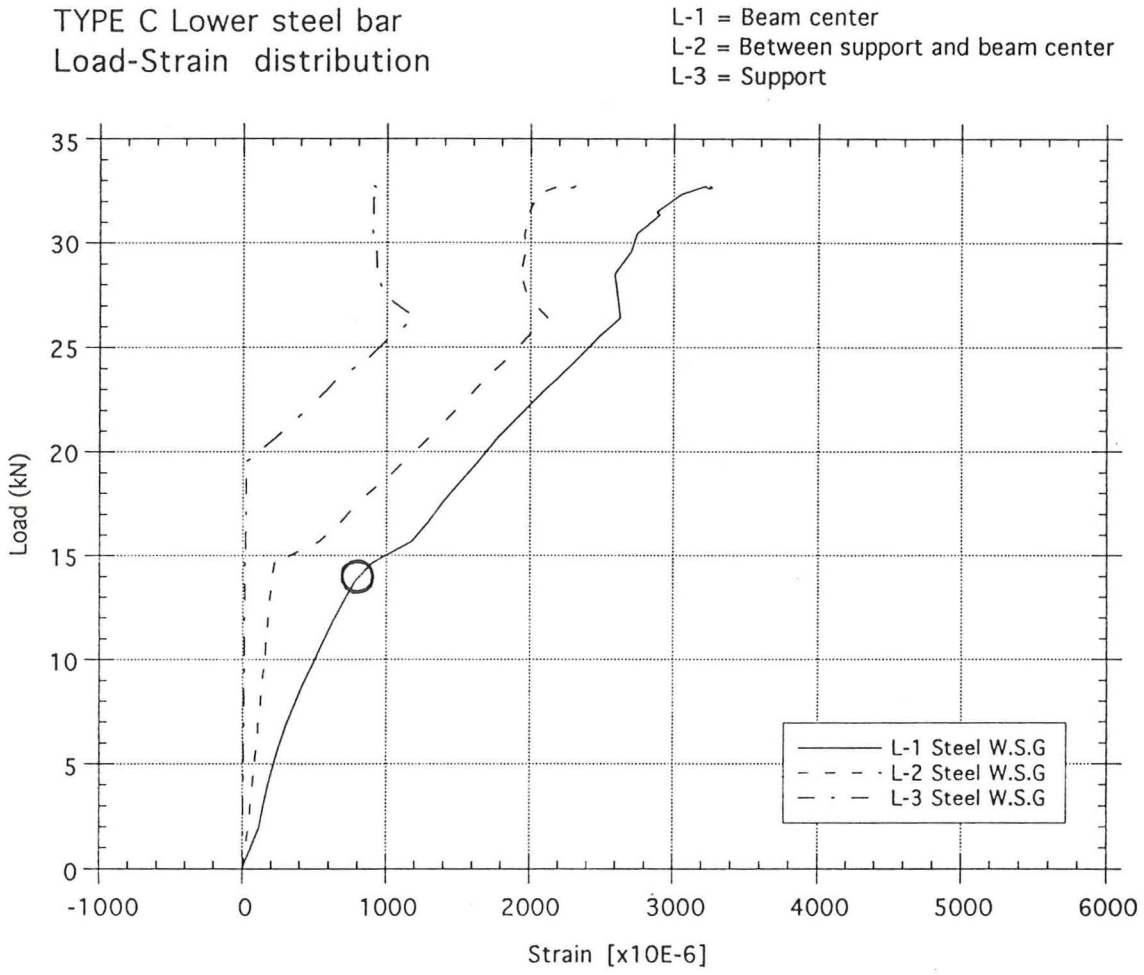

Figure 4.14 Strain distribution

4.2.3 Strain distribution in cross section

The graphs in figure 4.15 to 4.21 show the strain distribution in the cross section of the beam. The strain is showed at three different positions of the beam. The positions are beam center, 300 mm from beam center and at support. There is only one graph of type B due to slip of the gauges at two positions of this beam. The expected plain strain distribution according to beam theory can be observed in type A.

In type A the major crack occurs at the center of the beam where the strain gauge is located. The drastic change of strain at the support probably depends on slip of the PC-tendons and the steel bars. The unexpected behavior of the strain distribution in beam center, shown in figure 4.21, could be understood by considering the crack pattern of the type C beam. The major crack runs from just beside the beam center almost up to the level of the upper PC-tendon where it turns towards the center of the beam. This crack pattern corresponds to the high strain in the upper PC-tendon and the low strain in the lower PC-tendon and lower steel bar.

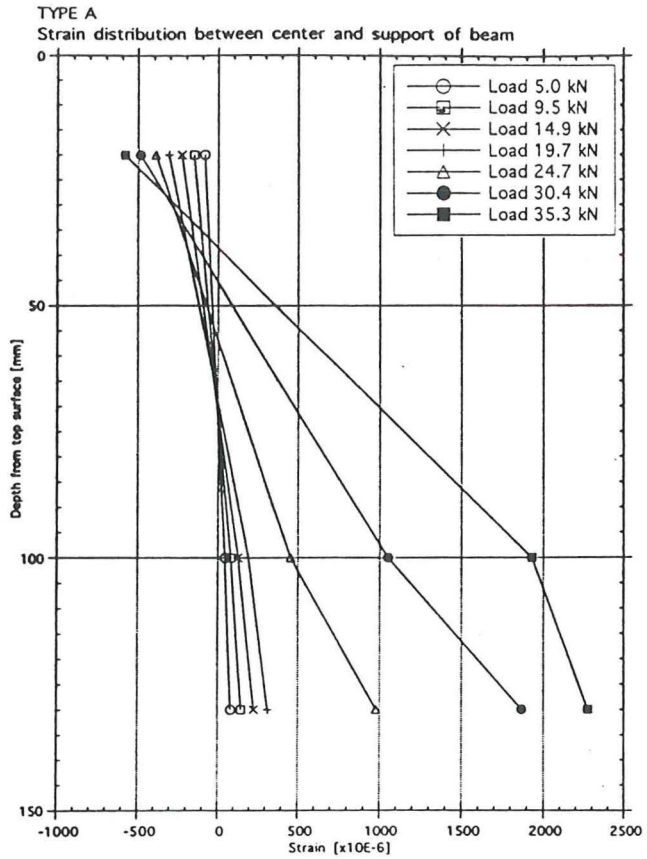

Figure 4.15

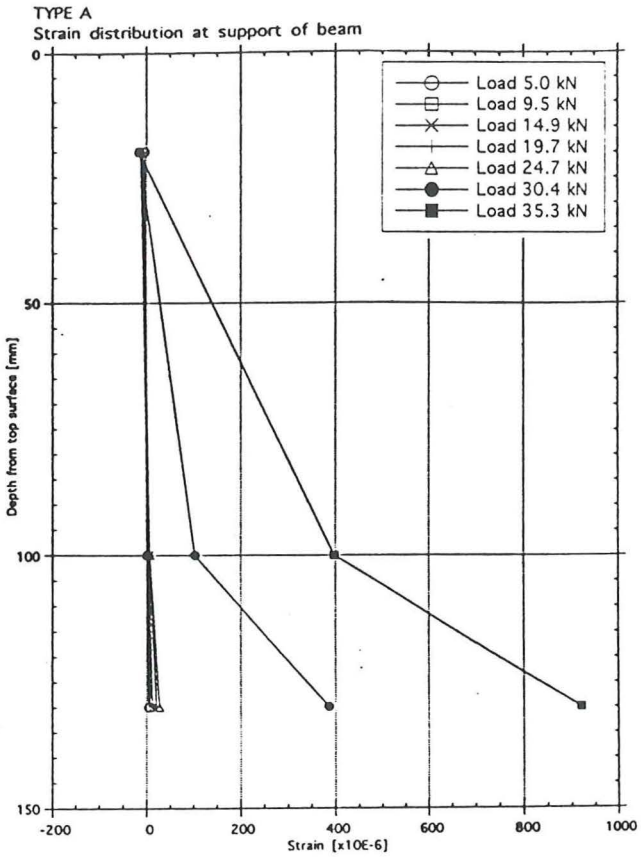

Figure 4.16

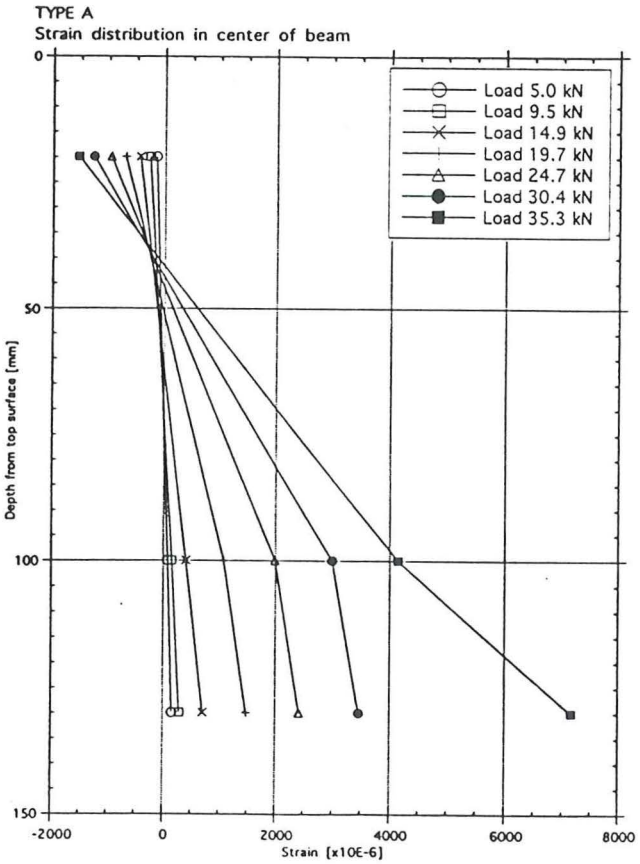

Figure 4.17

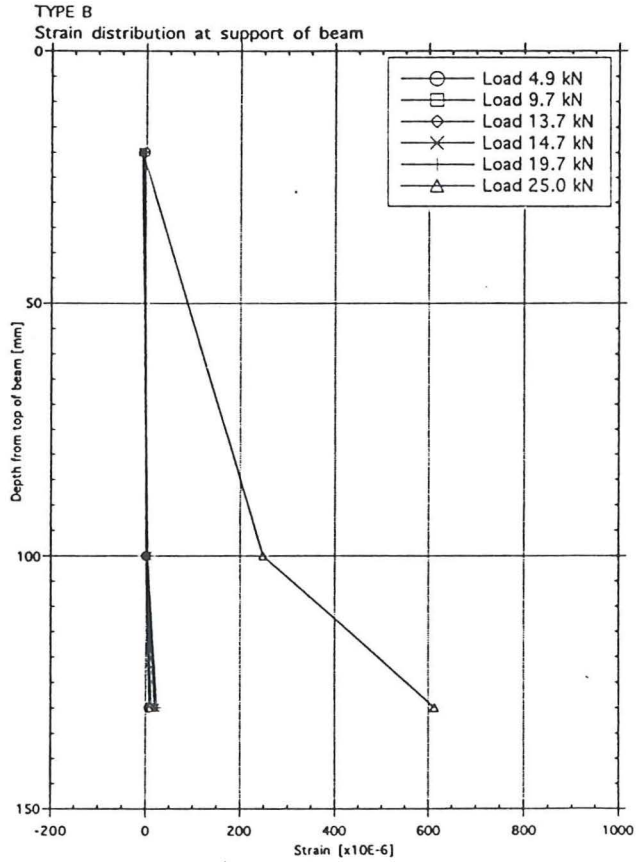

Figure 4.18

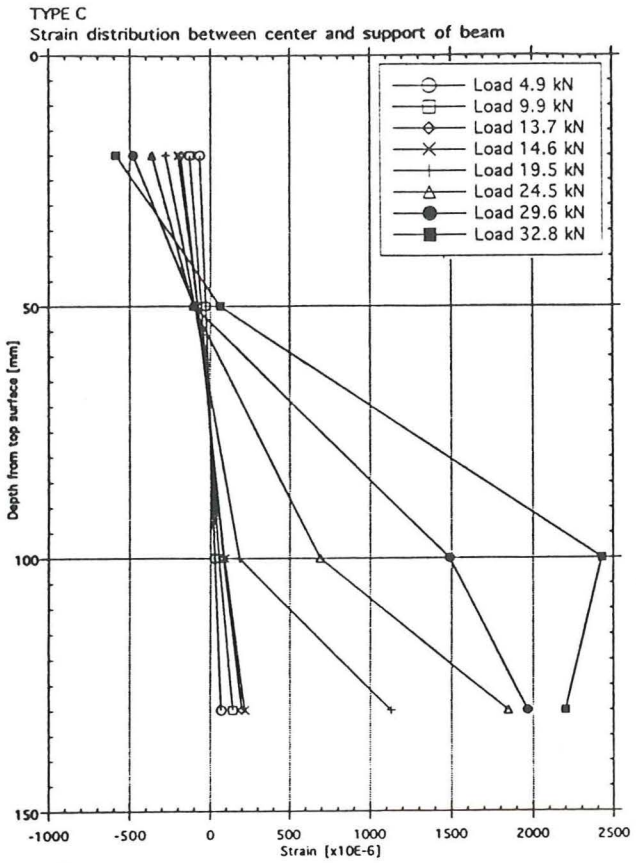

Figure 4.19

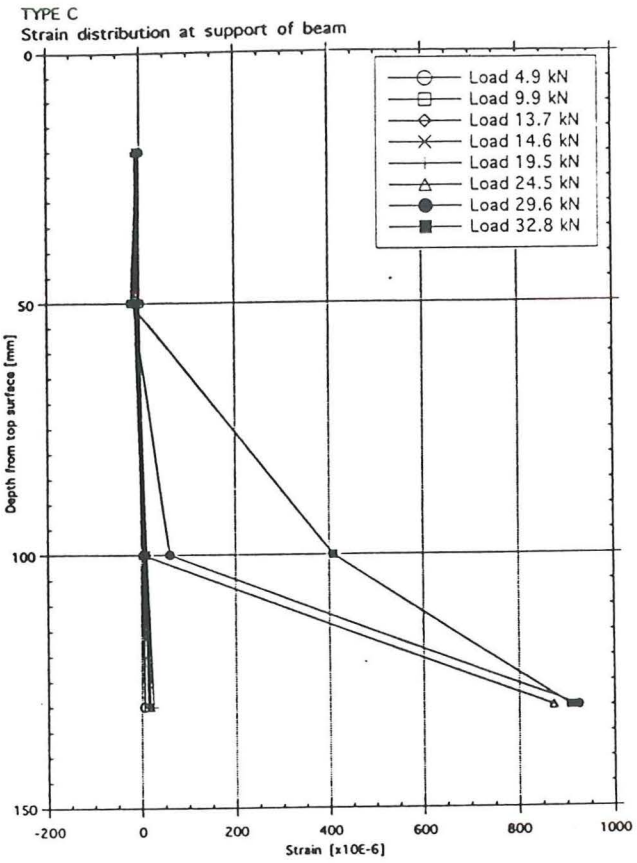

Figure 4.20

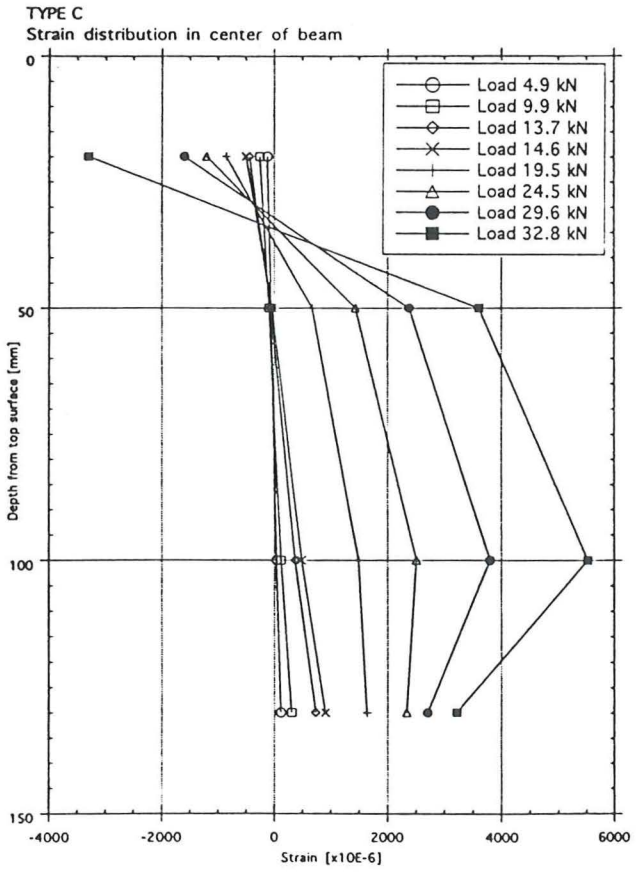

Figure 4.21

4.2.4 Strain distribution

The graphs in figure 4.22 to 4.30 show the strain at three positions of the beam under different load. The positions are beam center, 300 mm from beam center and at support. The measured values from the wire strain gauges of upper steel bar, tendons and lower steel bar are shown in separate graphs for each beam. The drastic change in strain occurs at a load of 25 kN for type B and C and at 30 kN for type A. The high values of the wire strain gauges in the lower steel bars of type A and B are due to yielding in the steel bars. The reason why this pattern not occurs in type C is that the position of the major crack is beside the beam center of type C while the strain gauge is located in the center of the beam.

In all of these graphs we can see an unexpected strain at the supports in the high load area, where the strain is expected to be equal to zero. This probably depends on slip of the tendons and the steel bars under high tensile force.

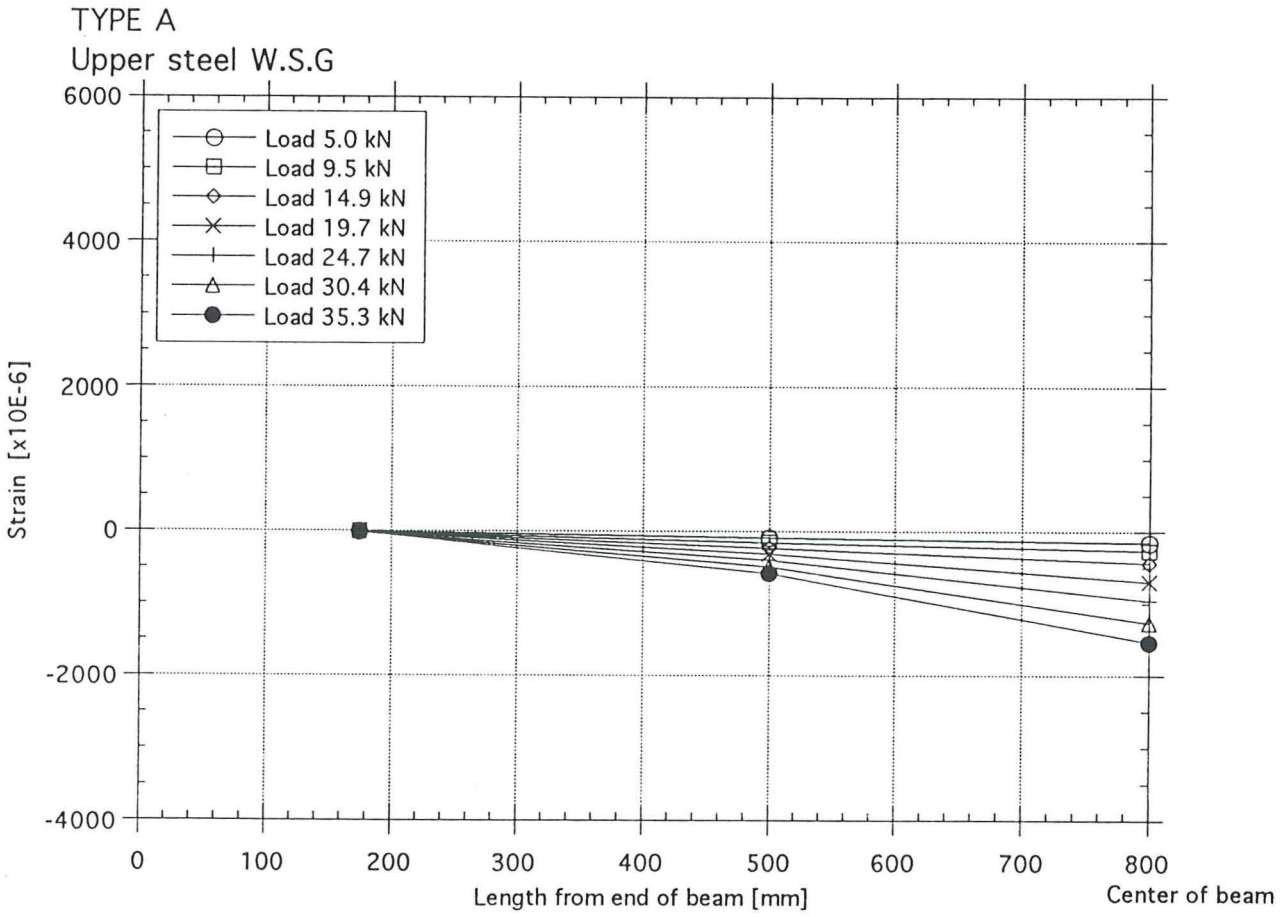

Figure 4.22 Strain in beam type A

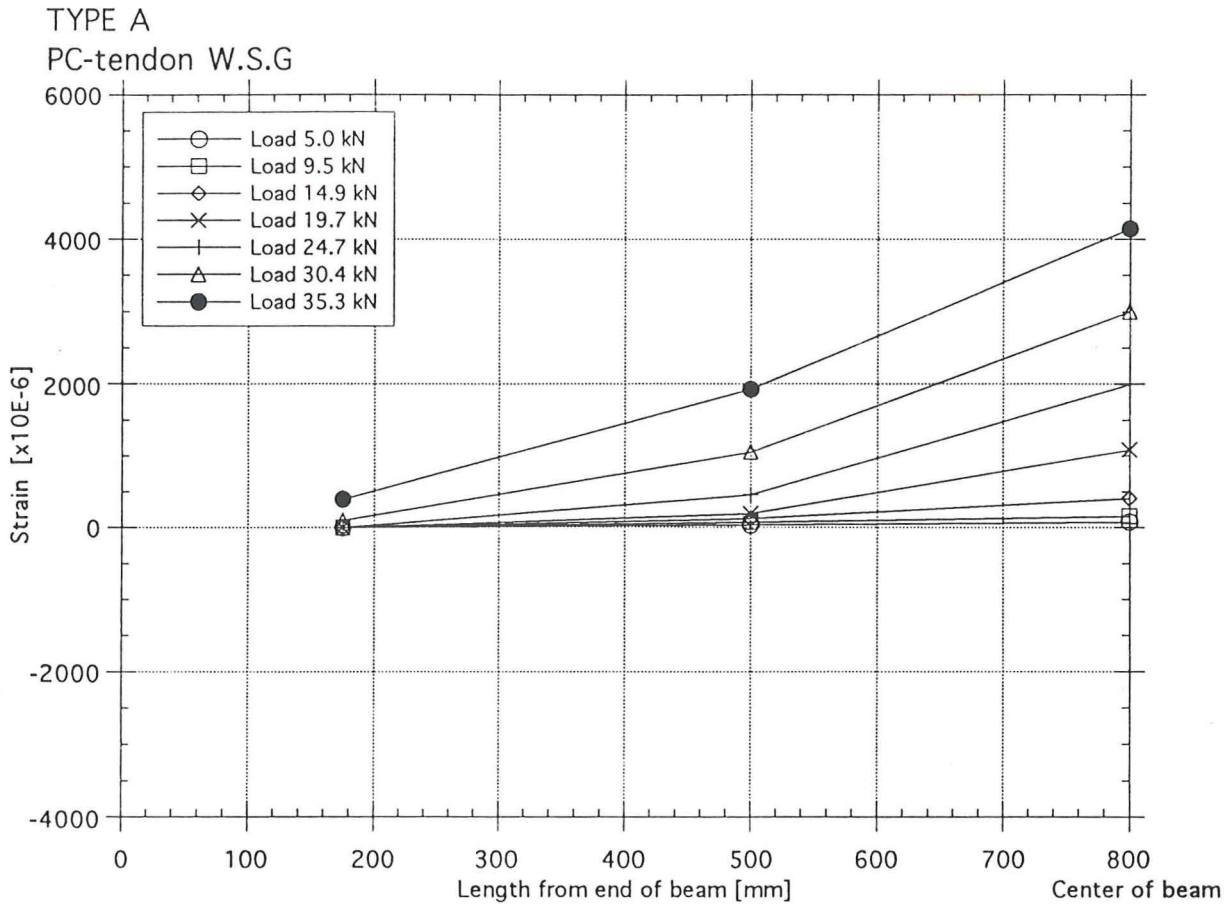

Figure 4.23 Strain in beam type A

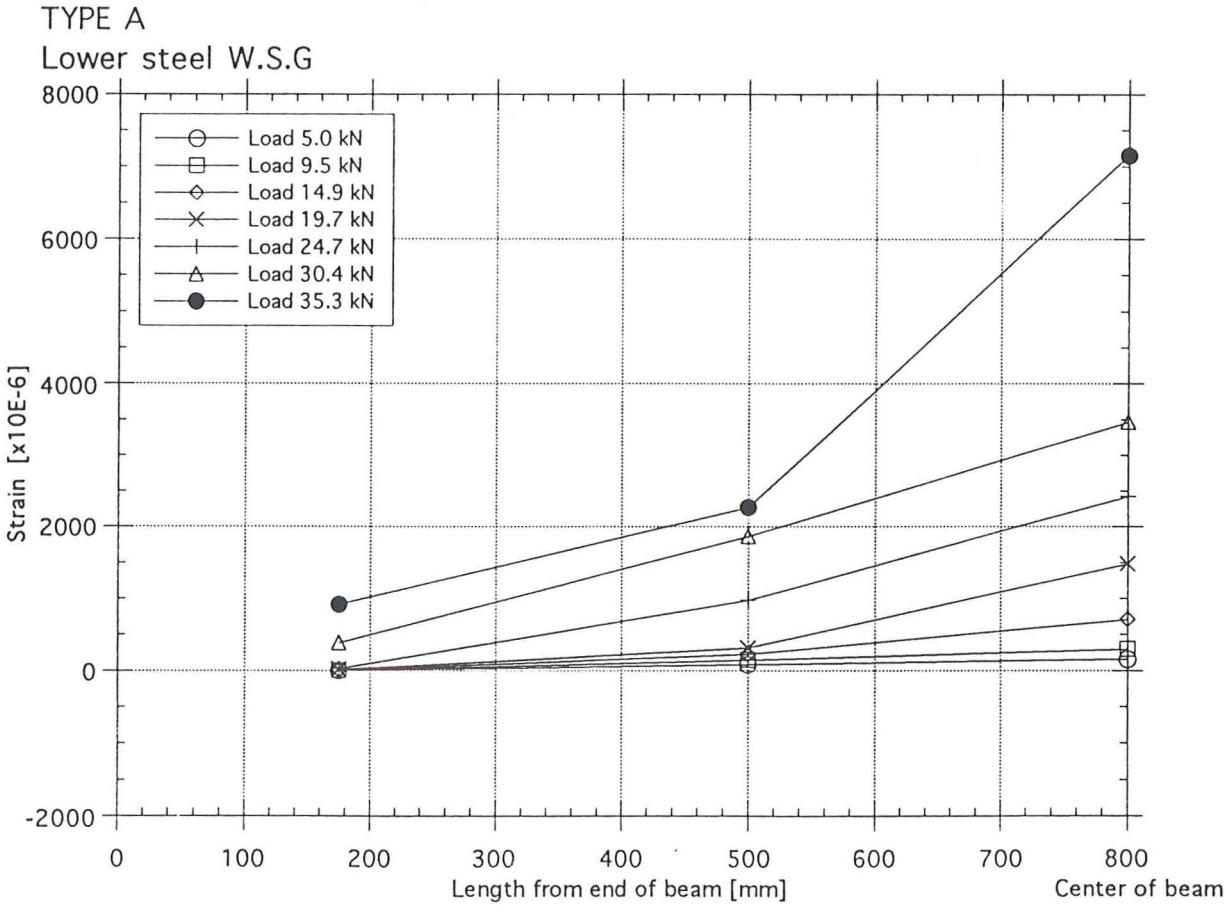

Figure 4.24 Strain in beam type A

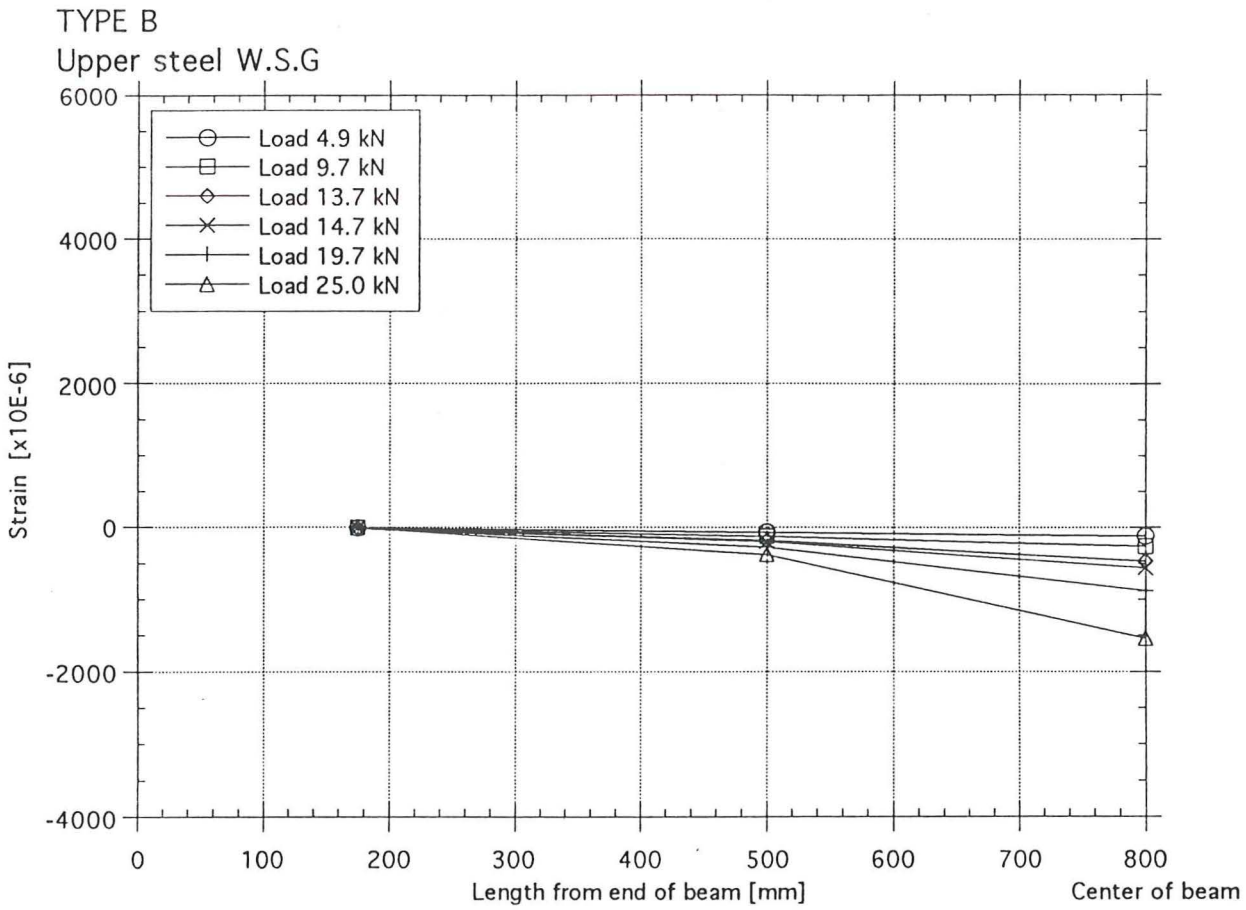

Figure 4.25 Strain in beam type B

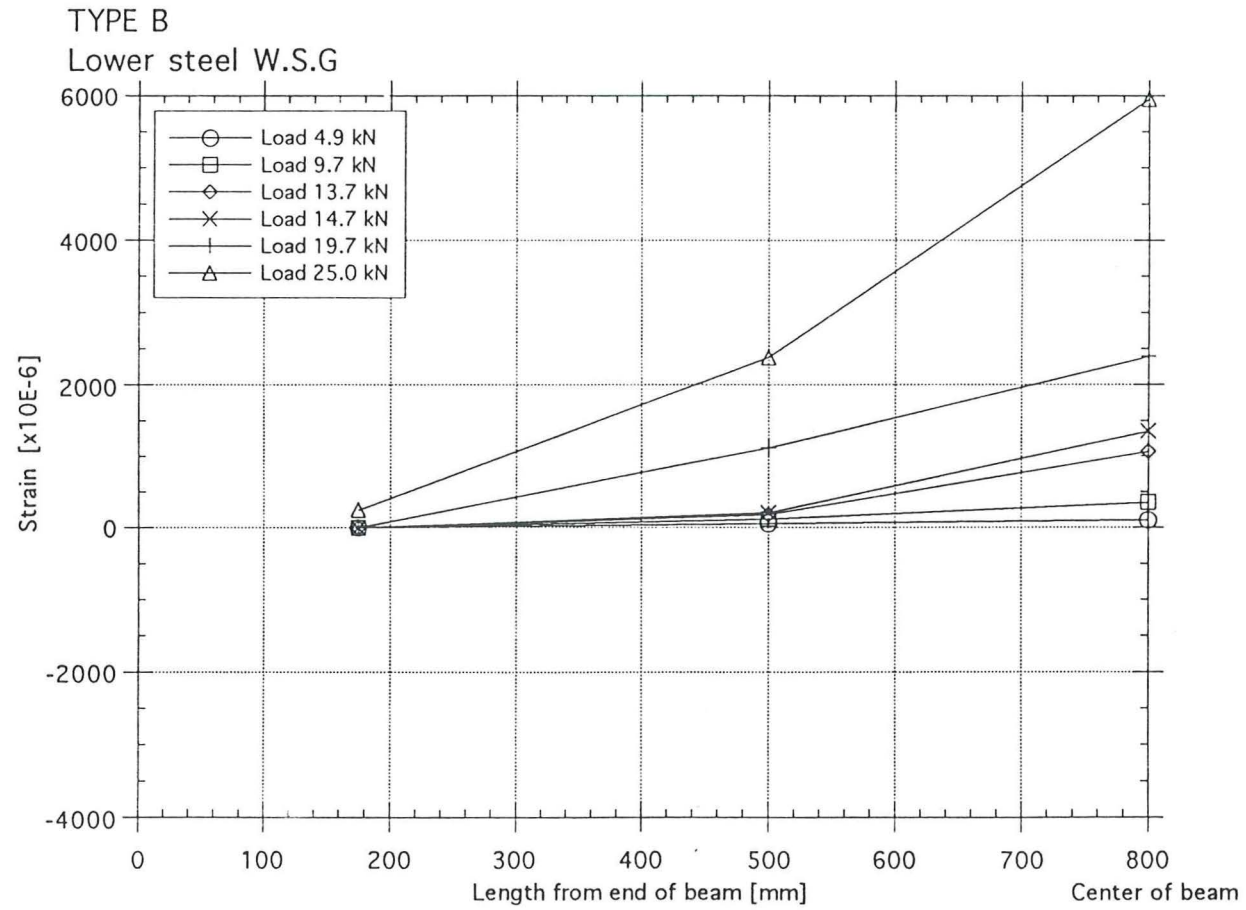

Figure 4.26 Strain in beam type B

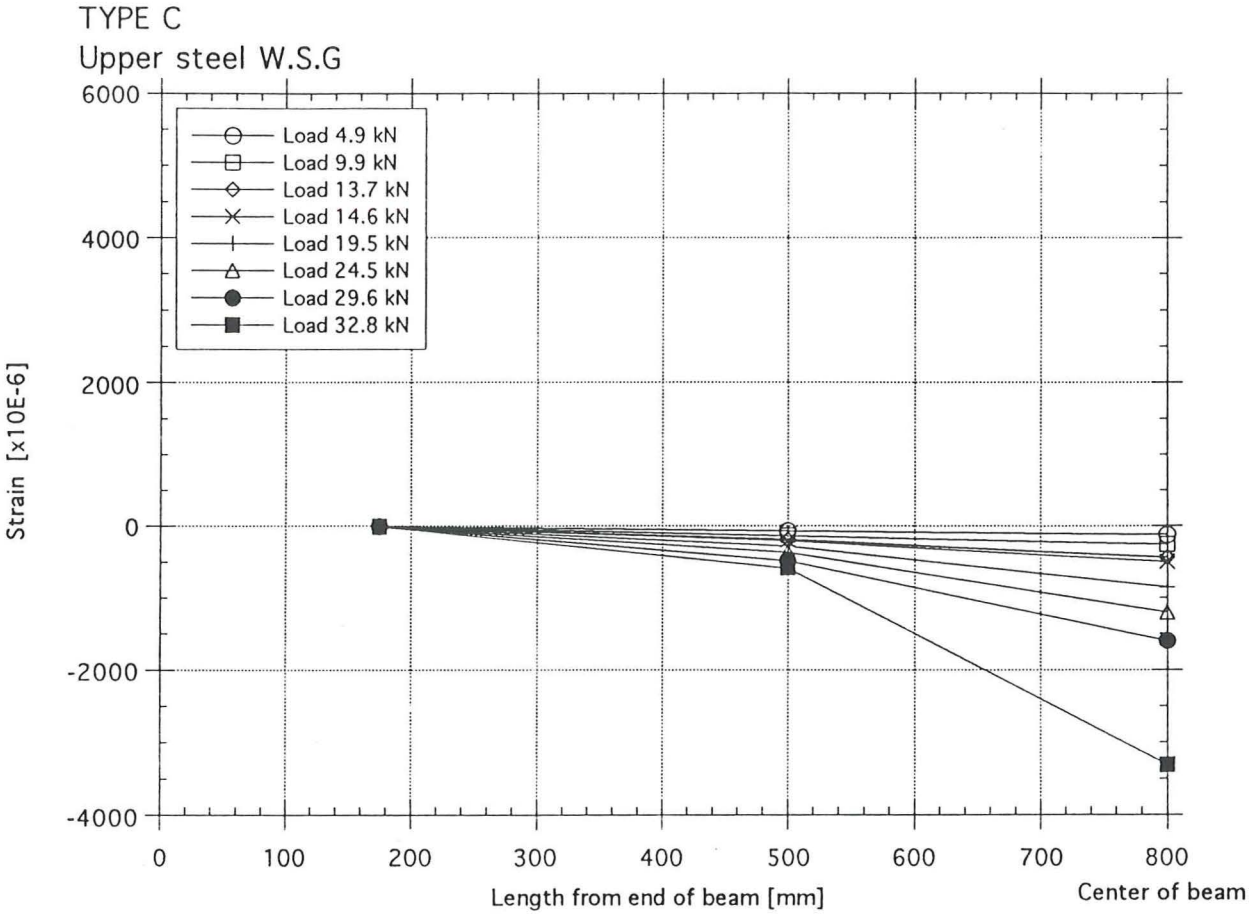

Figure 4.27 Strain in beam type C

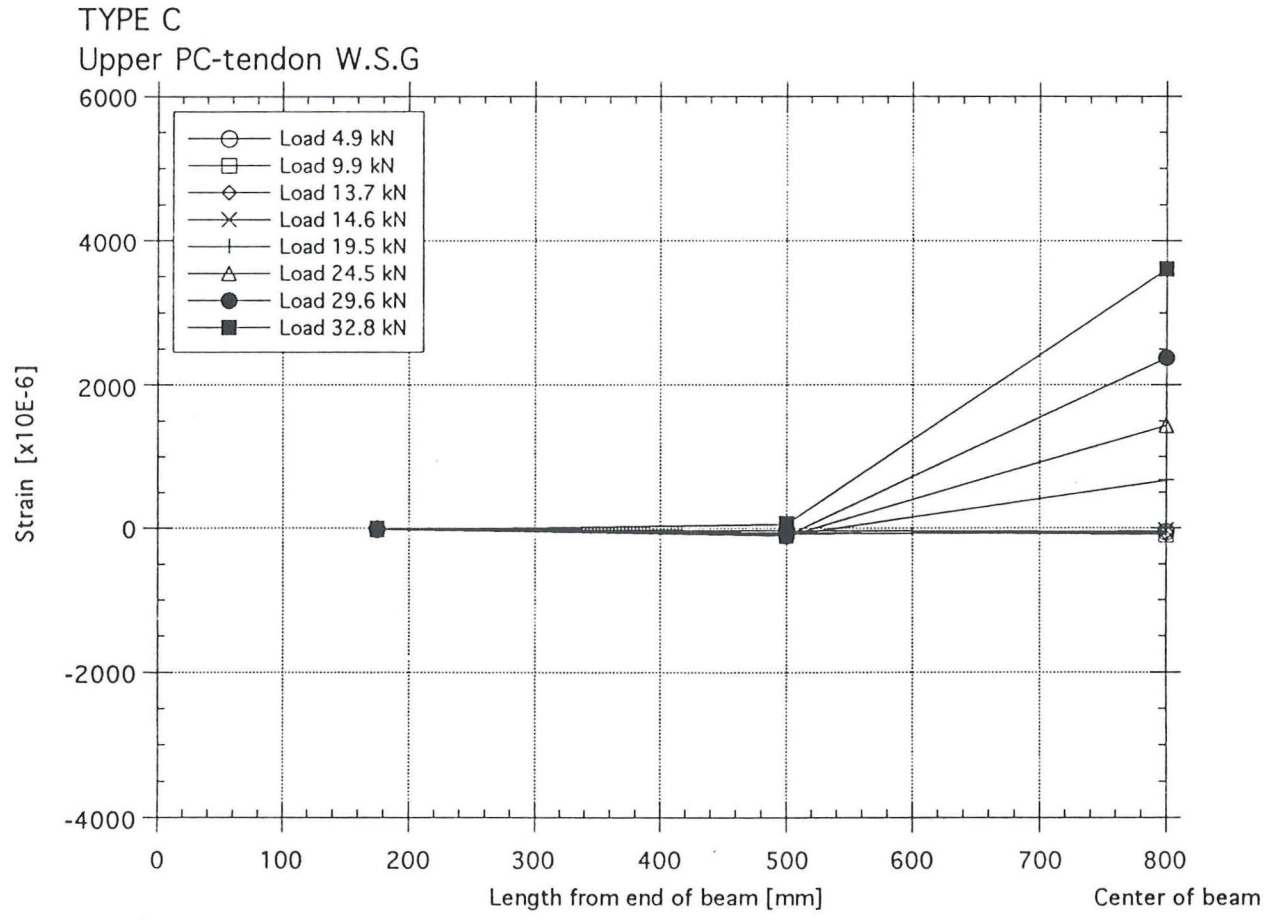

Figure 4.28 Strain in beam type C

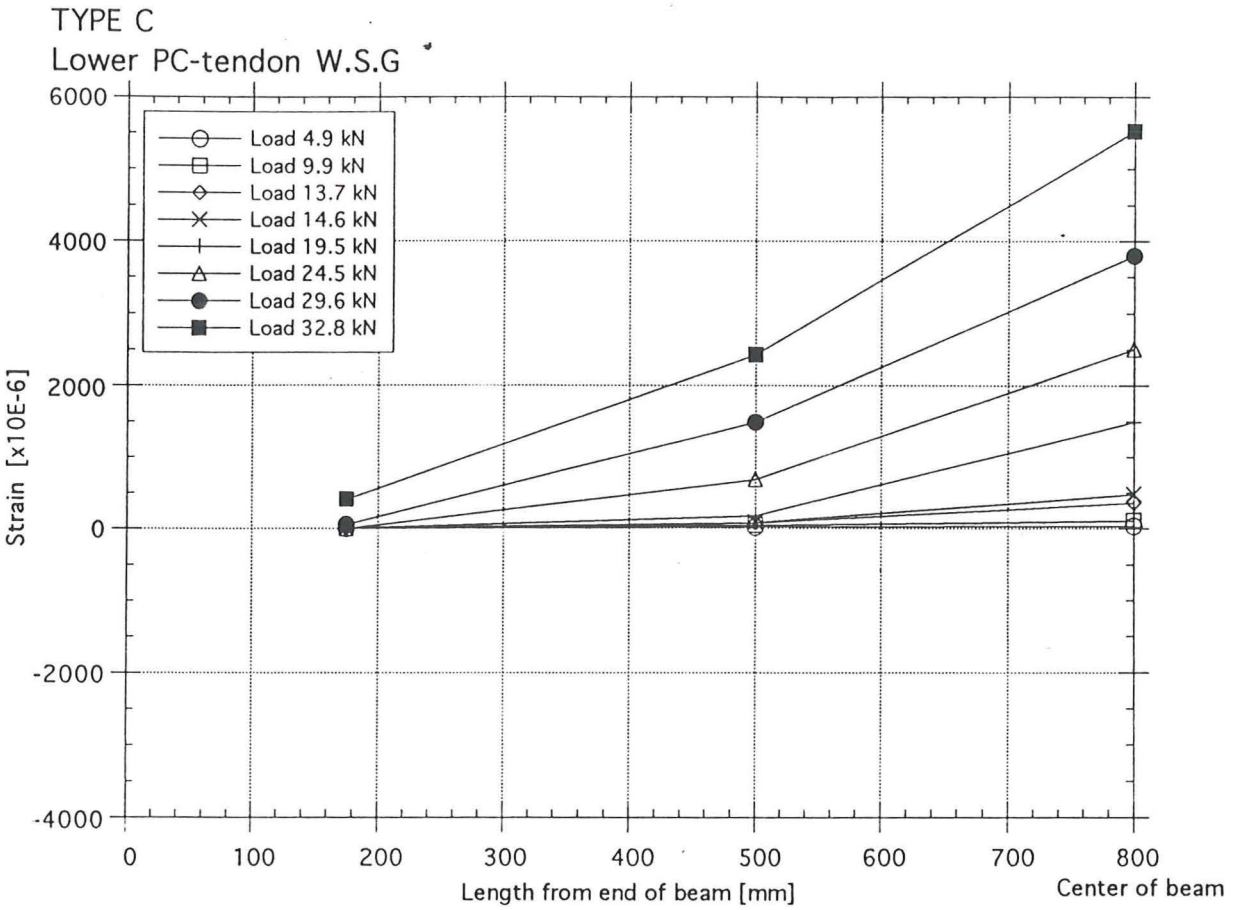

Figure 4.29 Strain in beam type C

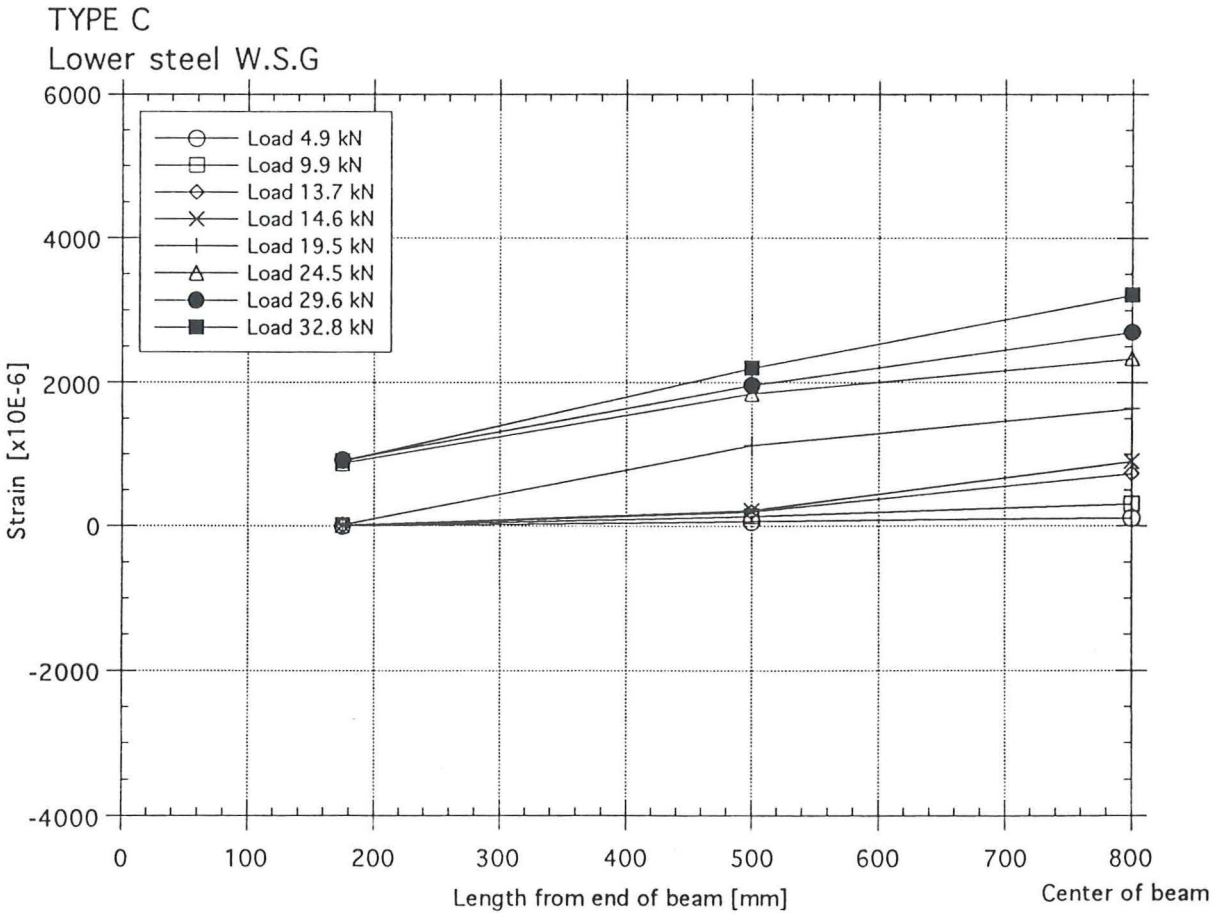

Figure 4.30 Strain in beam type C

4.2.5 Deflection in center of beam

The graphs in figure 4.31 to 4.34 show the moment in the center of the beam plotted against the center deflection. For comparison a dotted curve showing the calculated deflection at crack moment, concrete compression failure and at one moment in between is plotted. After the opening of cracks type A and C are nearly linear up to a center deflection of about 10 mm when the concrete becomes plastic. The almost linear relationship probably depends on the AFRP PC-tendons that shows an elastic behavior up to rupture.

Observe the shape of the curves in the turning point area between no crack and cracks. The neutral axis move slowly due to load application procedure. The soft shape of the curves can be due to the smaller difference in Young's modulus between AFRP and concrete compared to steel and concrete.

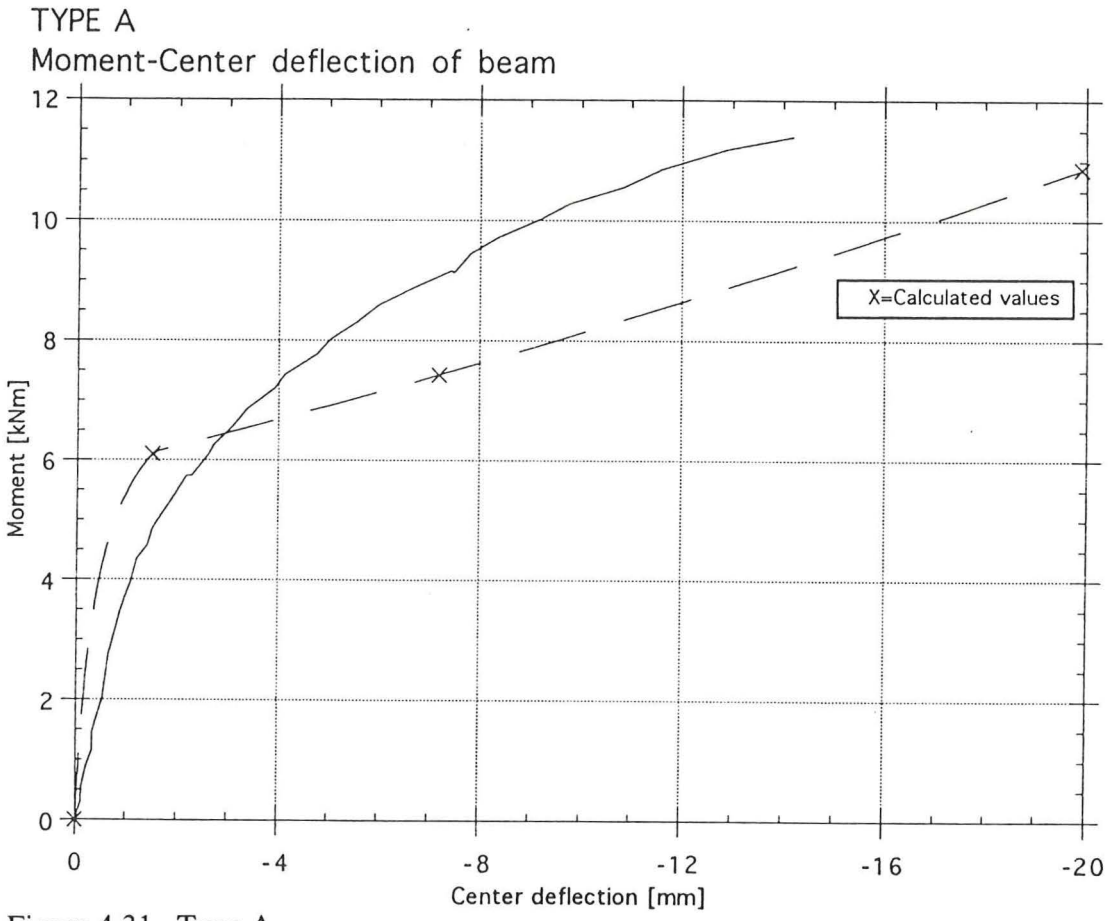

Figure 4.31 Type A

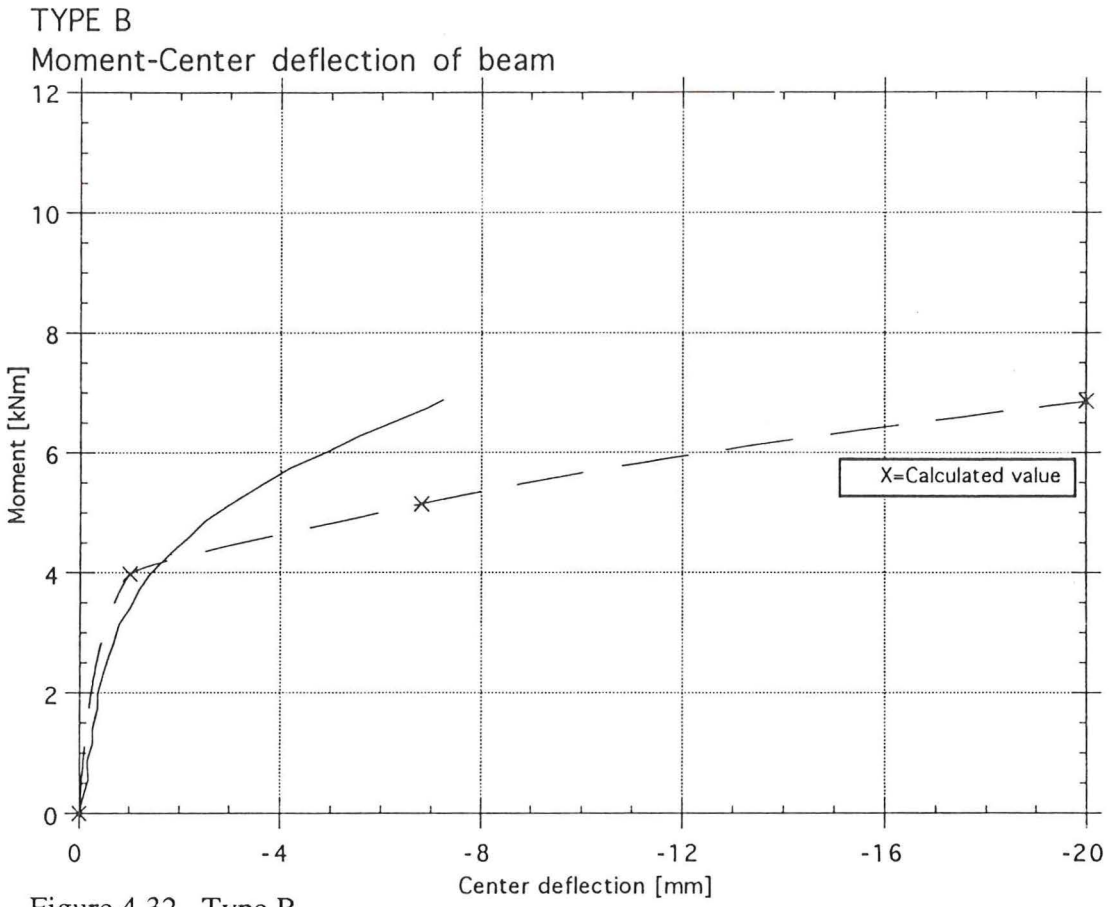

Figure 4.32 Type B

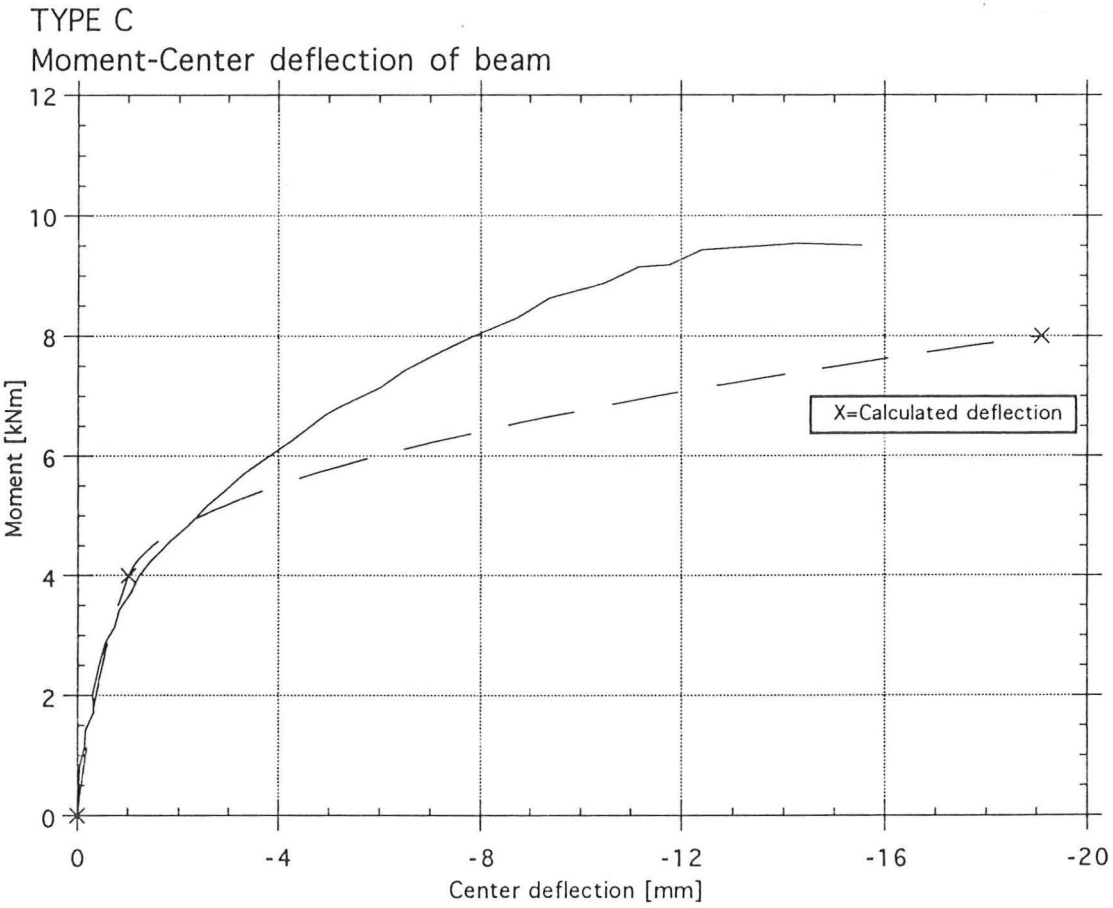

Figure 4.33 Type C

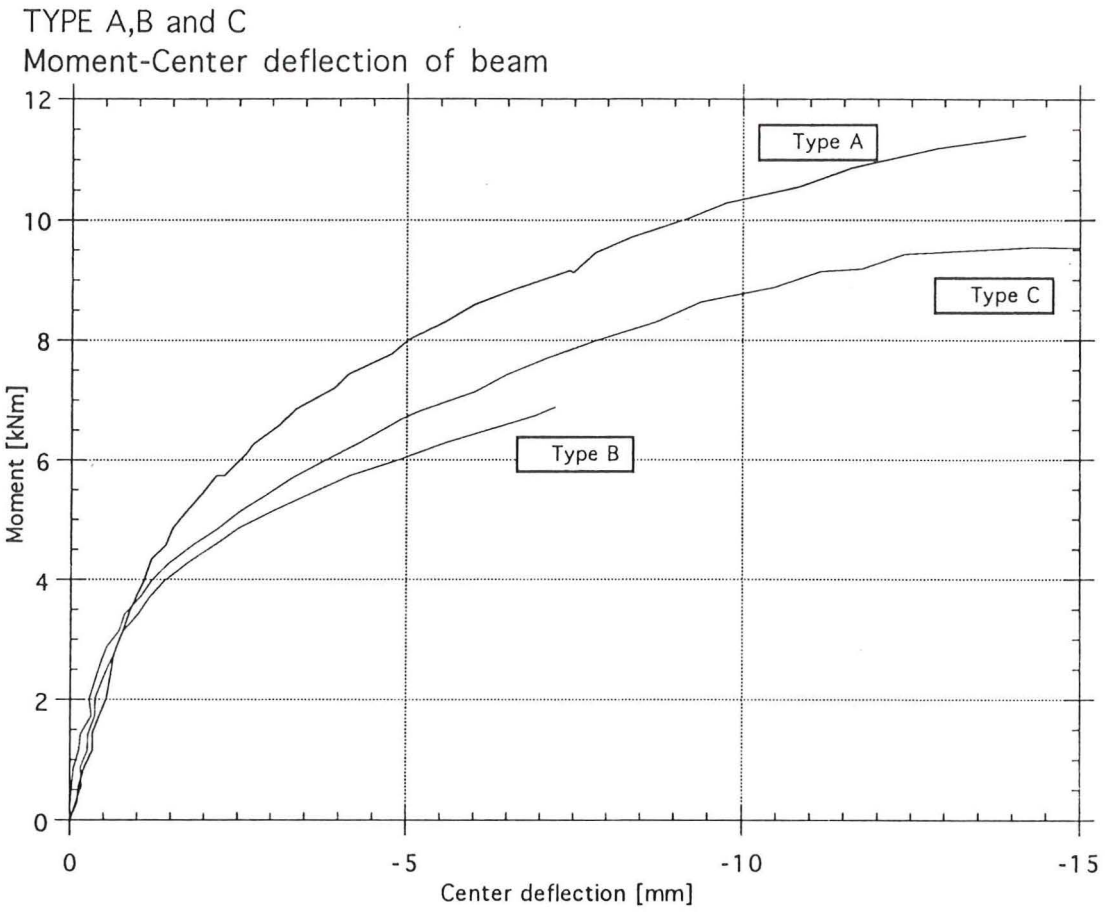

Figure 4.34 Comparison between type A, B and C

4.2.6 Crack width

The graphs in figure 4.35 to 4.38 show the crack width given by two π-gauges that were attached over the two largest cracks found after the first unloading. The average value is plotted in the graphs and finally these average values are compared in one graph. After passing the crack moment area the growth of the crack width is almost linear. The inclination of this line in type A and C is about the same, but in case of type B the inclination is smaller. The inclination depends mainly on the effective depth of the cross section, the diameter and prestress force of the PC-tendons. Type A and C (lower PC-tendon) have the same effective depth but different diameter and prestress force of the PC-tendons. Type B has different effective depth compared to type A but same diameter and prestress force of the PC-tendons. An assumption can be made that the effective depth of the cross section is more affective to the crack width than the diameter and prestress force of the PC-tendons.

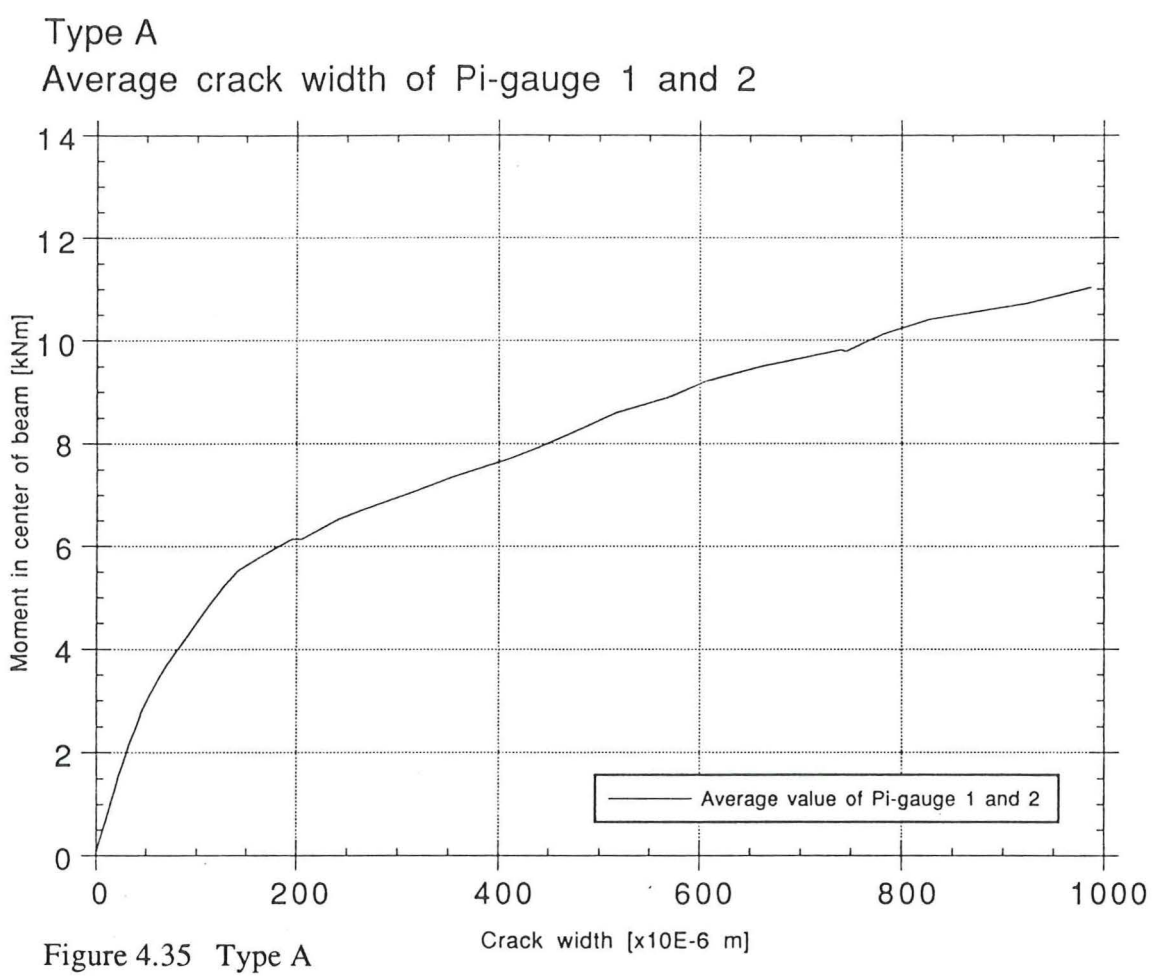

Figure 4.35 Type A

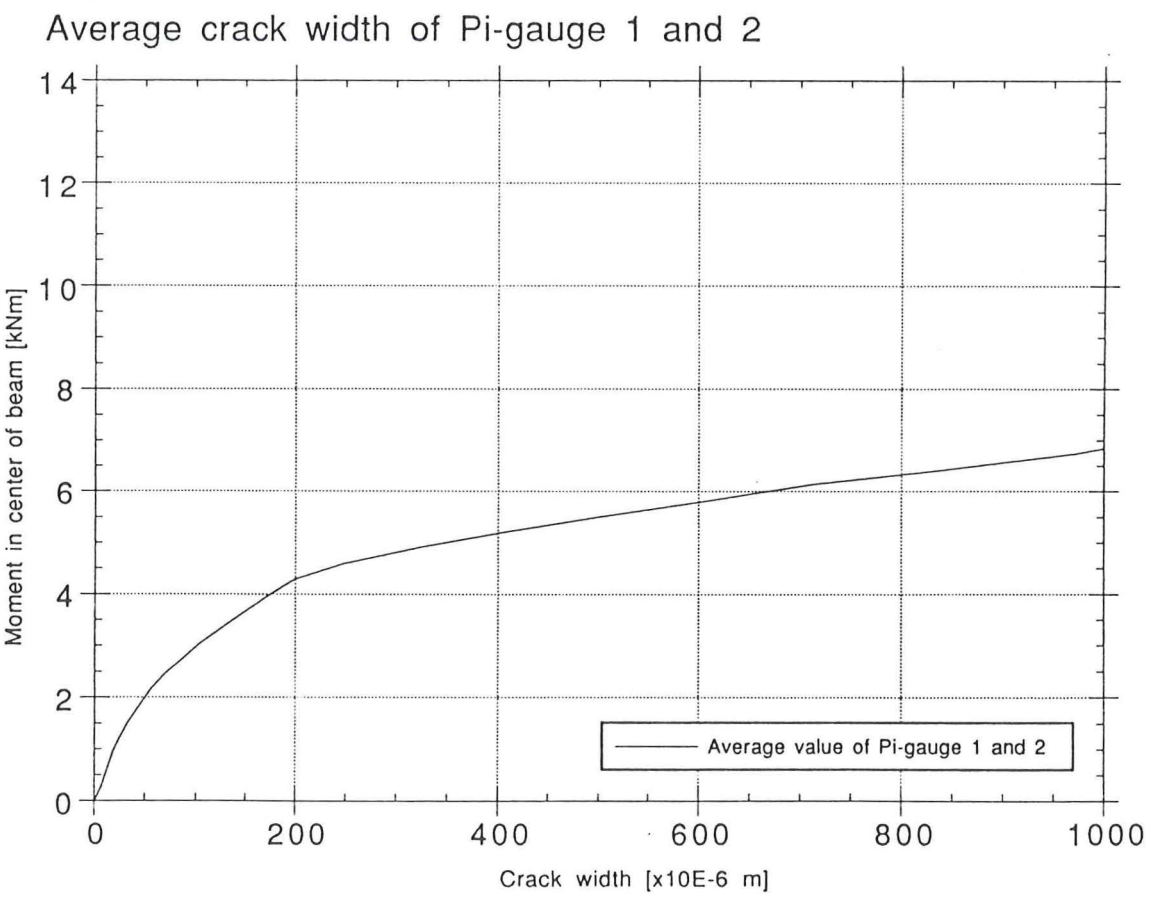

Figure 4.36 Type B

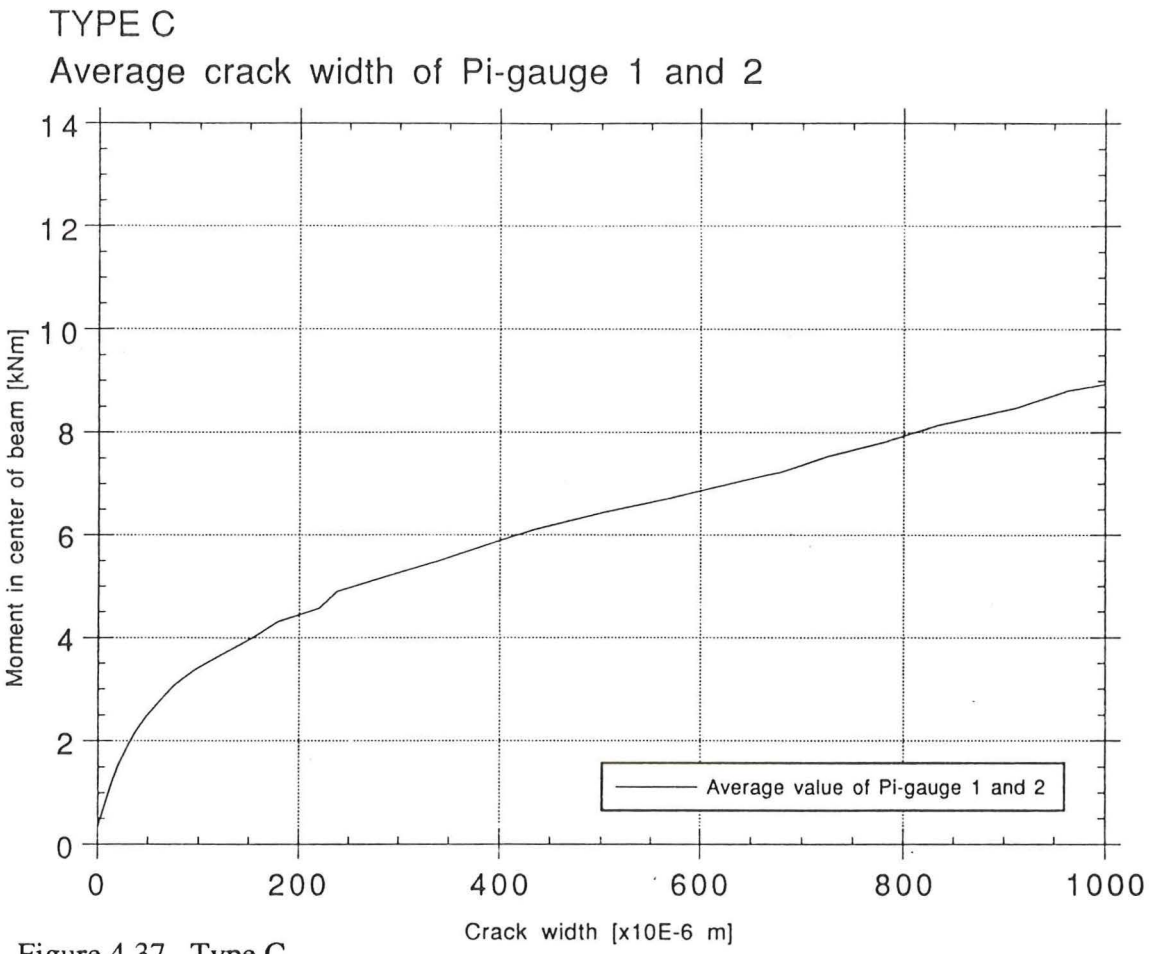

Figure 4.37 Type C

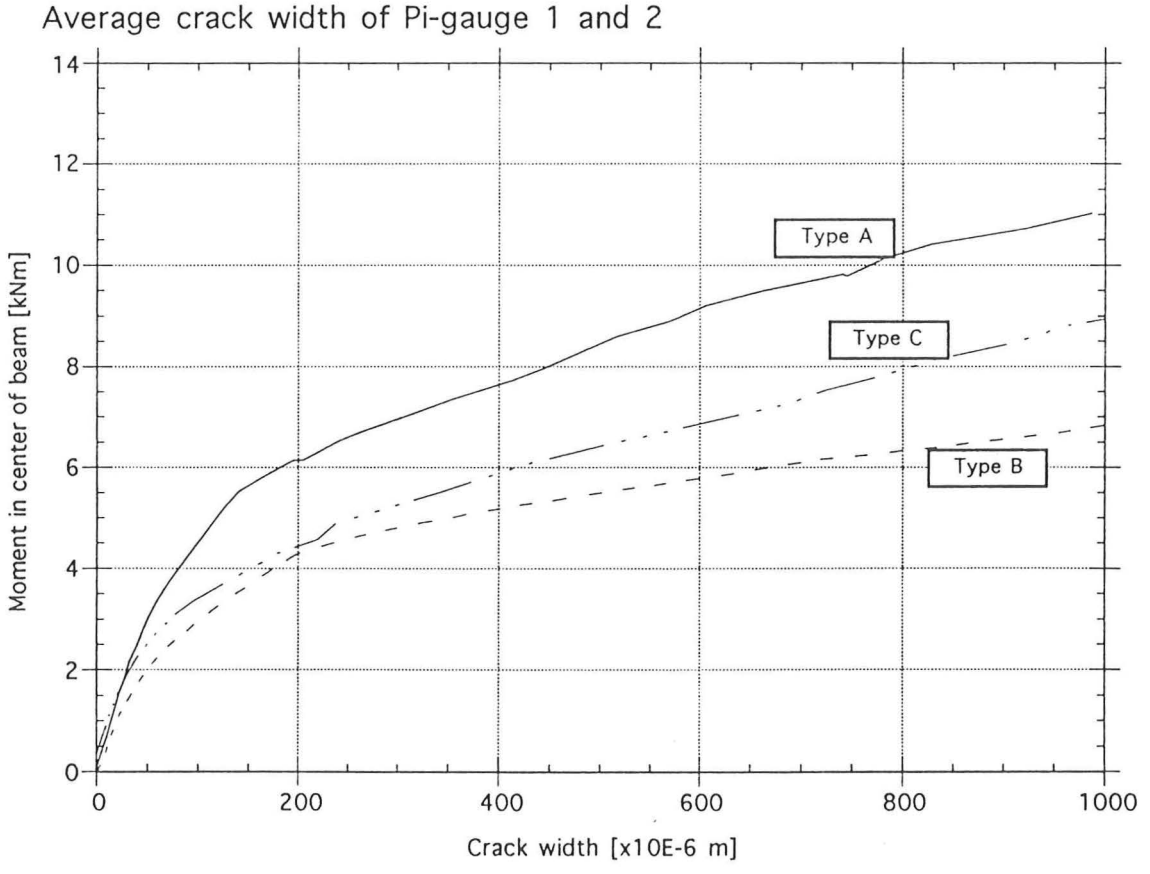

Figure 4.38 Type A, B and C

4.2.7 Crack pattern

The crack patterns are shown in figure 4.39. In type A and B a major crack occurs in the center of the beams. The major crack in type C occurs by the side of the center. The number of cracks is larger in type C and, as follows, the crack spacing is smaller. Many small cracks that may be split cracks occur in type A close to the supports, particularly at the ends of the beam. A large split crack occurs in type A from the PC-tendon up to the top surface. This split crack is probably caused by the design of the stirrups that are U-shaped and open against the top of the beam (see figure 2.1). Another reason could be the high tensile stress in the PC-tendon under loading. As the Poissons ratio (ν =0.6) of the braided AFRP PC-tendon is high the tendon slips from the center and outwards with stress concentrations at the ends of the PC-tendon as result.

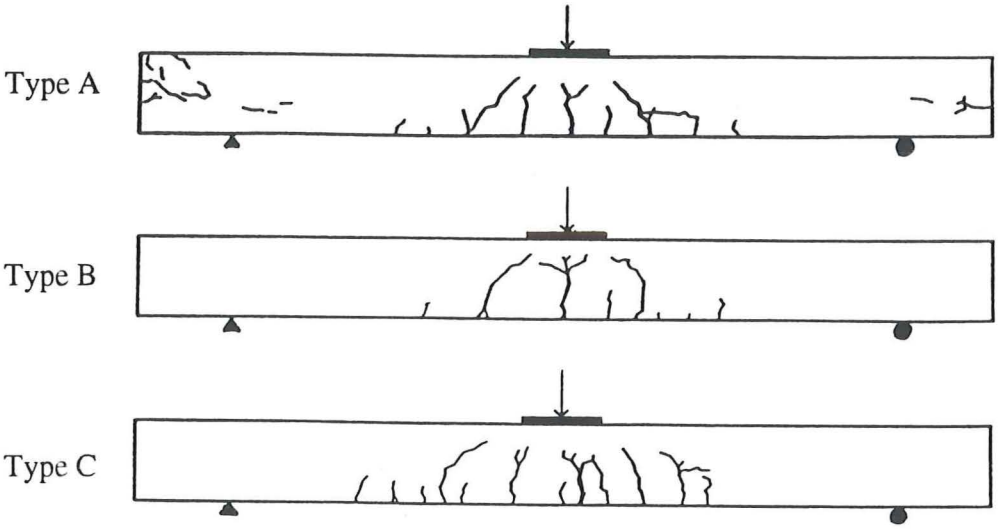

Figure 4.39 Crack pattern

5 Impact test

5.1 Test method

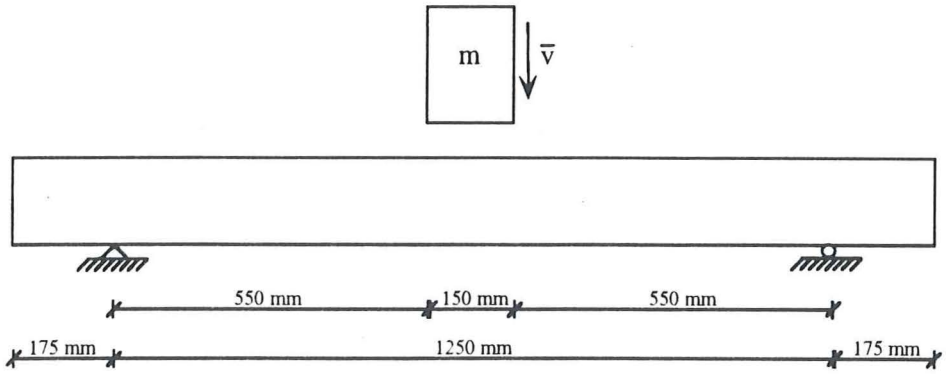

Figure 5.1 Test equipment

The impact test was carried out using an impact-apparatus with a falling weight. A mass (m) of 100 kg was dropped from different heights (h) to achieve the desired impact velocity. The velocity was calculated by the formula: $v=\sqrt{2gh}$. The acceleration was measured as the mean value of four accelerometers applied on the falling mass. The maximum impact force was determined by multiplying the mean acceleration with the weight of the mass and the results are shown in the upper curves of figure 5.2. An integration of the impact force gives $\int F\,dt=m\,v$, which is the momentum.

Strain gauges were attached to the reinforcement in the same way as in the static load test but with four additional strain gauges put on the upper and lower steel bars respectively (see figure 2.1). Outside the beam the measurement equipment differed from the one used in the static load test. At each support two load cells (4 load cells altogether) were attached to measure the reaction force. In order not to disturb the deflection of the beam 6 non-connective deflection meters were used for measurement.

5.2 Test results

5.2.1 Impact response

The initial impact velocity was 1 m/s with an increment of 1 m/s until the beam failed. After each load application a crack sketch was made and the test data was checked. The response results obtained in the impact tests are summarized in figure 5.2. The lower curves show the reaction at the support at different impact velocity. The area between the upper and lower curve of each beam represents the dynamic response. The type C beam shows the largest area while type B shows the smallest.

The results indicate that the response is basically linear up to a speed of 2-3 m/s. This reflects that the increment of momentum is linear and no or little energy is lost. The support responses are also smaller than those obtained during static tests.

For impact speeds which are higher than 2-3 m/s there is a change of the linear response. Consequently the increment of momentum is no longer linear and energy is lost. This energy loss most likely reflects crushing of the concrete.

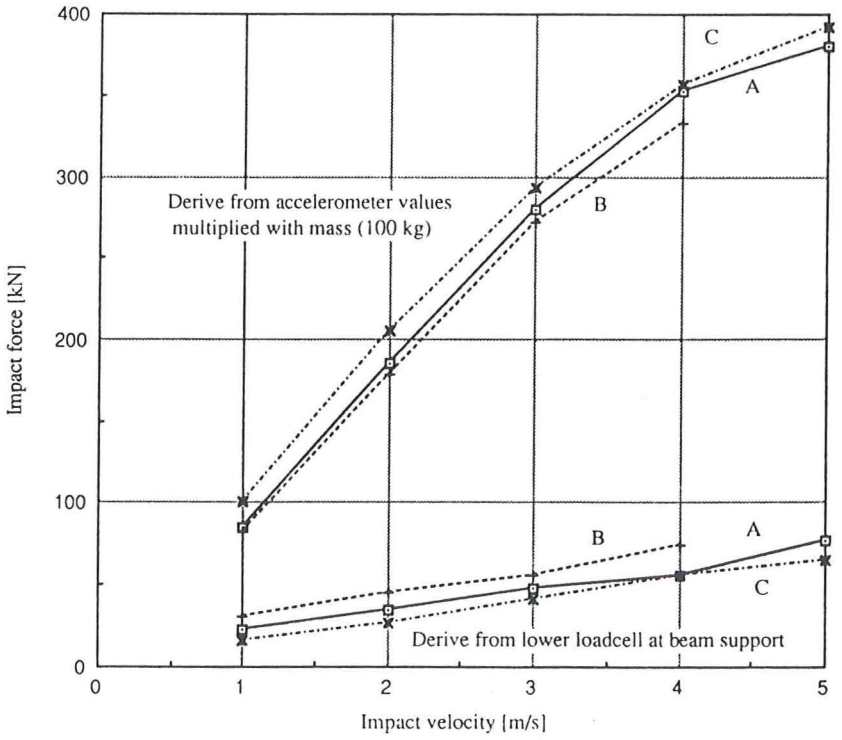

Figure 5.2 Impact and reaction force

5.2.2 Beam displacement

The graphs in figure 5.3 to 5.5 show the displacement in six locations of the beam at an impact velocity of 2 m/s. Earlier studies indicate that the impact properties are affected by the bonding property and rigidity of the reinforcement /5/. The use of materials as AFRP with low rigidity and large elastic elongation may resist impact force by the overall deformation.

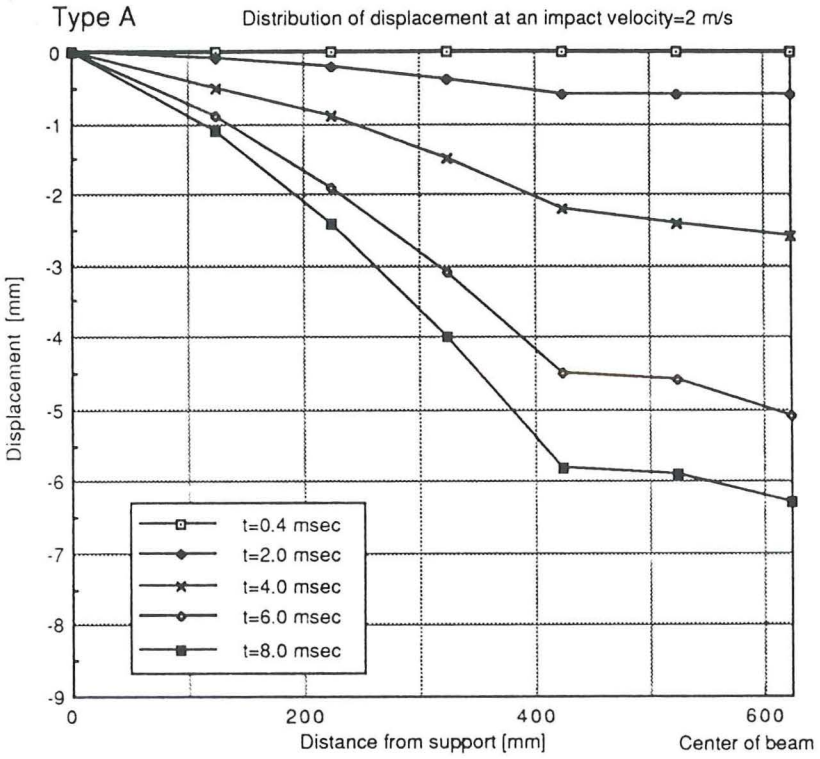

Figure 5.3 Beam displacement type A

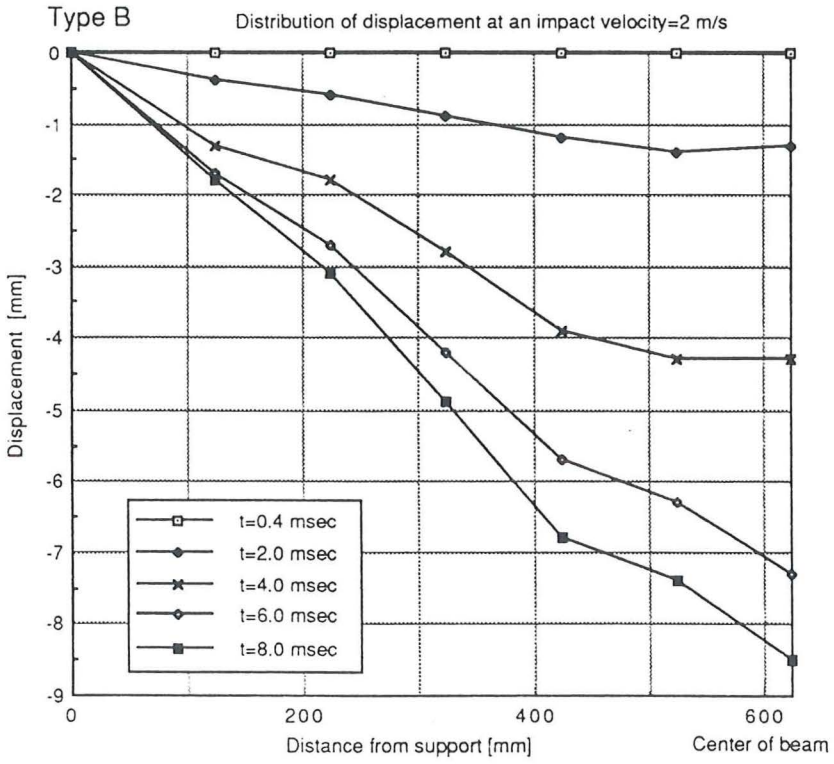

Figure 5.4 Beam displacement type B

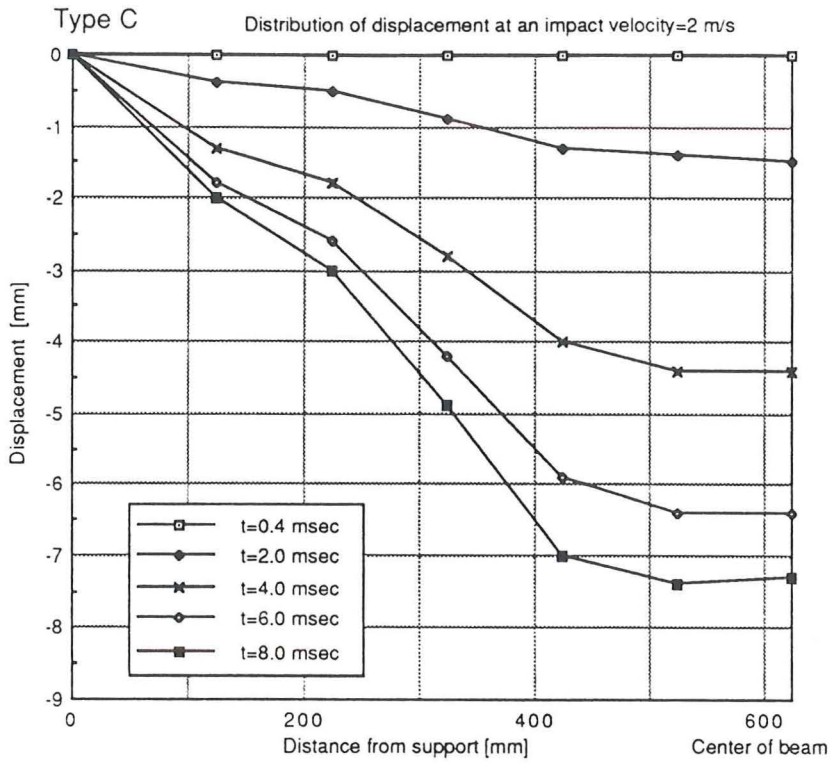

Figure 5.5 Beam displacement type C

5.2.3 Strain wave configurations

Figure 5.6 shows the strain response in time at the center of the beams at an impact velocity of 1 to 4 m/s. Eighty percent of the total sampling time is showed in the figures. The strain is measured on the upper and lower steel bars and the tension and compression response is positive and negative respectively. The beams vibrate with a motion where the strain response on the upper and lower steel bars shows a symmetrical pattern.

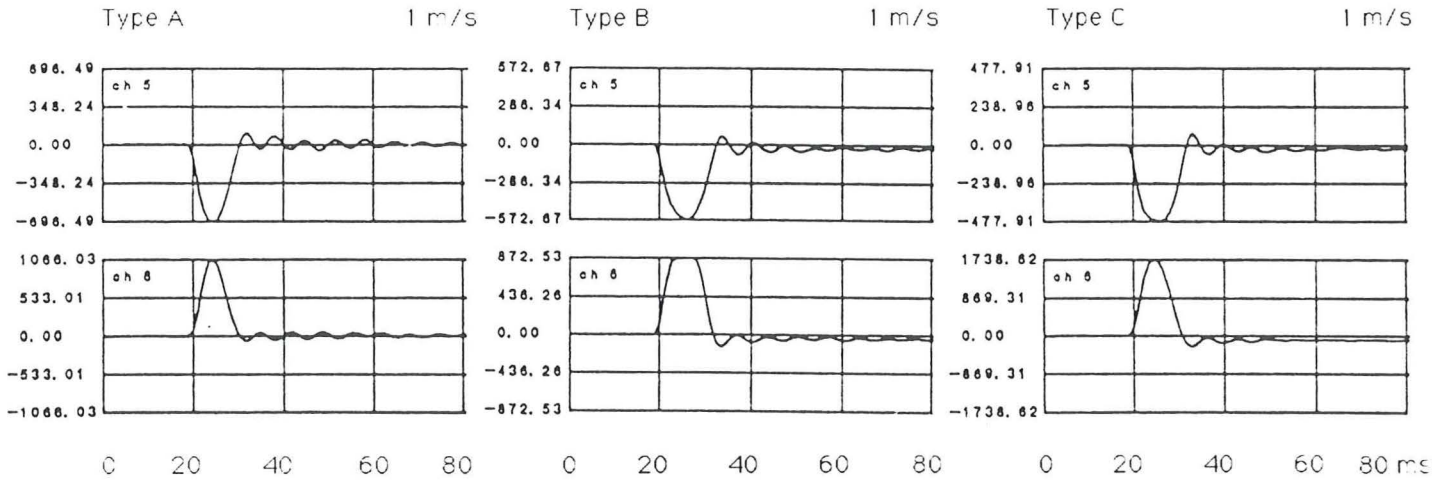

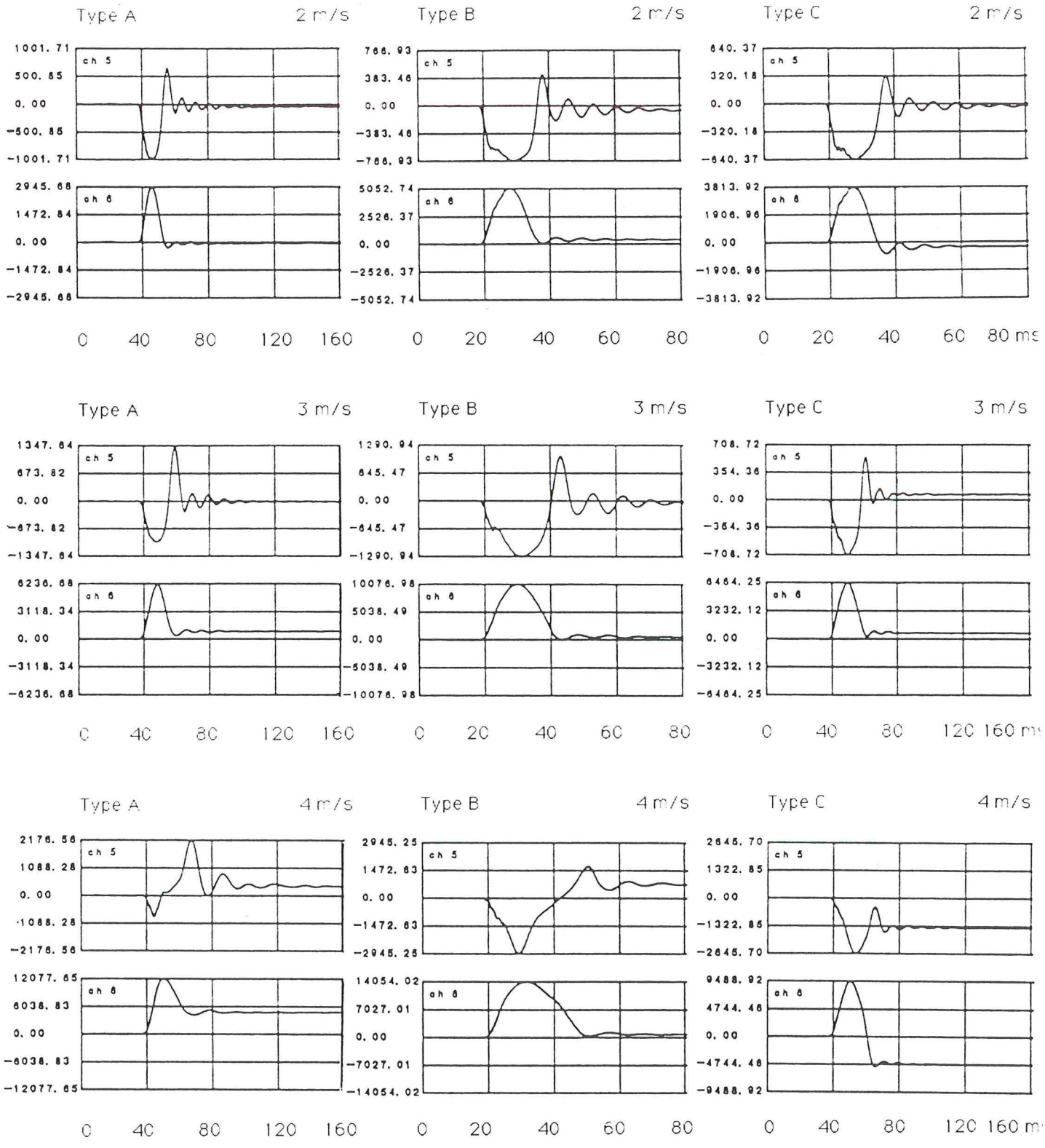

Figure 5.6 Strain in upper and lower steel bar [*10E-6]

5.2.4 Strain distribution

Figure 5.7 to 5.9 show the strain distribution along the beams at an impact velocity of 1 m/s. It can be seen that the main wave propagates from the loading point to the supporting point. Type B has the longest elapsed time until maximum strain is developed, but on the other hand this strain is not so high. The maximum strain was in type A 1066*10E-6 and occurred at t = 5 sec, in type B 872.5*10E-6 at t = 7 sec and in type C 1738*10E-6 at t = 5.7 sec.

In all three types the mode of strain distribution vibrates similarly to the fundamental mode. Earlier tests on concrete slabs reinforced with steel tendons show that they have a concentrated peak of high strain at the center of the beam /3/. In case of AFRP tendons the strain is well distributed all along the beam as seen in figure 5.7 to 5.9.

At the impact load test there is first a deflection of the beam downwards and then an upward reaction. This causes a change of strain in upper steel bars, first compression and then tension. The compression strain in the upper steel bar was highest in type A and smallest in type C.

The upper steel bar had a higher value of tensile strain in type A than in type B and C. This was also seen in the crack pattern at the top surface of the beams. A large number of these cracks occurred in type A but few in type C and no in type B. This behavior is mainly due to the initial prestress distribution in the beams.

The tensile strain of the lower steel bars is lowest in type A. Type B and C show the same strain values in the beginning of the test but in the end type C showed lower values than type B. At low impact load the strain in steel bars is mainly depending on the prestress distribution in the beam, but at higher impact load the effective depth and the position of the tendons have more influence.

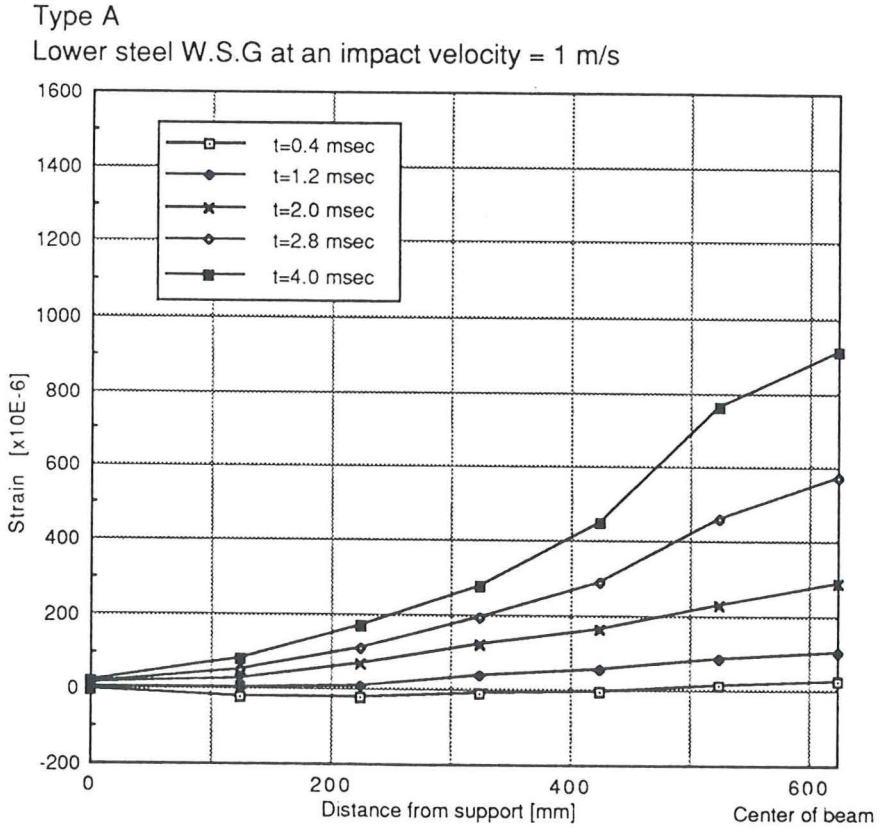

Figure 5.7 Strain distribution type A

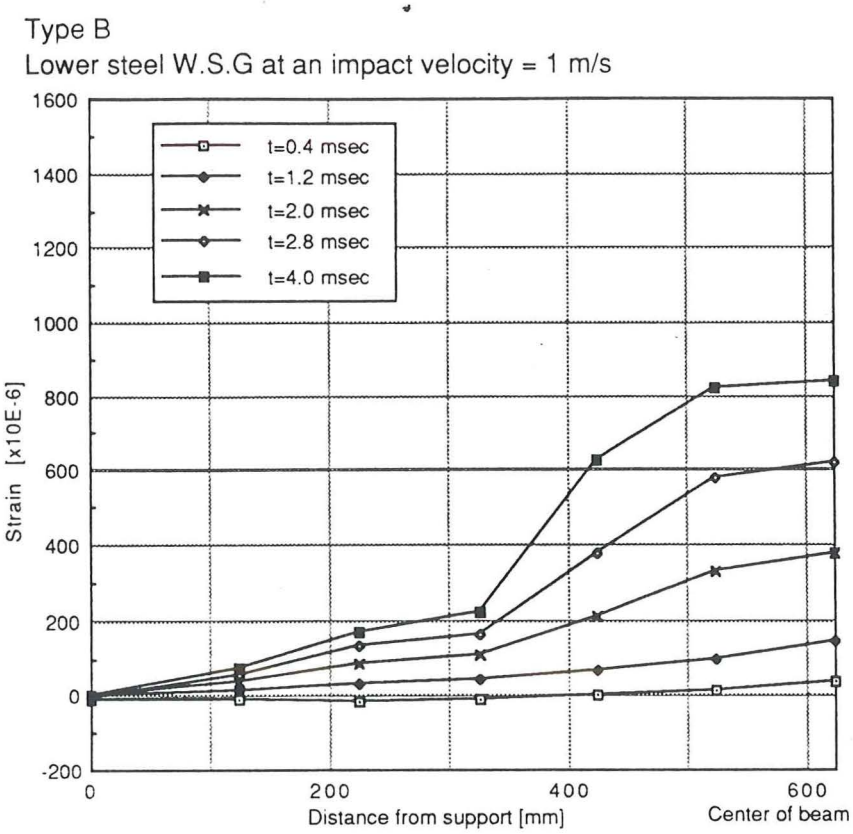

Figure 5.8 Strain distribution type B

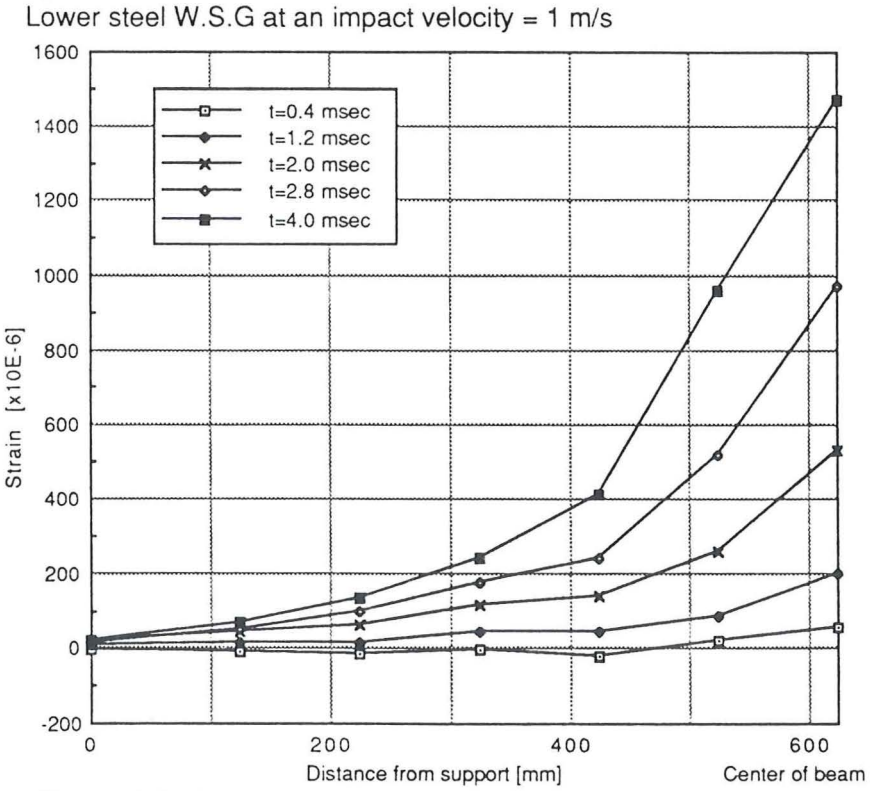

Figure 5.9 Strain distribution type C

5.2.5 Crack pattern

Figure 5.10 to 5.12 show the crack pattern in the three types of beams. Crack sketches after each loading and sketches of all four sides after failure are displayed in the figures.

In figure 5.10 the crack pattern of type A is shown. As in the static test major cracks occur in the center area of the beam with a V-shape of the beam as result. The cracks are either longitudinal or perpendicular to the longitudinal axis of the beam. This beam shows the same kind of behavior at the end of the test as type A did in the static test. The black areas show positions on the beam where the concrete had fallen off.

From other impact tests it can be seen that the cracks depend on the bond properties and the Young's modulus of the reinforcement /3/.

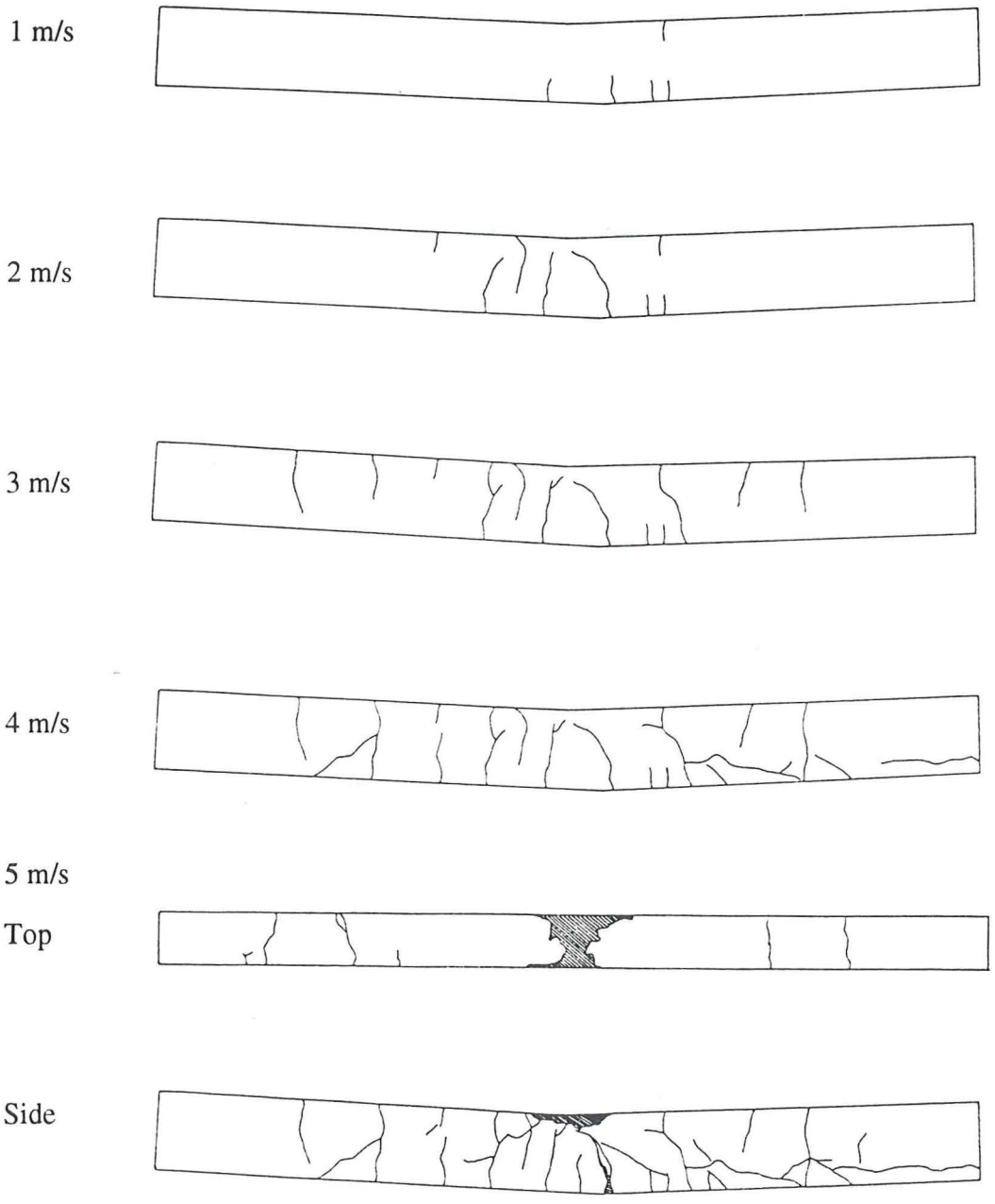

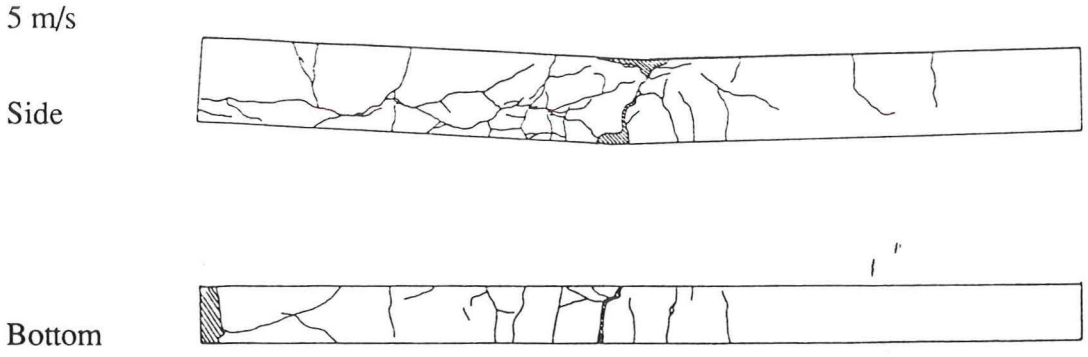

Figure 5.10 Crack pattern type A

The number of cracks is very small in figure 5.11. The beam of type B only shows cracks perpendicular to the longitudinal axis of the beam. The test was stopped at v=4 m/s.

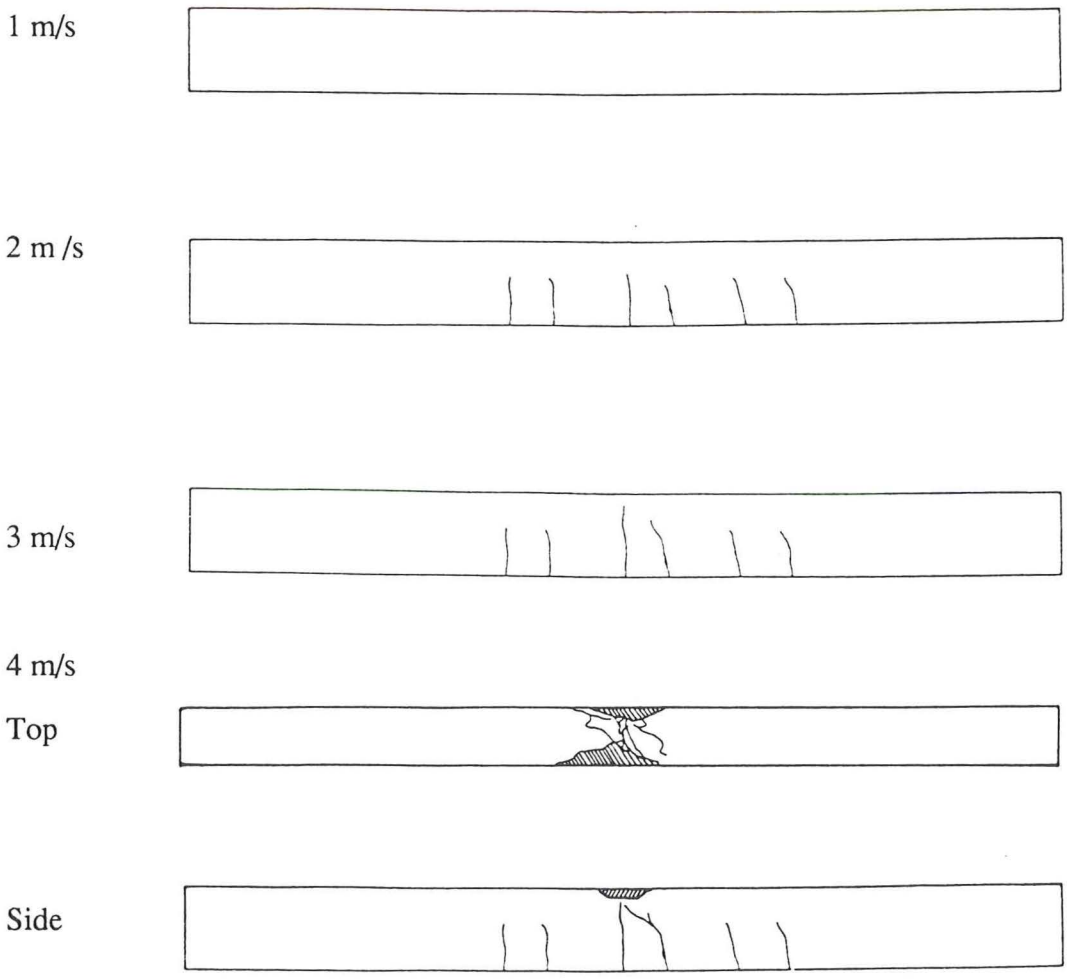

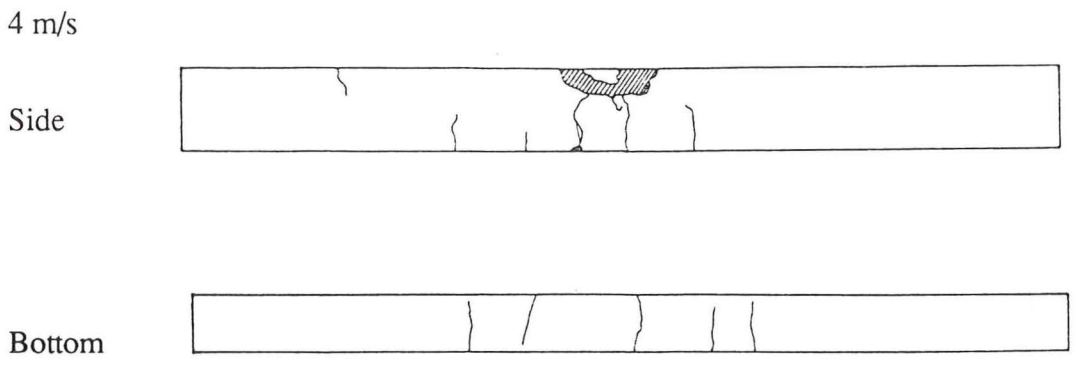

Figure 5.11 Crack pattern type B

Figure 5.12 shows the crack pattern of the type C beam. Concrete compression failure occurred at a velocity of 5 m/s. There are a few numbers of cracks in this beam compared to type A. Observe the longitudinal cracks on the top surface of the beam.

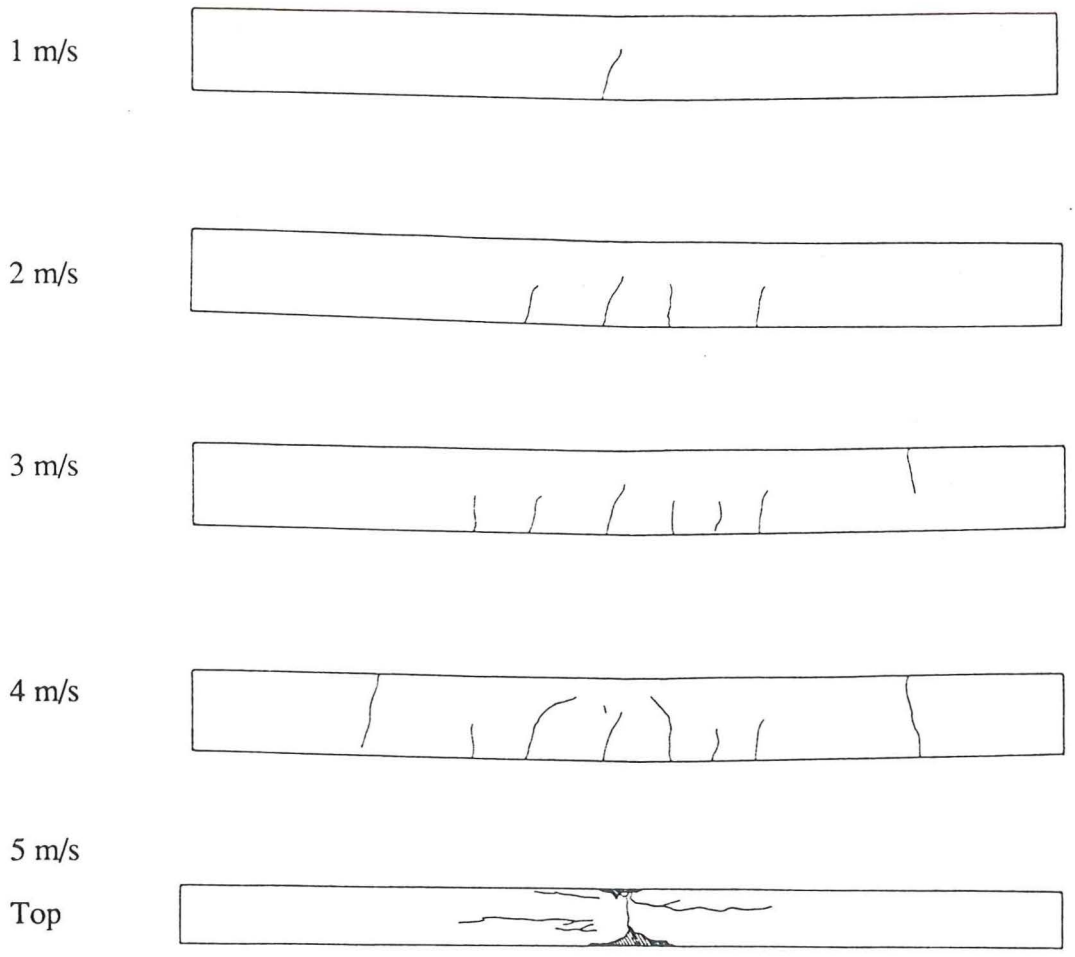

5 m/s

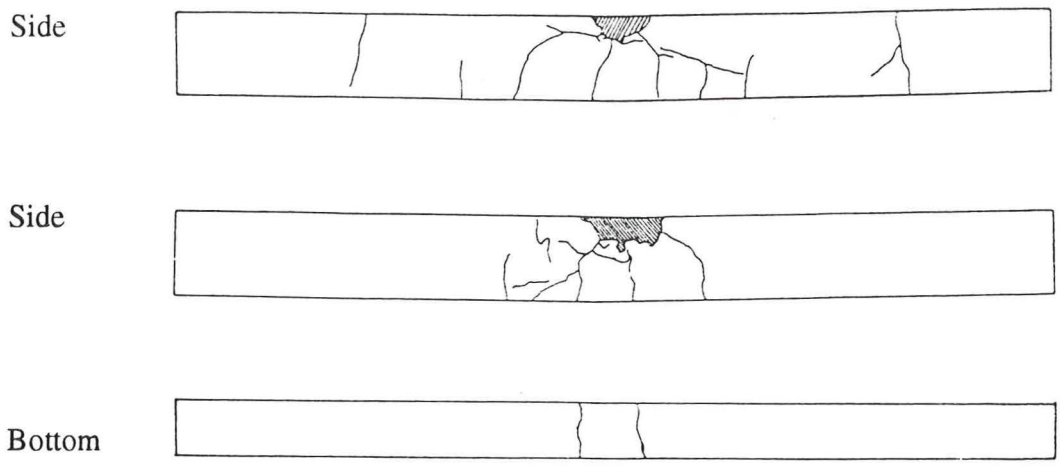

Figure 5.12 Crack pattern type C

The first crack at the top surface of the beams occurs in type A at an impact speed of v=1 m/s. In type B no such cracks were found and in type C the first top surface crack occurs at v=3 m/s.

At an impact speed v=4 m/s type A turned out to be the most cracked one. In type B the cracks were equally distributed over the central area of the beam. At low impact speed type C had fewer cracks than type B, but at v=4 m/s type C showed a larger number of cracks.

In case of longitudinal cracks they seem to appear where the PC-tendons are located. These cracks occur at v≈4-5 m/s. At this speed the stress in the PC-tendons is very high. The high Poissons ratio of the AFRP PC-tendons and high stress decreases the diameter of the tendons. The tendons start slipping in the center of the beam where the stress is highest. As the tendon slips the bond stress between the tendon and the concrete increases with split cracks in the concrete as result.

6 Load and failure process

It is difficult to make a complete comparison between the impact and static test. In the static load test the load application speed is low and the beams fail after approximately 30 minutes. The slow load application speed results in a transition from elastic to viscous response. In an impact test the duration of the load application is very short (in this test 0.2 msec) which results in mainly an elastic response. This difference can be found to a certain extent in the crack pattern at failure.

In addition to a difference in failure modes the strength properties of a beam subject to a load will in general depend on the load application. This can be described by an expression in terms of an effective duration of this stress:

$$R \approx R_0 \left(\frac{D}{D_0} \right)^{\frac{1}{\beta}} \qquad (1)$$

where R is the failure load with a duration D. Normally the value D is different from the reference value D_0. This results in a new value on the failure load R. The difference also depends on the time parameter β ($\beta_{CONCRETE}$ =20-30 and β_{AFRP} = 32 and $\beta_{PRESTRESSING\ STEEL}$ = 120). The difference in short-term and long-term strength of aramid is, due the β value, larger than in prestressing steel.

The beams were designed for concrete compression failure that is caused by an increase of the micro cracks between cement paste and aggregate. If the beams were designed for failure in the AFRP PC-tendons the following failure would have been most likely to occur in the tendons. In the static load test, with slow load application speed, the failure would occur because of growth of micro-cracks in the interphase between the fibers and the matrix. In the impact test the failure would occur because of existing defects in the fiber composite.

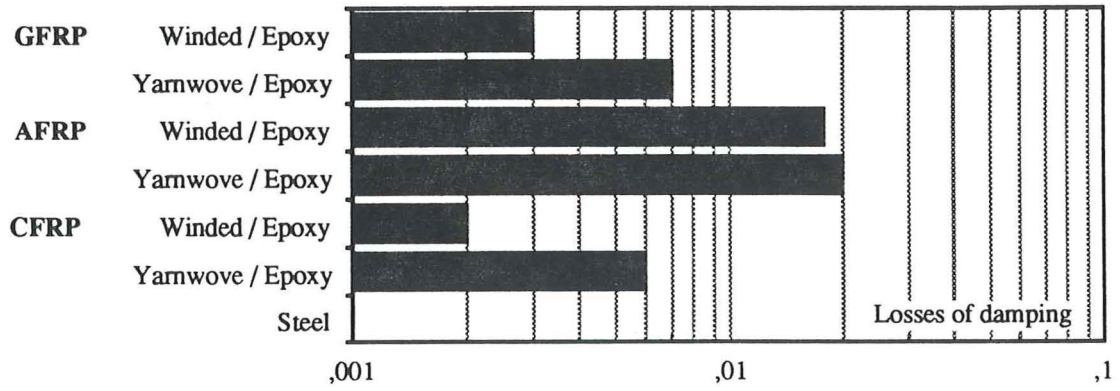

Figure 6.1 Losses due to damping

In figure 6.1 the losses of damping are shown for steel and different reinforced plastics. The graph shows that aramid fiber is a very good damper compared to steel. In a reinforced concrete structure exposed to large impact loads steel yields with a remaining plastic deformation as result. The strength in aramid fibers is more time dependent than the strength of steel. Concrete is a little more time dependent than aramid. In figure 6.2 the strength increases as the load application time decreases. In the tests the relation between static and impact load application time was about 10^7. In figure 6.2 the strength increases approximately 65% for aramid and only 14% for steel. The failure load in the impact test compared to the failure load in the static test seems to correspond with this theory.

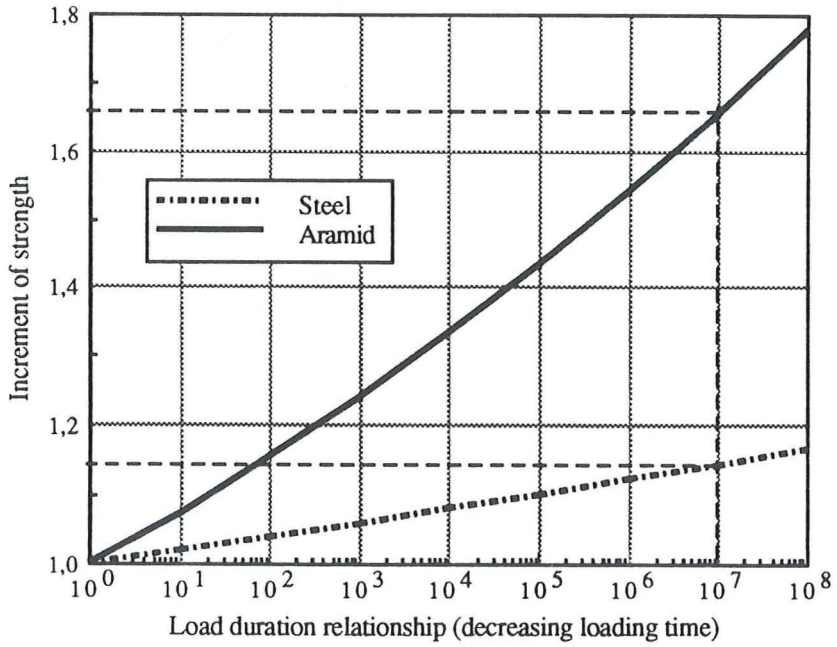

Figure 6.2 Time dependence of strength

7 Conclusions

In the static test beam type A was strongest and in the impact test type A and C could sustain the largest impact load. The lower Young's modulus of AFRP PC-tendons compared to steel is an advantage in absorbing impact energy. Earlier tests show that steel tendons have a concentrated peak of high strain at the center of the beam. When AFRP tendons are used the strain is well distributed all along the beam. A larger deflection of the beam gives a lower value on the retardation. The retardation is proportional to the impact force that will be lower.

The theoretical ultimate load of the static test was lower than the experimental one. The simple beam theory gives a too large beam displacement causing an early compression failure.

After concrete compression failure all static test specimens showed the same V-shape with major cracks in center of beam. In the impact load test the V-shape of the beam occurred in type A and C, maybe due to higher impact velocity than type B.

To distribute the energy over a large area of the beam the crack pattern should show many smaller cracks. Higher bond-strength PC-tendons would be required to achieve that kind of pattern.

At high load area split cracks may occur in AFRP PC-beams, especially when a high value on the effective depth is used. This occurs in type A of the static test and in type A and C of the impact test.

Acknowledgment

In closing, the authors wish to express their sincere thanks for the assistance and advice received from every involved employee at the Technical Research Institute of Mitsui Construction CO, LTD, Tokyo and a special thank to professor Norimitsu Kishi at Muroran Institute of Technology, Muroran.

References

/1/ Kishi, et al.: "The behavior of reaction forces of simply supported BR beam under impact loading", Transactions of the Japanese Concrete Institute

/2/ Mikami, et al.: "Dynamic behavior of concrete slabs reinforced by braided AFRP rods under impact loads", Transactions of the Japanese Concrete Institute, 1991

/3/ Mikami, et al.: "Experimental study on dynamic behavior of concrete slabs reinforced with braided AFRP rods under impact loads", Transactions of the Japanese Concrete Institute, 1991

/4/ Mikami, et al.: "Impact resistance of concrete slab reinforced with braided AFRP rods", Transactions of the Japanese Concrete Institute, 1992

/5/ Mikami, et al.: "Impact behavior of concrete slab reinforced by braided AFRP rods under heavy weight falling", Transactions of the Japanese Concrete Institute, 1992

/6/ Japan Society of Civil Engineers (JSCE): "Standard Specification for Design and Construction of Concrete Structures", part 1 (design), 1986

/7/ Tanigaki, et al.: "Flexural behaviors of partially pre-stressed concrete beams reinforced with braided aramid fiber rods", 11th JCI, 1989

/8/ Kishi, et al.: "Development of 3-layered shock-absorbing system for rock sheds", Transactions of the Japanese Concrete Institute

/9/ Sentler: "A strength theory for viscoelastic materials", D9:1987, Swedish Council for Building Research